Hepatitis B virus affects TLR2 signalling and Hippo pathway activity, thereby counter-regulates innate immunity and contributes to hepatocarcinogenesis

Inaugural Dissertation
for
the doctoral degree of
Dr. rer. nat.

from the Faculty of Biology
University of Duisburg-Essen
Germany

Submitted by

Xufeng Luo

Born in Luohe (Henan)

August 2020

The experiments underlying the present work were conducted at the Department of Gastroenterology and Hepatology at the University Hospital Essen at the University of Duisburg-Essen.

1. Examiner: Priv. Doz. Dr. Ruth Bröring
2. Examiner: Prof. Dr. Sven Brandau

Chair of the Board of Examiners: Prof. Dr. Ulf Dittmer

Date of the oral examination: 25th November 2020.

DOI: 10.17185/duepublico/73478
URN: urn:nbn:de:hbz:465-20231025-104715-0

FOR MY FAMILY

天下无难事，只怕有心人。

It's dogged that does it.

Wer willensstark ist, dem ist in der Welt nichts schwer.

Note

In the context of this doctoral work, the following articles were published or submitted:

1. Zhenhua Zhang, Martin Trippler, Catherine I Real, Melanie Werner, **Xufeng Luo**, Stefan Schefczyk, Thekla Kemper, Olympia E. Anastasiou, Yvonne Ladiges, Juergen Treckmann, Andreas Paul, Hideo A. Baba, Lena Allweiss, Maura Dandri, Guido Gerken, Heiner Wedemeyer, Joerg F Schlaak, Mengji Lu, Ruth Broering. (2020).
   Hepatitis B virus particles activate toll-like receptor 2 signalling initial upon infection of primary human hepatocytes.
   Hepatology. 2020 Jan 11. doi: 10.1002/hep.31112. Online ahead of print.

2. **Xufeng Luo**, Mengji Lu, Hideo A. Baba, Guido Gerken, Heiner Wedemeyer, Ruth Broering.
   Toll-like receptor signalling induces the Hippo pathway activity, thereby counter-regulating innate immunity against Hepatitis B virus.
   Manuscript prepared for submission

3. **Xufeng Luo**, Yaojie Liang, Mengji Lu, Hideo A. Baba, Stefan Schefczyk, Guido Gerken, Heiner Wedemeyer, Ruth Broering.
   HBsAg-induced inactivation of Hippo signalling increases YAP and BMI1 to induce hepatocarcinogenesis by affecting cell cycle and chromosomal instability.
   Manuscript in preparation

Table of Contents

Abbreviations

%	percent
°C	degrees Celsius
×g	gravity
µg	microgram
µl	microlitre
µm	micrometre
µM	micromolar
ALT	alanine aminotransferase
bp	base pair
BSA	bovine serum albumin
cccDNA	covalently closed circular DNA
CHB	chronic Hepatitis B
ChIP	chromatin immunoprecipitation
cm	centimetre
Co-IP	co-immunoprecipitation
DLR	dual-luciferase reporter
DMEM	Dulbecco's Modified Eagle Medium
DMSO	dimethyl sulfoxide
DNA	deoxyribonucleic acid
dsRNA	double-stranded RNA
E. coli	*Escherichia coli*
ECL	enhanced chemiluminescence
eGFP	enhanced green fluorescent protein
EMSA	electrophoretic mobility shift assay
EDTA	ethylenediaminetetraacetic acid
EGTA	ethylene glycol-bis-N,N,N′,N′-tetraacetic acid
ER	endoplasmic reticulum
ERK	extracellular signal-related kinase
ES	enrichment score
FBS	fetal bovine serum
FDR	false discovery rate

FFPE	formalin-fixed paraffin-embedded
FITC	fluorescein isothiocyanate
GEO	Gene Expression Omnibus
GSEA	gene set enrichment analysis
HBV	hepatitis B virus
HBcAg	HBV core antigen
HBeAg	HBV e antigen
HBx	HBV x protein
HBsAg	HBV surface antigen
HCC	hepatocellular carcinoma
HCV	hepatitis C virus
HE	hematoxylin and eosin
HEPES	4-(2-Hydroxyethl) piperazine-1-ethanesulfonic acid
Hpo	Hippo
HRP	horseradish peroxidase
IHC	immunohistochemistry
ICC	immunocytochemistry
IF	immunofluorescence
IFN	interferon
IgM	immunoglobulin M
i.p.	intraperitoneal
i.v.	intravenous
IRAK4	IL1 receptor-associated kinase 4
IRFs	IFN-regulatory factors
ISG	IFN-stimulated gene
kDa	kilodalton
KEGG	Kyoto Encyclopedia of Genes and Genomes
LATS1/2	large tumour suppressor 1/2
LPS	lipopolysaccharides
MEK	mitogen-activated protein kinase
ml	mililitre
mM	micromolar
MOB1A/B	MOB kinase activator 1A/B

MOI	multiplicity of infection
mRFP	monomeric red fluorescent protein
mRNA	messenger ribonucleic acid
Mats	Mob as tumour suppressor
MST1/2	Sterile 20-like kinase 1/2
MyD88	myeloid differentiation primary response protein 88
NA	nucleoside analogue
NES	normalised enrichment score
NF-κB	nuclear factor Kappa B
ng	nanogram
NTCP	sodium taurocolate cotransporting polypeptide
ORF	open reading frame
Pam3CSK4	Pam3CysSerLys4
PBS	phosphate buffered saline
PBMC	peripheral blood mononuclear cells
PEG	polyethylene glycol
PERK	PKR-like ER kinase
PMH	primary murine hepatocyte
PHH	primary human hepatocyte
PP2A	protein phosphatase 2A
PPRs	pattern recognition receptors
qPCR	quantitative real-time PCR
rcDNA	relaxed circular DNA
RIG-I	retinoic acid-inducible gene I
RLRs	RIG-I-like receptors
RNA	ribonucleic acid
RPMI	Roswell Park Memorial Institute medium
SAV	Salvador
SAV1	Salvador homolog 1
Sd	Scalloped
SDS	sodium dodecyl sulfate
shRNAs	small-hairpin RNAs
siRNAs	small-interfering RNAs

ssRNA	single-stranded RNA
TAZ	transcriptional coactivator with PDZ-binding motif
TBE	tris/borate/EDTA
TEAD1-4	TEA DNA-binding proteins 1-4
tg	transgenic
TLR	toll-like receptor
TNF	tumour necrosis factor
UPR	unfolded protein response
V	voltage
WB	western blot
WHO	World Health Organization
WT	wild type
Wts	Warts
YAP	Yes-associated protein
Yki	Yorkie

Figures

Tables

1. Introduction

1.1 Hepatitis B virus

Hepatitis B virus (HBV) is a partially double-stranded, circular, DNA virus, belonging to *Hepadnaviridae* family, in the *Orthohepadnavirus* genus[1,2]. HBV causes the hepatitis B disease in humans and non-human primates[3]. The virus particle consists of an external lipid bilayer and an internal, protein-based nucleocapsid[4]. HBV surface antigen (HBsAg), which includes small, medium, and large isoforms, is a transmembrane protein anchored in the lipid bilayer[5]. The viral genome and DNA polymerase both are enclosed in the nucleocapsid[6]. The HBV virion (Dane particle) features a diameter of approximately 42 nm[7], but pleomorphic forms exist, including filamentous and spherical bodies without nucleocapsids[8], and up to 90% of secreted particles are empty[9]. These filamentous and spherical bodies are not infectious and are produced in excess during the HBV life cycle[10]. The HBV genome consists of a partial, double-stranded, circular DNA, and the viral DNA polymerase attaches to the end of the full-length strand[11]. The genome ranges from 3020–3320 nucleotides long, for the full-length strand, whereas the short-length strand ranges from 1700–2800 nucleotides long, depending on the HBV genotype[12]. After HBV enters hepatocytes, by binding to the cell-surface receptor sodium taurocholate cotransporting polypeptide (NTCP), viral DNA is immediately translocated into the nucleus[13]. Subsequently, the partial, double-strand DNA is completed by cellular DNA polymerases, using the sense strand as a template, resulting in the formation of a covalently closed, circular DNA (cccDNA) in the nucleus[14]. The viral genes are transcribed by cellular RNA polymerase II, based on the cccDNA template. The HBV genome contains four overlapping open reading frames (ORFs), which encode HBsAg, the core protein (HBcAg), the DNA polymerase, and the HBx protein[14]. The HBsAg gene contains three in-frame start codons (ATG) that divide the gene into *preS1*, *preS2,* and *S* sections. Correspondingly, three different-sized polypeptides, referred to as large surface protein (*preS1*+*preS2*+*S*), medium surface protein (*preS2*+*S*), and small surface protein (*S*), can be produced (Figure 1). Nucleocapsids,

containing newly synthesised, partial, double-stranded DNAs, are released from hepatocytes as new virions (Figure 2) or are recycled to the nucleus, to replenish the cccDNA pool.

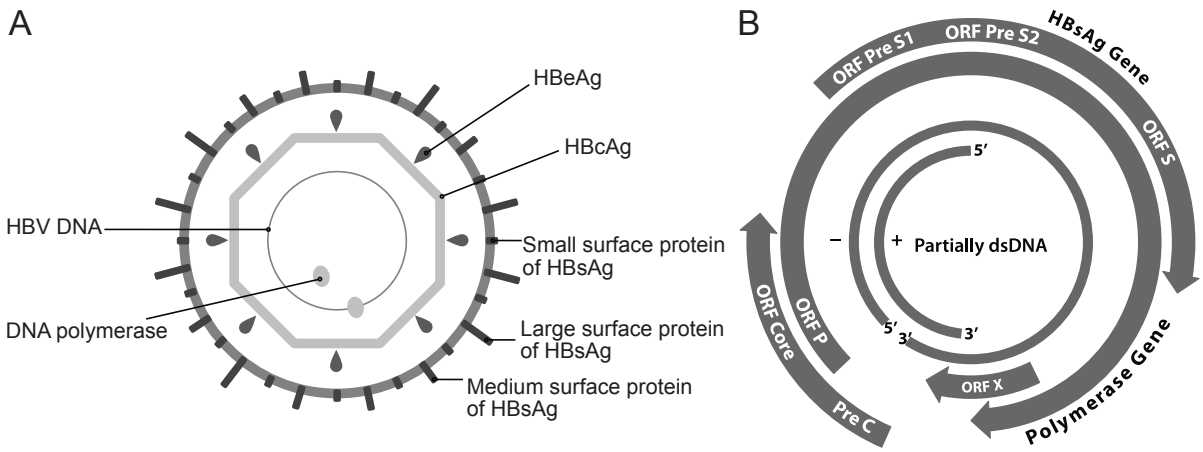

Figure 1: Schematic representation of the HBV virion and the HBV genome.
A. Schematic representation of the HBV particle, with the three envelope proteins (Small, Medium and Large surface protein of HBsAg), the core protein (HBcAg), e protein (HBeAg), partial, double-stranded DNA (HBV DNA), and DNA polymerase. **B**. The HBV genome. The bold outer lines represent the different classes of transcripts. The inner partial circles represent the HBV genome. The four major open-reading frames (ORFs) are indicated on the line. The core gene encodes the capsid protein. ORF P encodes the viral polymerase. ORF X encodes X protein. The three envelope proteins are encoded by a single ORF, with three in-frame start codons.

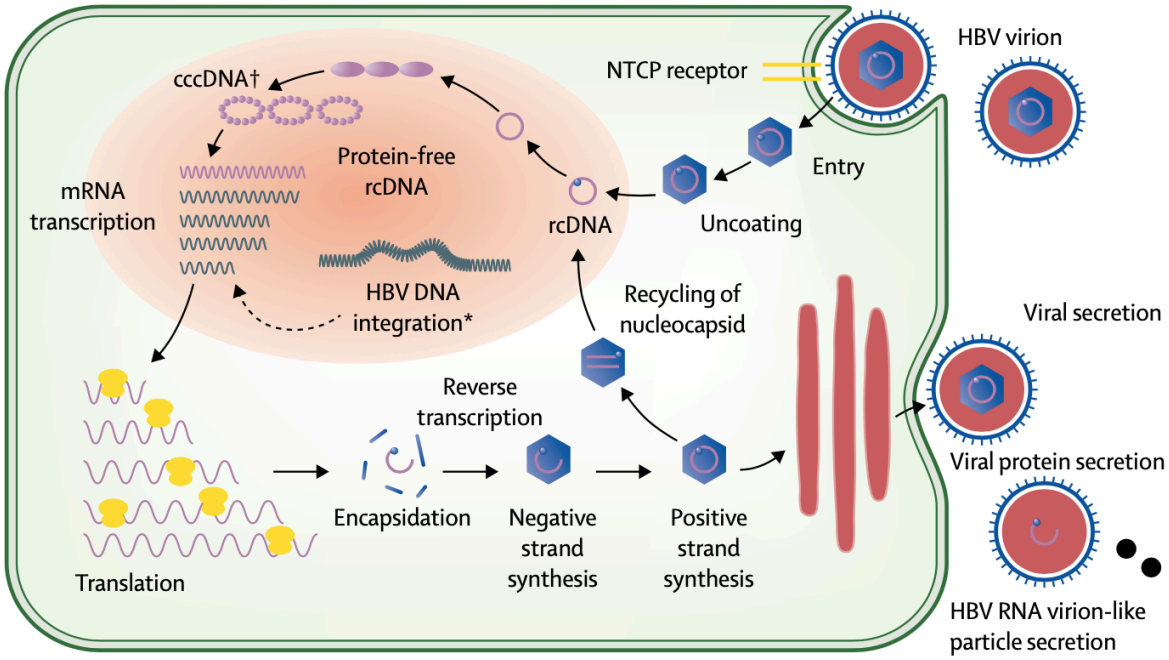

Figure 2. The life cycle of HBV.

After viral entry, the relaxed circular DNA (rcDNA) is delivered into the nucleus and converted into fully double-stranded DNA, which is converted by ligation into covalently closed circular DNA (cccDNA), which represents the stable form of HBV DNA and is responsible for its persistence in infected hepatocytes and transmission to progeny cells. The HBV genome contains four overlapping, frame-shifted, open reading frames, which support the pregenomic RNA synthesis of the core protein and HBV polymerase, and are transcribed into mRNAs that produce HBeAg, large, medium, and small HBsAg, and X protein. Nucleocapsids, containing newly formed rcDNAs, are then released from the hepatocyte as new virions or are recycled to the nucleus to replenish the cccDNA pool. cccDNA: covalently closed circular DNA; HBV: hepatitis B virus; NTCP: sodium taurocholate cotransporting polypeptide; rcDNA: relaxed circular DNA; *Integrated HBV DNA sequences can produce HBsAg and generate mutant viral proteins that play roles in hepatocarcinogenesis. †cccDNA is the stable form of intrahepatic HBV DNA, responsible for the persistence of HBV. Adopted from Steo, WK. *et al. Lancet* 2018; 392: 2313-24.

1.1.1 HBV genotypes and their global distributions

HBV can be divided into nine genotypes (A to I), which differ in more than 7.5% of their nucleotide sequences and can be further subdivided into sub-genotypes, with nucleotide divergence greater than 4%[15,16]. Genotype A is widespread in Northern Europe, Western Africa, and sub-Saharan Africa[17-19]. Genotypes B and C are common in Asia[20]. Genotype D is dominant in Europe, Africa, Mediterranean countries, and India[16,21,22]. Genotype E is localised in sub-Saharan Africa[23-25], and

genotypes F and H are restricted to Central and South America[24,25]. Genotype G has been reported in France, Germany, Japan, and the United States[24-27]. Genotypes I and J were discovered recently. Genotype I was first described in 2008 and was considered as a recombination of genotypes A, C and G. Phylogenetic analysis revealed that the genotype J is rather gibbon than human HBV, and may result from recombination with human genotype C. Hence, the acceptance of the notation of genotypes I and J is not universal[28]. Genotypes A-D, F, and I can be further subdivided into at least 35 sub-genotypes[15] (Figure 3).

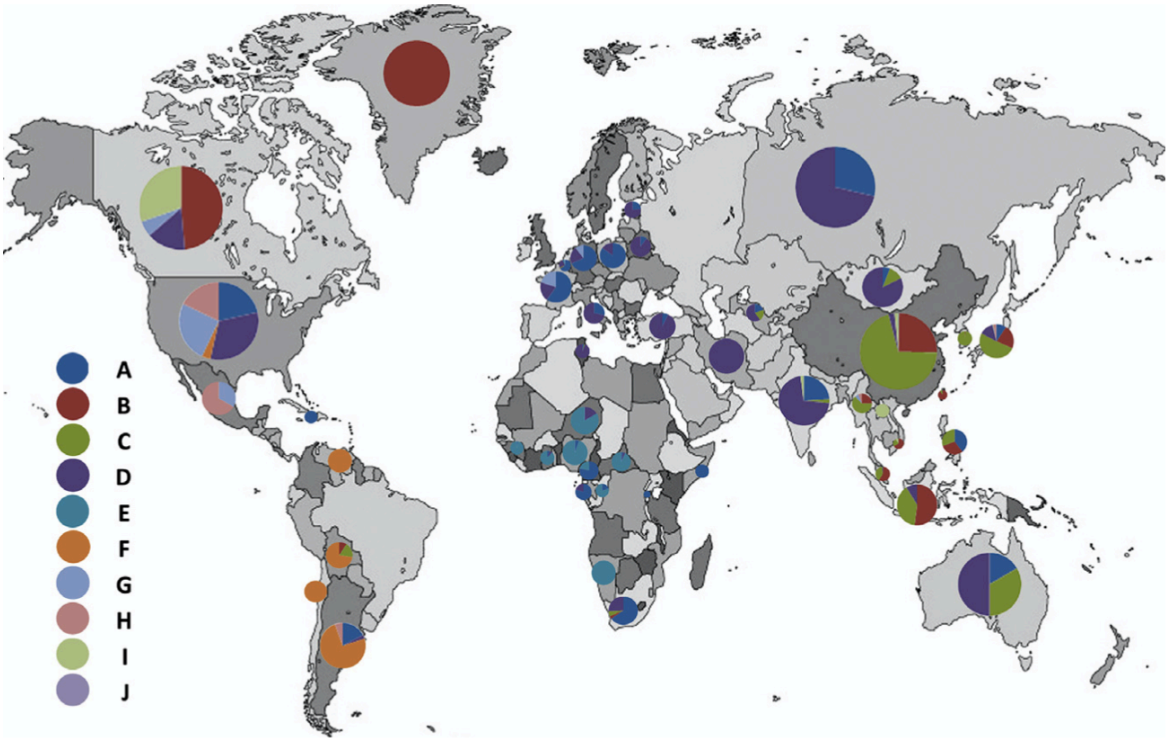

Figure 3. Geographic distribution of the various HBV genotypes.
The HBV genotyping data illustrates that the different HBV genotypes may have different geographic distributions. Only those countries/regions with more than five, full-length genome sequences available were included. This dataset included 46 countries/regions and 3,179 full-length genome sequences. This geographic distribution of HBV genotypes may not represent the actual seroprevalence of HBV in any country/region, due to the potential for sampling errors and the bias of including only whole-genome analyses. In addition, the size of each circle is not representative of the prevalence of HBV infection or the burden of disease for each specified geographic region. Adopted from Shi *et al*. *Infect Genet Evol* 2013; 16: 355-361.

1.1.2 HBV infection

HBV infections represent serious threats to human health and can develop into lifelong, chronic infections. Without antiviral interference, chronically infected individuals are at high risk of developing liver fibrosis, cirrhosis, and hepatocellular carcinoma (HCC)[29-32]. Globally, approximately 2 billion people have been infected with HBV, including more than 290 million chronic HBV infections[33]. In adults, HBV is especially prevalent in the African Region and the Western Pacific Region, according to the World Health Organization (WHO) Region division[34,35]. Vaccination programs against HBV have reduced the numbers of new infections in children, worldwide; however, the prevalence of HBV infections in children remains high (3%) in Africa[36-38].

Hepatitis B cannot be distinguished from other forms of virus-induced hepatitis by clinical examinations alone, such as ultrasounds, computed tomography scans, and magnetic resonance imaging. Therefore, laboratory tests are essential for the diagnosis of hepatitis B, such as blood tests to identify the presence of viral DNA and antigens and antibodies against HBV. HBV infections can result in either acute infections or chronic infections, which can be distinguished by monitoring the levels of HBV-DNA, HBsAg, HBeAg, antibodies against HBc, and alanine aminotransferase (ALT) in the blood (Figure 4)[30,39,40]. The risk of developing a chronic HBV infection has been directly associated with the age at which a person experiences a primary HBV infection. A primary infection at a younger age is associated with a higher risk of developing chronic hepatitis B (CHB). More than 90% of infected new-borns develop CHB[41], and up to 50% of 1- to 5-year-old infected children develop CHB[42]. In contrast, no more than 5%-10% of healthy adults (19 years and older) develop CHB after primary infection[43].

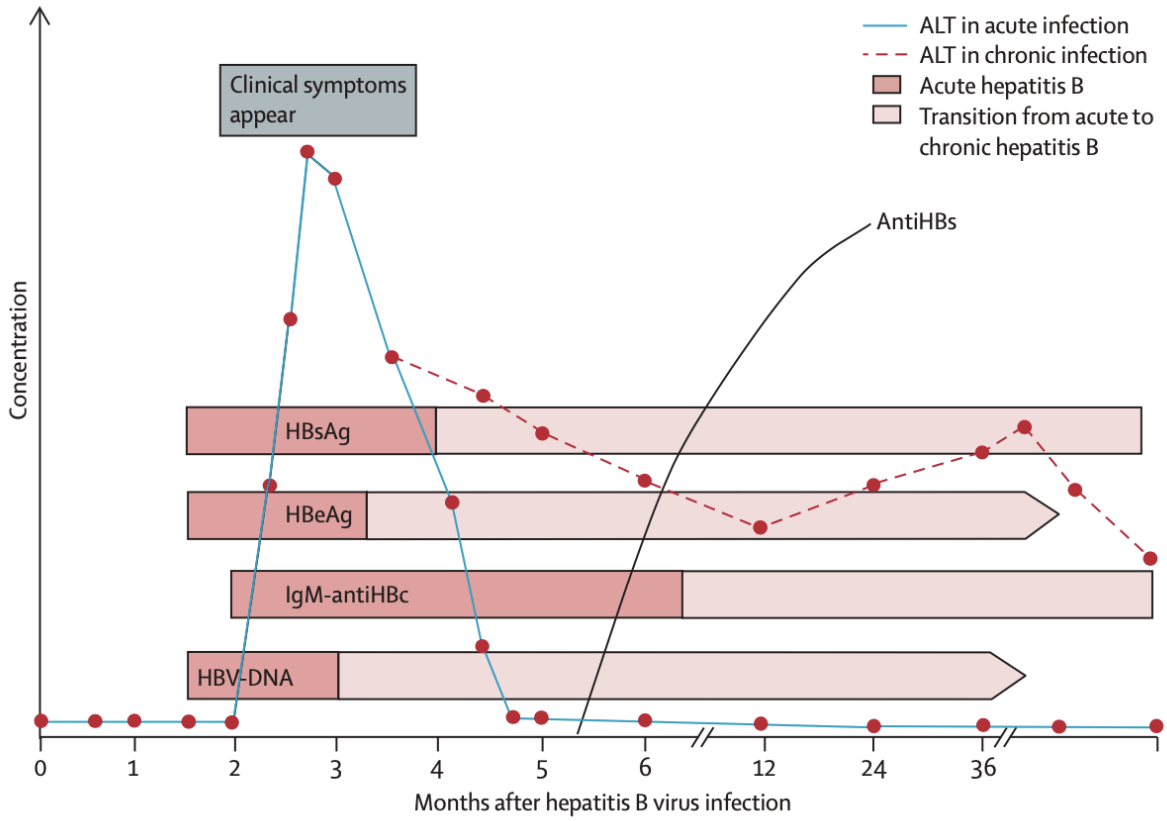

Figure 4. Serological and clinical changes after acute HBV infection.
Shaded bars indicate the duration of seropositivity in self-limited acute hepatitis B infections. Pointed bars indicate that HBV-DNA and HBeAg can become seronegative during chronic infections. Only IgG anti-HBc is detectable after the resolution of acute hepatitis or during chronic infection. Adopted from *Liaw* et al. *Lancet*. 2009; 373: 582-92

Acute HBV infection is characterised by the presence of HBsAg and antibodies against HBc (IgM type). HBcAg is encoded by the *preC* gene and is later processed in the endoplasmic reticulum (ER) to produce hepatitis B e antigen (HBeAg)[44]. HBeAg and HBcAg are encoded by the same open-reading frame. HBcAg forms the nucleocapsid, whereas HBeAg is secreted and accumulates in the serum, as an immunologically distinct, soluble antigen. During the acute stage of infection, patients also present with high levels of serological HBeAg[45] (Figure 4), which indicates a high level of HBV replication and the high infectious risk posed by the blood and body fluids of these patients. Approximate 90%-95% of HBV-infected adults do not progress to the chronic phase and instead, recover naturally[46]. Adaptive immunity has generally been recognised to be a crucial player in the clearance of HBV

infection. Adaptive immunity is comprised of a complex web of effector cell types[47]. CD4 T-cells are robust producers of cytokines, which are required for the efficient development of effector CD8 cytotoxic T-lymphocytes and B-cell antibody production[47]. CD8 T-cells eliminate HBV-infected hepatocytes, through cytolytic and non-cytolytic mechanisms, to reduce the levels of circulating virus[48], whereas B-cell antibody production neutralises free viral particles and prevents viral reinfection[49]. These antiviral immune responses are induced in adults after acute HBV infection, leading to the elimination of HBV. However, in individuals with weak immune systems or underlying medical immune suppression, HBV replication and reproduction are allowed to persist in the liver, eventually resulting in chronic infection[45,46].

Chronic HBV infection is characterised by the persistence of HBsAg, which can be detected in the serum for at least six months. The natural history and disease course of chronic HBV infection involve dynamic interactions between HBV and the host immune system[45], and the immune response can vary widely among individuals. Immune cell reactivity is robust in 90%-95% adults, whereas a small proportion of adults exhibit a weak immune response in response to HBV particles. Without antiviral therapy, a substantial proportion of infected patients will develop fibrosis, cirrhosis, and hepatocellular carcinoma (HCC), whereas others experience a lifelong, quiescent disease. Currently, the different phases of chronic HBV infection are characterised according to the kinetics of serum HBV DNA, HBeAg, HBsAg, and ALT[50] (Figure 5). The chronic HBV infection can be divided into HBeAg-positive, HBeAg-negative and HBsAg-negative phases according to the serological persistence of HBeAg and HBsAg. The HBeAg-positive and HBeAg-negative phases can be both subdivided into chronic infection and chronic hepatitis phases. During the chronic infection (HBeAg-positive) phase, also known as the immune-tolerant phase, high levels of serum HBV DNA are detectable, accompanied by normal serum ALT levels and near-normal liver histology[30,50]. The chronic hepatitis (HBeAg-positive) phase, also known as the immune-clearance phase, features immune-mediated liver necroinflammation, fibrosis, and fluctuating serum ALT concentrations[30]. HBeAg

disappearance and anti-HBe antibody appearance both occur at the end of this phase. In the HBeAg-negative chronic phase, also known as the inactive-carrier stage[50], ALT concentrations return to the normal range and HBV DNA levels fall below 2000 IU/ml[51]. A proportion of HBeAg-negative chronic hepatitis patients are characterised by fluctuations in serum HBV DNA levels and ALT concentrations[50]. A small proportion of HBeAg-negative chronic hepatitis patients can achieve HBsAg seroclearance naturally[52] (known as functionally cured HBV infection), although intrahepatic HBV maintains low levels of replication and transcription in these patients due to the continued presence of cccDNA and integrated viral DNA[53].

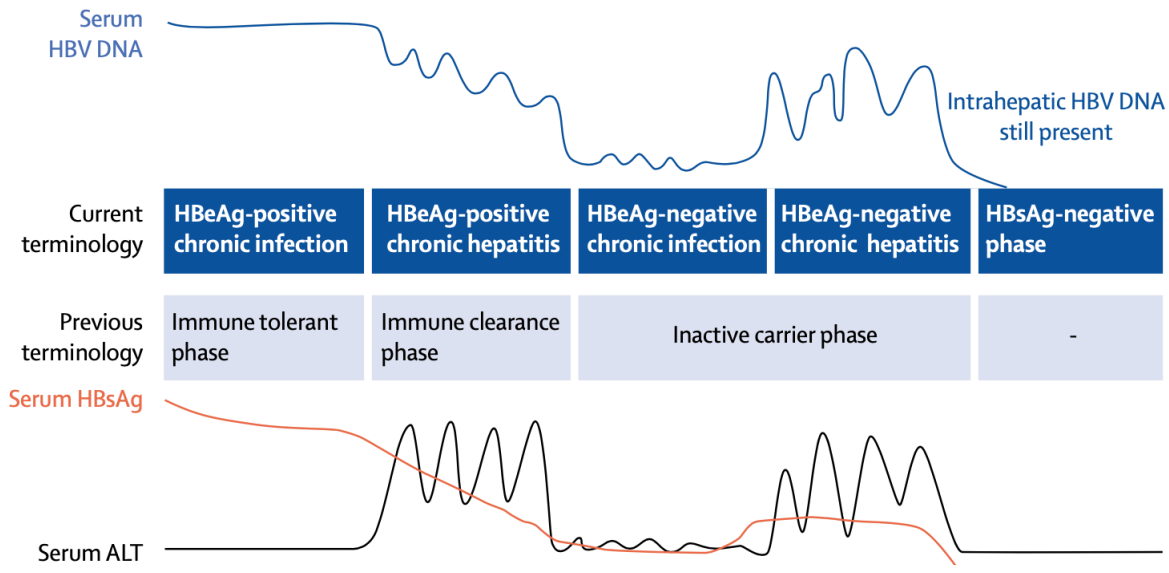

Figure 5. Different phases of chronic HBV infection, according to the kinetics of serum HBV DNA, HBsAg, and ALT.

The natural history and disease course of chronic HBV infection involve dynamic interactions between the virus and the host immune responses. Different phases of chronic HBV infection have been described, with changing denominations over time, and differing biochemical and virological profiles. ALT: alanine aminotransferase; HBV: hepatitis B virus. Adopted from Steo, W. K. *et al*. *Lancet* 2018; 392: 2313–24

1.2 HBV infection and immune defence

In high-prevalence areas, HBV is primarily spread through mother-to-child transmission[54]. In addition, HBV can also spread by exposure to infected blood and

bodily fluids. Sexual transmission can also occur when people engage in sex without proper protection[55,56]. HBV can survive outside of the body for at least seven days[57,58]. During this time, unvaccinated individuals are vulnerable to HBV infection if the virus enters their bodies. Most individuals do not present with any symptoms immediately following infection. However, some individuals suffer from acute illness, characterised by jaundice, dark urine, extreme fatigue, vomiting, nausea, and abdominal pain, which can last for several weeks. Even worse, a small subset of individuals develop severe hepatitis, which might lead to death[56,59-61]. The immune response largely determines viral clearance and disease pathogenesis following HBV infection. After HBV enters hepatocytes through the NTCP receptor, the virus begins to replicate, without causing direct cell damage[62,63]. Commonly, the host immune system is able to monitor and control HBV spread and infection by producing inflammatory factors, CD4 and CD8 T-cells, and B-cells, which are responsible for causing cytotoxic liver pathologies[64,65]. However, HBV acts as a stealth virus, often evading the innate immune response. The virus replicates without inducing intrahepatic interferon (IFN) or IFN-stimulated gene (ISG) responses[66-70]. Similarly, no cytokine induction can be detected in the serum of human patients with acute HBV infections[71,72]. Although some studies, examining *in vitro* models, have suggested that early HBV exposure may induce a slight innate immune response, these studies have been hampered by a lack of optimal model systems[73,74]. Recently, Cheng *et al.* and Mutz *et al.* developed new *in vitro* HBV infection models, which revealed that HBV infection does not trigger rapid, innate, immune responses[70,75,76]. Studies have suggested that HBV acts as a stealth virus, efficiently spreading throughout the liver, without activating the innate immune system[66,77].

1.2.1 Innate immune signals in acute and chronic HBV infection

The innate immune system is the first-line host defence against various infections, consisting of cell-surface and intracellular pattern recognition receptors (PRRs), which include toll-like receptors (TLRs), cytoplasmic retinoic acid-inducible gene I (RIG-I)-like receptors (RLRs), cytosolic DNA sensors, and nucleotide-binding

oligomerisation domain (NOD)-like receptors. Innate and adaptive immunity perform different tasks during the body's defence. TLRs are responsible for recognising pathogens when they encounter components associated with bacteria, viruses, parasites or fungi[78,79]. Although TLRs are critical for immune defence, the dysregulation or suppression of TLR signalling has been strongly associated with HBV infections and the pathogenesis of liver inflammation[80,81].

In humans, TLR1, TLR2, TLR4, TLR5, and TLR6 are type I transmembrane proteins, with ectodomains[82], whereas TLR3, TLR7/8, and TLR9 are receptors that localise to the endolysosome and are responsible for recognising double-stranded RNA (dsRNA), single-stranded RNA (ssRNA), and DNA[83,84]. TLR1/2 recognises triacyl lipoprotein, TLR3 recognises dsRNA, TLR4 recognises lipopolysaccharides (LPS), TLR5 recognises flagellin, TLR6 recognises diacyl lipoprotein, TLR7/8 recognises ssRNA, and TLR9 recognises CpG-DNA[85]; after recognition, TLRs rapidly activate downstream adaptors, such as nuclear factor-kappa b (NF-κB) and IFN-regulatory factors (IRFs), producing inflammatory cytokines and type I and III IFNs for the host defence[86-88]. In the past decades, scientists have insisted that HBV acts as a stealth virus because PRRs do not appear to recognise HBV particles and no cytokine release could be detected in response to HBV infection. However, our recent work demonstrated that HBV particles could be recognised by TLR2 in primary human hepatocytes (PHHs), following activation of NF-κB after 1-2 hours post exposure[89]. A recent study also demonstrated that HBV exposure in PHHs was able to induce a rapid, innate immune response through the NF-κB signalling pathway[90].

During acute infections, investigations have shown that HBV induces a negligible activation of IFN or ISGs, in chimpanzees and human patients[91,92]. However, several recent studies, utilising newly developed experimental systems, have suggested that host PRRs may recognise HBV particles and mediate the production of cytokines to limit HBV replication[93]. Therefore, the specific mechanisms underlying HBV

recognition and PRR signalling remain poorly understood and further exploration of these processes is urgently needed.

Immune responses to chronic HBV infections have been investigated for decades; however, conflicting results continue to be reported. Several studies have indicated that TLR function and expression are impaired in hepatocytes, nonparenchymal cells, and peripheral immune cells during chronic HBV infections[94-96]. Furthermore, HBeAg has been suggested to contribute to impaired TLR2 expression and the induction of tumour necrosis factor (TNF) in the HepG2 cell line[97]. Similarly, serum HBsAg levels have been correlated with impaired TLR2 expression and cytokine production in peripheral blood mononuclear cells (PBMCs) derived from CHB patients[94]. These studies suggested the existence of a complicated interaction between HBV and TLRs. Understanding these interactions is urgently necessary and critical for the clinical application of TLR agonists as an immunotherapeutic treatment in CHB patients.

1.2.2 Hippo signalling pathway in the innate immune response

The Hippo signalling pathway controls tissue growth, which is critical for the maintenance of normal organ size[98,99]. This pathway was originally discovered in *Drosophila* and is relatively well-conserved in mammals. Dysfunction of Hippo pathway components has been linked to various cancers, including HCC[100,101], breast cancer[102,103], thoracic cancer[104-106], genitourinary cancer[107,108], gynaecologic cancer[109,110], skin cancer[111,112], bone cancer[113,114] and brain cancer[115,116]. The core components of the mammalian Hippo pathway include sterile 20-like kinase 1/2 (MST1/2), Salvador homolog 1 (SAV1/WW45), large tumour suppressor 1/2 (LATS1/2), MOB kinase activator 1A/B (MOB1A/B), Yes-associated protein (YAP), transcriptional coactivator with PDZ-binding motif (TAZ), and TEA DNA-binding proteins (TEAD1-4). The corresponding proteins in *Drosophila* are Hippo (Hpo), Salvador (Sav), Warts (Wts), Mob as tumour suppressor (Mats), Yorkie (Yki), Scalloped (Sd)[117-119]. MST1/2, SAV1, LATS1/2, and MOB1A-B are upstream factors of YAP and TEAD1-4, and their phosphorylation states are important for Hippo

activation and YAP nuclear translocation[117-119]. Normally, the dynamic equilibrium of phosphorylated YAP is controlled by upstream core components; however, when phosphorylation becomes inhibited, YAP accumulates in the nucleus, where it forms a transcription factor complex with its nuclear partner, TEAD. The dephosphorylation of components in the Hippo signalling pathway has been associated with its inactivation[118].

In addition to crucial functions associated with cell growth, the Hippo signalling pathway also plays a key role in the innate immune response[120,121]. In *Drosophila*, Hpo is activated rapidly by the Toll receptor after the detection of gram-positive bacterial infections. Activated Hpo phosphorylates Yki, which inhibits the nuclear translocation of Yki, decreasing *Cactus* (*NFKBIA* orthologue) expression and activating the rapid innate immune response[99]. Similarly, TLRs recognise bacterial infections in mice and activate MST1/2, to control the production of reactive oxygen species and to clear the infection[122]. The Hippo signalling pathway not only functions in the antibacterial innate immune response but also in the antiviral innate immune response. The downstream effector YAP/TAZ directly interferes with and abolishes the virus-induced activation of TANK-binding kinase 1[123]. Thus, the Hippo signalling pathway plays a crucial role in the innate immune response.

1.3 Chronic HBV infection and hepatocarcinogenesis

Chronic HBV infection is a key risk factor for CHB, fibrosis, cirrhosis, and HCC. HBV infection increases the risk of hepatic cancer 15–20-fold and is responsible for approximately 78% cases of all HCC cases, worldwide[124,125]. The efficient suppression of HBV viremia and necroinflammation, through nucleos(t)ide analogue treatment, has been shown to decrease HCC incidence; however, HCC can occur even in the absence of HBV replication[126,127]. HBV genomic integration has been identified in 85%–90% of HBV-associated HCCs and usually occurs prior to HCC development. The integration of HBV DNA not only occurs in HCC patients but has also been identified in chronically infected patients, without tumorigenesis[128,129].

During the progression of CHB from the carrier state to HCC, mutations accumulate in the viral genome, associated with the *preS* region and the *X* gene region[130]. Whether the risk of HCC is affected by the viral status of chronic patients, such as the virus genotype, HBeAg serostatus, or the accumulation of mutations, remains poorly understood. Viral status has been suggested to play important roles not only in chronic liver diseases but also in the response to antiviral therapies[131-133]. Chronic HBV-associated HCC could be caused by a combination of generalised processes, including fibrosis and cirrhosis, however HCC also occur under cirrhosis-free condition, suggesting direct oncogenic effects associated with HBV infection.

1.3.1 Role of HBsAg in hepatocarcinogenesis

During chronic HBV infections, HBsAg continues to be produced and accumulates in hepatocytes, resulting in the typical histological finding of “ground glass” hepatocytes. HCC occurs more frequently among those patients who suffer from high levels of HBsAg than in those with a low level of HBsAg[126,127]. Furthermore, patients with residual HBsAg titres that exceed 1000 IU/ml are at an increased risk of HCC development[134].

The *HBsAg* gene encodes three proteins of different molecular weights: the approximately 43 kDa, full-length HBsAg large surface protein; the approximately 25 kDa medium surface protein, without the preS1 region; and the approximately 17 kDa small protein, which only contains the S region[135,136]. HCC has been reported to occur more frequently in *HBsAg* knock-in transgenic mice than in wild-type (WT) mice[124,136-138]. Numerous studies have addressed that the HBx protein (16 kDa) is a viral oncoprotein that causes liver cell transformations through its co-transcriptional activity, which exerts effects on cell cycle regulation and DNA repair[139-141]. HBsAg is another small protein expressed by HBV, and a previous study has shown that *HBsAg* knock-in transgenic mice develop HCCs 3 months earlier than *HBx* knock-in transgenic mice, which demonstrated that HBsAg also plays an important direct role in the development of HBV-related HCC, though an independent mechanism from

that associated with HBx[142]. The medium surface protein also has transactivation abilities and was shown to transactivate c-myc, c-fos, and cHaras[143,144]. Recently, preS2 was reported to contribute to the malignant transformation of the HepG2 HCC cell line by upregulating telomerase reverse transcriptase expression and inducing telomerase activation[145]. Furthermore, preS2 activates protein kinase C and leads to the phosphorylation of the preS domain, which activates the c-Raf-1/mitogen-activated protein kinase (MEK)/extracellular signal-related kinase (ERK) signal transduction cascade[146]. The truncated form of the *preS2/S* gene is commonly identified in integrated viral genomes[147]. Similarly, the accumulation of HBsAg, *preS1/2* mutants, and C-terminally truncated medium HBsAg protein are frequently identified in humans and function as oncogenic factors[146,148,149]. Large HBsAg proteins containing *preS* mutations can induce ER stress, mediating oxidative DNA damage and chromosome instability[150]. Therefore, the mechanisms through which HBsAg interacts with other factors to induce HCC has attracted widespread interest.

1.3.2 Hippo signalling pathway in hepatocarcinogenesis

The Hippo signalling pathway controls organ size, tissue regeneration, stem cell self-renewal, and tumour development. The Hippo cascade phosphorylates YAP, resulting in YAP cytoplasmic retention and proteolysis[151-153]. YAP activation has been described during liver regeneration and has been identified in several cancer types, including HCC[101] and hepatoblastoma[154]. Moreover, YAP nuclear translocation has been observed in approximately 65% of HCC cases[155]. In HCC, the core components of Hippo signalling are usually not mutated; however, upregulated YAP levels have been associated with gene amplification and post-transcriptional regulation[156]. An increase in YAP activity is an early event in hepatic tumorigenesis[157], and the overexpression of YAP in mice is sufficient to induce HCC[158]. Alterations in the Hippo signalling pathway, including the knockouts of *MST1/2*[101], *SAV1*[159,160], *LATS1/2*[161] and *NF2*[162,163] and the overexpression of YAP, in mouse hepatocytes, has been shown to induce dedifferentiation, which is a feature of hepatic progenitor cells. Increased proliferation might lead to the accumulation of oncogenic mutations in

hepatocytes[164]. Moreover, the inactivation of Hippo signalling pathway is a pivotal cause for HCC progression in humans[101]. Therefore, further investigations of the Hippo signalling pathway could provide additional information regarding its role in HCC.

1.4 Aims and objectives

Whether HBV induces the innate immune response has been debated for decades. Our previous study demonstrated that HBV particles are able to activate TLR2 signalling, to initiate the innate immune response in human primary hepatocytes[89]. However, the induction of the rapid, innate immune response by the TLR2-mediated regulation of downstream signalling is not well-understood. Thus, further studies examining the mechanisms through which HBV particles trigger TLR2-mediated downstream cascades and the regulation of the rapid, innate immune response must be performed to better understand how HBV-infection affects innate immunity and possibly to improve HBV therapeutic strategies.

The Gene Expression Omnibus (GEO) is a powerful, publicly accessible microarray database for use in bioinformatic analyses. Microarray datasets associated with acute HBV infection were reanalysed to identify eligible pathways associated with HBV infection, through gene set enrichment analysis (GSEA). Previously, scientists insisted that HBV acted as a stealth virus, capable of evading host immunity to maintain infective behaviour. However, increasingly, studies have demonstrated that HBV may be detected by TLRs at an early stage[89,90,165]. To validate the reanalysis results associated with the TLRs-NF-κB signalling pathways, primary murine hepatocytes were isolated and treated with TLR ligands (LPS, Pam3CSK4) and HBV particles, *in vitro*. To visualise changes in protein expression patterns in hepatocytes, immunocytochemistry was performed. Liu *et al.* recently reported that Hippo signalling plays a crucial role in innate immunity[99]. Based on preliminary results, a dual-luciferase reporter (DLR) assay and chromatin immunoprecipitation (ChIP) and electrophoretic mobility shift assay (EMSA) were combined to demonstrate the direct

regulation of the *Nfkbia* promoter by the YAP/TEAD4 transcription factor complex. To confirm this regulation, gain and loss of function experiments were performed by generating the stable overexpression or knockdown subclones. Finally, to verify all of these findings *in vivo*, Pam3CSK4 or LPS were administered in mice. Human primary hepatocytes were also isolated and exposed to HBV particles.

HCC develops more often in patients without high-level HBsAg. The accumulation of HBsAg results in “ground glass” hepatocytes, cell aneuploidy, and cell proliferation[136], which indicates the oncogenic potential of HBsAg. Similarly, HCC develops more frequently in HBsAg-transgenic mice[136], and our previous work showed that the oncogene BMI1 is upregulated in HBsAg-transgenic mice and could be increased by HBV exposure in primary murine hepatocytes, as well as in HCC patients with HBV infections[125]. However, the regulation of BMI1 expression during the development of HCC has not been well-studied. Thus, studies examining the effects of the HBsAg-induced increase in BMI1 and the associated development of HCC should be conducted.

Similarly, an HBsAg overexpression-associated microarray database was reanalysed to identify potential pathways associated with HBsAg overproduction. After associated pathways were selected, haematoxylin and eosin (HE) and immunohistochemical staining were performed on WT and HBsAg-transgenic mouse liver sections, to determine changes in key components belonging of the identified pathways. Based on our preliminary methodology, dual-luciferase reporter (DLR) assay and chromatin immunoprecipitation (ChIP) were performed to determine the direct regulation of the *Bmi1* promoter by the YAP/TEAD4 transcription factor complex. Because BMI1 is associated with the cell cycle, DNA damage, and chromosomal instability, related factors were detected after developing a series of gain- and loss-of-function models associated with YAP and BMI1. Verteporfin, a YAP inhibitor, were administered to transgenic mice *in vivo,* to validate these findings.

The final aim of this thesis was to simulate an HBV infection-induced innate immune response, *in vitro*, to reveal the specific mechanisms through which HBV interacts with host immunity and to examine the specific mechanisms through which HBsAg regulates BMI1 expression and affects BMI1-mediated DNA damage, cell proliferation, chromosomal instability, and aneuploidy in HBsAg-transgenic mice.

2. Material and Methods

2.1 Material

2.1.1 Chemicals and reagents

Table 1: Chemicals and reagents

Chemical/reagents	Manufacturer
2-mercaptoethanol	Sigma, St.Louis, Missouri, USA
Agarose	Thermo Scientific, Vilnius, LT
Ampicillin, sodium salt	Sigma, Steinheim, Germany
Acrylamide	Sigma-Aldrich, Darmstadt, Germany
Bovine serum albumin (BSA)	Roth, Karlsruhe, Germany
C29	MedChemExpress, Monmouth Junction, New Jersey, USA
Canada balsam	Sigma-Aldrich, Darmstadt, Germany
Calcium chloride ($CaCl_2$)	Fluka, Neu-Ulm, Germany
Collagen I, Rat Tail	Corning, Bedford, MA, USA
Collagenase Type IV	Worthington-biochem, Lakewood, NJ, USA
Chloroform	Sigma-Aldrich, Darmstadt, Germany
Dimethyl sulfoxide (DMSO)	Sigma-Aldrich, Darmstadt, Germany
dNTPs (10 mM)	Sigma-Aldrich, Darmstadt, Germany
Dulbecco's Modified Eagle Medium (DMEM)	Gibco, Paisley, UK
DMEM/F12(1:1) medium	PAN-Biotech, Aidenbach, Germany
Dulbecco's Phosphate Buffered Saline (DPBS)	Gibco, Paisley, UK
Ethylenediaminetetraacetic acid (EDTA)	Sigma-Aldrich, Darmstadt, Germany
Ethylene glycol-bis(β-aminoethyl ether)-N,N,N′,N′-tetraacetic acid (EGTA)	Sigma-Aldrich, Darmstadt, Germany
Ethanol	AppliChem, Darmstadt, Germany

ECL solution	Millipore, Darmstadt, Germany
FastStart Universal SYBR Green Master (Rox)	Roche, Basel, Switzerland
Fetal bovine serum (FBS)	Millipore, Darmstadt, Germany
Fluoroshield™ with DAPI	Sigma-Aldrich, Darmstadt, Germany
FuGENE® HD Transfection Reagent	Promega, Madison, Wisconsin, USA
GelRed nucleic acid gel stain	Biotium, Fremont, California, USA
GeneRuler 1 kb DNA Ladder	Fermentas, Vilnius, Lithuania
Glutathione Sepharose 4B	GE Healthcare, Uppsala, Sweden
Glycerol	Sigma-Aldrich, Darmstadt, Germany
Glycin	Roth, Karlsruhe, Germany
Glycose	Sigma Cell Culture, St. Louis, MD, USA
Halt™ Protease Inhibitor Cocktail (100×)	Thermo Scientific, Rockford, IL, USA
HEPES Buffer Solution (1 M)	Merck, Darmstadt, Germany
HiPerFect Transfection Reagent	Qiagen, Hilden, Germany
Hoechst 33342	Sigma-Aldrich, Darmstadt, Germany
Hydrochloride (HCl)	Sigma-Aldrich, Darmstadt, Germany
Hydrogen peroxide solution	Sigma-Aldrich, Darmstadt, Germany
IPTG	Sigma-Aldrich, Darmstadt, Germany
Isopropanol	Sigma-Aldrich, Darmstadt, Germany
LA Taq® DNA Polymerase	Takara, Kusatsu, Japan
LB Broth	Sigma-Aldrich, Darmstadt, Germany
L-Glutathione reduced	Sigma-Aldrich, Darmstadt, Germany
L-Glutamine	Sigma-Aldrich, Darmstadt, Germany
Lipofectamine™ RNAiMAX Transfections reagent	Invitrogen, Vilnius, Lithuania
Lipofectamine™ LTX Reagent with PLUS™ reagent	Invitrogen, Vilnius, Lithuania
Magnesium chloride $MgCl_2$	Sigma-Aldrich, Darmstadt, Germany
Methanol	J.T.Baker, Netherland
Mouse Hepatocyte Medium	PRIMACYT, Schwerin, Germany
N,N′-Methylenebis(acrylamide)	Sigma-Aldrich, Darmstadt, Germany

Normal Donkey Serum	Millipore, Darmstadt, Germany
Non-fat milk powder	Roth, Karlsruhe, Germany
Opti-MEM™ I Reduced Serum Medium	Gibco, Paisley, UK
Paraformaldehyde	Sigma-Aldrich, Darmstadt, Germany
Phosphate-buffered formaldehyde solution 4.5 %, acid-free (pH 7)	Roth, Karlsruhe, Germany
PTC596	Selleckchem, Houston, TX, USA
QIAzol Lysis Reagent	Qiagen, Hilden, Germany
Recombinant Rnase Inhibitor	Takara, Kusatsu, Japan
Restriction endonucleases	Thermo Fisher, Waltham, MT, USA
Roti®-Mix PCR 3	Roth, Karlsruhe, Germany
Roth Hexanukleotid Random-Primer-Mix	Roth, Karlsruhe, Germany
Roth poly d(T)12-18 Primer	Roth, Karlsruhe, Germany
Rotiphorese® NF-Acrylamid/Bis-Lösung 30 % (29:1)	Roth, Karlsruhe, Germany
RPMI 1640 medium	Gibco, Paisley, UK
SMART® MMLV Reverse Transcriptase	Takara, Kusatsu, Japan
Sodium dodecyl sulfate	MP BIOMEDICALS, Eschwege, Germany
Sodium Chloride	AppliChem, Darmstadt, Germany
Sodium hydrogen carbonate	Merck, Darmstadt, Germany
Spongostan standard	ETHICON, Soeborg, Denmark
TBE 10×	Gibco, Paisley, UK
T4 DNA Ligase	Thermo Scientific, Hampton, NH, USA
TEV Protease	Sigma, St.Louis, Missouri, USA
Tissue Freezing Medium	Leica, Richmond, IL, USA
Trypan blue	Sigma-Aldrich, Darmstadt, Germany
Trypsin-EDTA solution (0.05%)	Gibco, Paisley, UK
Tween-20	Sigma-Aldrich, Darmstadt, Germany
Ultrapure LPS	Invivogen, San Diego, CA, USA

Vertepofin	Sigma-Aldrich, Darmstadt, Germany
XMU-MP-1	Selleckchem, Houston, TX, USA
Xylene substitute	Thermo Scientific, Hampton, NH, USA
Zeocin	Invivogen, San Diego, CA, USA

2.1.2 Buffers and solutions

Table 2: Buffers and solutions

Buffer/Solution	**Composition**
Blocking solution I for western blot	5% (w/v) non-fat milk powder in TBS-T
Blocking solution II for western blot	5% (w/v) BSA in TBS-T
10 mM Citrate buffer	2.94 g sodium citrate trisodium salt dihydrate in 1 Liter distilled water, pH6.0
1 mM EDTA buffer	0.372 g EDTA in 1 Liter distilled water, pH8.0
10× TBS	250 mM Tris, 1.5 M NaCl, pH7.4
TBS-T	0.1% Tween-20 in TBS
10× Tris-glycine SDS running (TGS) buffer	Dissolve 30 g of Tris base, 144 g of glycine, and 10 g of SDS in water.
1× TGS buffer	100 ml 10× TGS buffer in 1 Liter water
Aqueous electroblot transfer buffer	336 mM tris, 260 mM glycine, 140 mM tricine, and 2.5 mM EDTA
4% PFA buffer	4% (w/v) PFA in 0.1 M PBS, pH7.4
15% sucrose buffer	75 g “Rnase free” sucrose in 500 ml 0.1 M PBS, pH7.4. Mix and filter sterilize with a 0.45 µm filtration unit, store at 4°C
30% sucrose buffer	150 g “Rnase free” sucrose in 500 ml 0.1 M PBS, pH7.4. Mix and filter sterilize with a 0.45 µm filtration unit, store at 4°C
Permeabilization buffer for ICC	0.2% Triton-X-100, 0.2% BSA in PBS

staining	
Blocking buffer for ICC staining	0.02% Triton-X-100, 5% BSA in PBS
10% SDS	10 g SDS in 100 ml distilled water
1.5 M Tris, pH 8.8	181.65 g Tris base in 1 L diH_2O, pH8.8
0.5 M Tris, pH6.8	60.6 g Tris base in 1 L diH_2O, pH6.8
RIPA buffer	150 mM NaCl, 1% Nonidet P-40, 0.5% sodium deoxycholate, 0.1% SDS, 25 mM Tris supplemented with protease and/or phosphatase inhibitors
5× binding buffer (EMSA)	50 mM Tris-HCl (pH8.0), 750 mM KCl, 2.5 mM EDTA, 0.5% Triton-X-100, 62.5% glycerol (v/v), 1 mM DTT

2.1.3 Commercial kits

Table 3: Kits

Kit	**Manufacturer**
BCA kit	Thermo Scientific, Rockford, IL, USA
DNeasy Blood & Tissue kit	QIAGEN, Hilden, Germany
EZ ChIP kit	Millipore, Darmstadt, Germany
E.Z.N.A.® Gel Extraction Kit	Omega BIO-TEK, Norcross, GA, USA
DAB Substrate Kit, Peroxidase Kit	Vector, Burlingame, CA, USA
Direct IP	Thermo Scientific, Rockford, IL, USA
HA-tag IP	Thermo Scientific, Rockford, IL, USA
HE fast stain kit	Roth, Karlsruhe, Germany
KAPA Taq ReadyMix PCR Kit	Kapa Biosystems, Basel, Switzerland
Plasmid mini extraction kit	Omega BIO-TEK, Norcross, GA, USA
Plasmid Maxi extraction kit	QIAGEN, Hilden, Germany
Steady-Glo® Luciferase Assay System	Promega, Madison, Wisconsin, USA
Autofluorescence Quenching Kit	Vector, Burlingame, CA, USA
Dual-Luciferase® Reporter Assay System	Promega, Madison, Wisconsin, USA

ABC HRP Kit (Peroxidase, Mouse IgG)	Vector, Burlingame, CA, USA
ABC HRP Kit (Peroxidase, Rabbit IgG)	Vector, Burlingame, CA, USA

2.1.4 Laboratory equipment and instruments

Table 4: Equipment and instruments

Equipment/Instrument	**Manufacturer**
Autoclave, VX-150	Systec, Wettenberg, Germany
Bacteria shaking incubator	New Brunswick™ Innova®, Hamburg, Germany
CFX96 Touch Real-Time PCR Detection System	Bio-rad, Hercules, California, USA
SDS-page gel maker	Bio-rad, Hercules, California, USA
Mini-PROTEAN Tetra Vertical Electrophoresis Cell	Bio-rad, Hercules, California, USA
Mini-PROTEAN Tetra Handcast Systems	Bio-rad, Hercules, California, USA
NanoPhotometer	IMPLEN, Munich, Germany
Centrifuge 5910R	Eppendorf AG, Hamburg, Germany
Centrifuge 5424	Eppendorf AG, Hamburg, Germany
Centrifuge 5424R	Eppendorf AG, Hamburg, Germany
Concentrator plus	Eppendorf AG, Hamburg, Germany
CO2 incubator	Thermo Fisher, Waltham, MT, USA
CytoFLEX s	Beckman Coulter, Brea, California, USA
E-box VX2 Gel Documentation Imaging	Vilber, Collégien, France
Heidolph Reax 2 overhead shaker	Heidolph, Schwabach, Germany
Ice machine	Scotsman, Vernon Hills, IL, USA
IKA Magnetic Stirrers	IKA, Staufen, Germany
KERN 4200 EW Precision balance	KERN & SOHN GmbH, Balingen,

	Germany
KERN Analytical balance, 120-5DM	KERN & SOHN GmbH, Balingen, Germany
Laboratory dishwashing machine G7883	Miele, Gütersloh, Germany
Lab Heating and Drying Ovens	Thermo Fisher Scientific, Rockford, IL, USA
Microwave	Severin, Sundern, Germany
Milli-Q® Water Purification System	Merck, Darmstadt, Germany
pH-meter, HI2215	Hanna, Singapore
Pipetus	Hirschmann, Eberstadt, Germany
Pipet stepper	Eppendorf, Hamburg, Germany
Power supply, PowerPac	Bio-rad, Hercules, California, USA
SureCycler 8800 Thermal Cycler	Agilent, Santa Clara, California, USA
Ultrasonic homogenisers	BANDELIN electronic GmbH, Berlin, Germany
Zeiss Axio Observer.Z1 and Apotome	Zeiss, Jena, Germany
Olympus BX51, Upright epifluorescence microscope	Olympus, Shinjuku City, Tokyo, Japan
AMD EVOS fl Digital microscope, Inverted digital fluorescence microscope	Thermo Fisher, Waltham, Massachusetts, USA
Rocky 3D rotator	Boekel Scientific, Feasterville, PA, USA
Shaking incubator	Eppendorf, Hamburg, Germany
ADVANCED Fluorescence and ECL Imager	INTAS, Göttingen, Germany
Thermomixer	Eppendorf, Hamburg, Germany
Vortexer	Phoenix, Garbsen, Germany
Water bath	GFL, Burgwedel, Germany

2.1.5 Laboratory supplies and consumables

Table 5: Supplies and consumables

Supply/Consumable	Manufacturer
Cell scraper	TPP, Trasadingen, Switzerland
12 Well Chamber, glass slide, removable	Ibidi GmbH, Gräfelfing, Germany
8 Well Chamber, glass coverslip	Ibidi GmbH, Gräfelfing, Germany
Filter Cap Cell Culture flasks (25, 75 and 175 cm^2)	CELLSTAR, Kremsmünster, Austria
Nitril gloves	WRP, Sepang, Selangor, Malaysia
Filter bottle (500 ml)	TPP, Trasadingen, Switzerland
Glass Pasteur Pipettes	BRAND, Wertheim, Germany
Petri Dishes	CELLSTAR, Kremsmünster, Austria
Pipette tips (10/20, 20,100, 200, 1000 µl)	STARLAB, Hamburg, Germany
Pipette (5 ml, 10 ml, 25 ml, 50 ml)	CELLSTAR, Kremsmünster, Austria
PCR rubes	STARLAB, Hamburg, Germany
PCR plate	Bio-rad, Hercules, California, USA
Scalpels	Mediware, Wesel, Germany
Falcon tube (15 ml, 50 ml)	Sarstedt, Nümbrecht, Germany
Eppendorf tube (0.5 ml, 1.5 ml, 2 ml, 5 ml)	Eppendorf, Hamburg, Germany
Tissue culture dishes (10 cm)	CELLSTAR, Kremsmünster, Austria
Sterile cell strainer (100 µm)	BD Falcon, Erembodegem, Belglum
Sterile filter (0.2 µm, 0.45 µm)	Sartorius, Göttingen, Germany
Syringes (1 ml, 2 ml, 5 ml, 10 ml)	BD, Erembodegem, Belglum
Coverslip	Engelbrecht, Edermünde, Germany
Tissue culture plates (96, 48, 24, 12, 6-well plate)	CELLSTAR, Kremsmünster, Austria

2.1.6 Antibodies

Table 6: Antibodies

Antibody	Application	Dilution	Manufacturer
Anti-mouse β-actin, mouse	WB	1:2000 in 5%Milk	Cell Signalling, Danvers, MA, USA
Anti-mouse TEAD4, mouse	ChIP, WB	10µg per ChIP; 1:500 in 5%Milk	Abcam, Cambridge, UK
Anti-mouse MST1, rabbit	WB	1:1000 in 5%BSA	Cell Signalling, Danvers, MA, USA
Anti-mouse MST2, rabbit	WB	1:1000 in 5%BSA	Cell Signalling, Danvers, MA, USA
Anti-mouse p-MST1/2, rabbit	WB	1:1000 in 5%Milk	Cell Signalling, Danvers, MA, USA
Anti-mouse YAP, rabbit	WB, IHC, ICC	1:1000 in 5%BSA; 1:100 in PBS	Cell Signalling, Danvers, MA, USA
Anti-mouse p-YAP, rabbit	WB	1:1000 in 5%BSA	Cell Signalling, Danvers, MA, USA
Anti-mouse SAV1, rabbit	WB	1:1000 in 5%BSA	Cell Signalling, Danvers, MA, USA
Anti-mouse MOB1, rabbit	WB	1:1000 in 5%BSA	Cell Signalling, Danvers, MA, USA
Anti-mouse LATS1/2, rabbit	WB	1:1000 in 5%Milk	Abcam, Cambridge, UK
Anti-mouse BMI1, mouse	WB, IHC, ICC	1:1000 in 5%Milk or PBS	Abcam, Cambridge, UK
Anti-mouse IRAK1, rabbit	WB	1:1000 in 5%Milk	Cell Signalling, Danvers, MA, USA
Anti-mouse IRAK4, rabbit	WB	1:1000 in 5%Milk	Cell Signalling, Danvers, MA, USA
Anti-mouse MyD88, rabbit	WB	1:1000 in 5%Milk	Cell Signalling, Danvers, MA, USA
Anti-mouse TLR2, rabbit	WB	1:1000 in 5%Milk	Cell Signalling, Danvers, MA, USA

Anti-mouse TLR4, rabbit	WB	1:1000 in 5%Milk	Cell Signalling, Danvers, MA, USA
Anti-mouse IκBα, mouse	WB	1:200 in 5%Milk	Santa Cruz, Dallas, Texas, USA
Anti-mouse p-IκBα, rabbit	WB	1:1000 in 5%Milk	Cell Signalling, Danvers, MA, USA
Anti-mouse NF-κB, rabbit	WB, IHC, ICC	1:1000 in 5%BSA or PBS	Cell Signalling, Danvers, MA, USA
Anti-mouse p-NF-κB, rabbit	WB	1:1000 in 5%BSA	Cell Signalling, Danvers, MA, USA
Anti-mouse PP2A, rabbit	WB	1:1000 in 5%BSA	Cell Signalling, Danvers, MA, USA
Anti-mouse p-PP2A, rabbit	WB	1:1000 in 5%BSA	Cell Signalling, Danvers, MA, USA
Anti-HBsAg, rabbit	WB, IHC, ICC	1:1000 in 5%Milk	AVIVA system biology, San Diego, CA, USA
Anti-mouse Pericentrin, rabbit	ICC	1:1000 in PBS	Abcam, Cambridge, UK
Anti-mouse p16INK4a, rabbit	WB	1:500 in 5%Milk	Abcam, Cambridge, UK
Anti-mouse p19ARF, rat	WB	1:500 in 5%Milk	Abcam, Cambridge, UK
Anti-mouse p53, mouse	WB	1:1000 in 5%Milk	Santa Cruz, Dallas, Texas, USA
Anti-mouse Cyclin D1, mouse	WB, ICC	1:1000 in 5%Milk	Santa Cruz, Dallas, Texas, USA
Anti-mouse IgG-HRP	Secondary antibody	1:2000 in 5%Milk	Sigma-Aldrich, Saint Louis, MO, USA
Anti-mouse ki67, rabbit	IHC, ICC	1:1000 in 5%BSA	Abcam, Cambridge, UK
Anti-rabbit IgG-	Secondary	1:2000 in 5%Milk	Cell Signalling,

HRP	antibody		Danvers, MA, USA
Anti-mouse Caspase 3, rabbit	WB, ICC	1:1000 in 5%Milk; 1:1000 in PBS	Cell Signalling, Danvers, MA, USA
Anti-mouse pH2AX, rabbit	WB, ICC	1:500 in 5%BSA or PBS	Cell Signalling, Danvers, MA, USA
Donkey Anti-Rabbit IgG H&L (Alexa Fluor® 488)	IF	1:2000 in PBS	Abcam, Cambridge, UK
Donkey anti-Mouse IgG (H+L) Alexa Fluor 594	IF	1:500 in PBS	Invitrogen, Carlsbad, CA, USA
Donkey anti-Rabbit IgG (H+L) Alexa Fluor Plus 680	IF	1:200-1:2000 in PBS	Invitrogen, Carlsbad, CA, USA
Donkey anti-Rabbit IgG (H+L) Alexa Fluor 594	IF	1:1000 in PBS	Invitrogen, Carlsbad, CA, USA

WB: western blot; IHC: immunohistochemistry; ICC: immunocytochemistry; IF: immunofluorescence

2.1.7 Plasmids

Table 7: Plasmids

Plasmid	Description	Reference
pGL3-basic	Promoter reporter plasmid	Promega
pRL-TK	Reference reporter plasmid	Promega
pcDNA3.1	Expression plasmid	Promega
His-GST-TEV-pET(2G-T)	Expression plasmid	Addgene
peGFP	Expression plasmid	Takara

pmRFP	Expression plasmid	Takara
psiRNA-h7SK-GFPzeo	Knock down plasmid	Invivogen

The pcDNA3.1 vector merely overexpresses the gene of interest. The peGFP vector overexpresses the gene of interest as fusions to the N-terminus of eGFP. The pmRFP vector overexpresses the gene of interest as fusions to the C-terminus of RFP. The pET His6 GST TEV LIC cloning vector (2G-T) overexpresses the gene of interest as fusions to the N-terminus of His6-GST-TEV.

2.1.8 siRNA and shRNA sequences

The siRNAs were synthesised from GenePharm (Shanghai, China) with a 2'Ome modification and a TT at the end of sequence to prevent off-target immune induction. The shRNA target sequences were the same as those of the siRNAs. The shRNAs integrated into psiRNA-h7SK-GFPzeo were synthesised from Biomers (Ulm, Germany). To form the short-harpin structure of shRNAs, the 21 nucleotide gene-specific sequence was designed and synthesised in the backbone of forward oligo: ACCTC----------TCAAGAG----------TT (5'→3') and reverse oligo: CAAAAA----------CTCTTGA----------G (5'→3'). All siRNAs and shRNAs sequences information are given in Table 8.

Table 8: siRNA and shRNA sequences

siRNA	**Sequence (5'→3')**
siRNA Negative control	CAACAAGATGAAGAGCACCAATT
siYAP#1	CTGGTCAAAGATACTTCTTAATT
siYAP#2	GAAGCGCTGAGTTCCGAAATCTT
siTEAD4#1	GCTGAAACACTTACCCGAGAATT
siTEAD4#2	CCCTCTCTGTGAGTACATGATTT
siBMI1	TCAAATGATGTTGTTAGTAAATT
siSTK3#1	CCCATGATGGAACGAGAAATATT
siSTK3#2	CCTTCTTTCATGGACTACTTTTT
siSTK4#1	CCGTCTTTCCTTGAATACTTTTT

siSTK4#2	GCCCTCACGTAGTCAAGTATTTT
siMOB1a#1	GCTTGGATCTAAAGACAGATATT
siMOB1a#2	GAGGACCTCAATGAATGGATTTT
siMOB1b#1	GCTGGAAACAAATGCGACAAATT
siMOB1b#2	CTGGATGATGAGACATTATTTTT
siSAV1#1	GCACAAGAAGATTACAGATATTT
siSAV1#2	CTACATCTCTAGGGAATTTAATT
siLATS1#1	GCAACATTCAATTAACCGAAATT
siLATS1#2	TAGTCAATTCTTGGTACTTAATT
siLATS2#1	CGCAAGAATAGCAGAGATGAATT
siLATS2#2	CGCCTTCTATGAGTTCACCTTTT
shRNA	**Sequence (5'→3')**
Scramble	CAACAAGATGAAGAGCACCAA
shYAP	CTGGTCAAAGATACTTCTTAA
shTEAD4#1	GCTGAAACACTTACCCGAGAA
shTEAD4#2	CCCTCTCTGTGAGTACATGAT
shBMI1#1	GCAGATTGGATCGGAAAGTAA
shBMI1#2	CCAGCAAGTATTGTCCTATTT
shSTK3#1	CCCATGATGGAACGAGAAATA
shSTK3#2	CCTTCTTTCATGGACTACTTT
shSTK4#1	CCGTCTTTCCTTGAATACTTT
shSTK4#2	GCCCTCACGTAGTCAAGTATT
shLATS1#1	GCAACATTCAATTAACCGAAA
shLATS1#2	TAGTCAATTCTTGGTACTTAA
shLATS2#1	CGCAAGAATAGCAGAGATGAA
shLATS2#2	CGCCTTCTATGAGTTCACCTT

2.1.9 Bacteria strains

Table 9: Bacteria strains

Strain	Genotype	Manufacturer
BL21(DE3)	BNN93 *hflA150::Tn10* (Tet^R)	Novagen, Darmstadt, Germany
TOP10	F^- *mcr*A Δ*(mrr-hsd*RMS-*mcr*BC*)* *φ80lac*ZΔM15 Δ*lac*X74 *rec*A1	Invitrogen, Carlsbad, CA, USA
GT116	F^- *mcr*A Δ*(mrr-hsd*RMS-*mcr*BC*)* *φ*80*lac*ZM15 Δ*lac*X74 *rec*A1 *end*A1 Δ*sbc*C-*sbc*D	Invivogen, San Diego, CA, USA

BL21(DE3) competent *E. coli* was chosen for high level protein expression and purification. One Shot™ TOP10 chemically competent *E. coli* was chosen for plasmids preparation. LyoComp GT116 was used for shRNA plasmids preparation.

2.1.10 Primers

Table 10: Quantitative PCR primers

Gene	Sequence (5'→3')	Annealing Temp. (°C)
mActb forward	AAATCGTGCGTGACATCAAA	55
mActb reverse	CAAGAAGGAAGGCTGGAAAA	
mNfkbia forward	TCCTGCAGGCCACCAACTA	55
mNfkbia reverse	TCAGCACCCAAAGTCACCAA	
mCtgf forward	GTGTGCACTGCCAAAGATGGTGC	55
mCtgf reverse	GCACGTCCATGCTGCACAG	
hACTB forward	TCCCTGGAGAAGAGCTACGA	55
hACTB reverse	AGCACTGTGTTGGCGTACAG	
hYAP forward	GGTTGGGAGATGGCAAAGAC	55
hYAP reverse	GGGTCCTGCCATGTTGTTGT	
hNFKBIA forward	GAGACCTGGCCTTCCTCAACT	55

hNFKBIA reverse	TTCTGGCTGGTTGGTGATCA	
hCTGF forward	GGAGCGCCTGTTCCAAGAC	55
hCTGF reverse	CTGCAGGAGGCGTTGTCATT	

m, murine; h, human.

Expressions of murine *Il6, Il1β, Tnf* and human *IL6, IL1β*, *TNF* were detected by commercially available primer sets (QuantiTec Primer Assay, Qiagen; sequences are not given by the manufacturer).

Table 11: Chromatin immunoprecipitation primers

Gene	**Sequence (5'→3')**
Nfkbia-fragment1-forward	TTGCTCTGCTAGGCATTCACAA
Nfkbia-fragment1-reverse	CCGTATGGGAACCACATTTTTC
Nfkbia-fragment2-forward	TCAAAAAGTTCCCTGTGCATGA
Nfkbia-fragment2-reverse	CCAAGCCAGTCAGACTAGAAAAAGA
Bmi1-fragment1-forward	GGGAGACTCTTAAGCATCTGGATT
Bmi1-fragment1-reverse	TCACACACAAACTCCAAACAGAATG
Bmi1-fragment2-forward	GCCCGACTACACCGACACTAAT
Bmi1-fragment3-reverse	GTCACGTGCTCCCCTCATTC
Bmi1-fragment3-forward	CGCTCGGTGCCCATTG
Bmi1-fragment2-reverse	GCGGGCGGAAAAGACAA
neg-control-*Ctgf*-forward	CAGTGGAGATGCCAGGAGAAA
neg-control-*Ctgf*-reverse	CCCCGGTTACACTCCAAAAA
pos-control-*Ctgf*-forward	CTTCTTGGTGTTGTGCTGGAAAC
pos-control-*Ctgf*-reverse	GACCCCTTGACACTCCACATTC

neg, negative; pos, positive.

Table 12: Primers for construction of overexpression plasmids

Gene	**Sequence (5'→3')**	**Accession No.**
pcDNA3.1-m*Yap*-forward	GCTCTAGAATGGAGCCCGCGCAAC	NM_009534
pcDNA3.1-m*Yap*-reverse	GGGGTACCGCTCCCTGCAGCTCTATAACCAC	
peGFP-m*Yap*-forward	GAAGATCTATGGAGCCCGCGCAA	NM_009534

peGFP-m*Yap*-reverse	GGGGTACCAACCACGTGAGAAAG CTTTCT	
pcDNA3.1-m*Tead4*-forward	GCTCTAGAATTACCTCCAACGAGT GGAGCTC	NM_001080979
pcDNA3.1-m*Tead4*-reverse	GGGGTACCCTACCATTGCTCTCCA AGTCTCTCAT	
pcDNA3.1-m*Vgll4*-forward	GCTCTAGAATGCTGTTTATGAAGA TGGACCTGT	NM_177683
pcDNA3.1-m*Vgll4*-reverse	GGGGTACCCCTTCAGGAGACCAC AGAGG	
pcDNA3.1-m*Stk3*-forward	GCTCTAGAATGGAGCAGCCGCCG	NM_019635
pcDNA3.1-m*Stk3*-reverse	GGGGTACCTCAGAAATTCTGCTGC CTCCTCT	
pcDNA3.1-m*Stk4*-forward	GCTCTAGAATGGAGACCGTGCAG CTG	NM_021420
pcDNA3.1-m*Stk4*-reverse	GGGGTACCTCAGAAGTTCTGTTGC CTCCTCT	
pmRFP-HBsAg-HA-forward	GAAGATCTGGTGGTGGCGGTTCA GGCGGAGGTGGCTCT ATGGGGC AGAATCTTTCC	NC_003977.2
pmRFP-HBsAg-HA-reverse	GGGGTACCTCAGGCATAATCTGG CACATCATAAG	
pcDNA3.1-m*Bmi1*-forward	GCTCTAGAATGCATCGAACAACCA GAAT	NM_007552
pcDNA3.1-m*Bmi1*-recerse	GGGGTACCCTAACCAGATGAAGTT GCTGATG	
peGFP-m*Bmi1*-forward	GAAGATCTATGCATCGAACAACCA GAAT	NM_007552
peGFP-m*Bmi1*-recerse	GGGGTACCCCAGATGAAGTTGCT GATGAC	
pET-m*Tead4*-forward	ATTATTACCTCCAACGAGTGGAGC T	NM_001080979
pET-m*Tead4*-reverse	GGGGTACCTCATTCTTTCACAAGT CGGTAGATGTGG	

Table 13: Primers for gene reporter system

Gene	**Sequence (5'→3')**
m*Bmi1*-FL-forward	GGGGTACCGAGCTAGCACCCTTTTGAAGTG
m*Bmi1*-FL-reverse	GAAGATCTAATGAATGCGAGCCAAGC
m*Nfkbia*-FL-forward	GGGGTACCAGCTGATAGAAGCAGCAGGTTTC
m*Nfkbia*-FL-reverse	GAAGATCTGCGGCGCCCTATAAACG
m*Nfkbia*-TB1-forward	GGGGTACCTGAGTGCAGGCTGCAGGG
m*Nfkbia*-TB1-reverse	GAAGATCTATGAGCCACTGGGGTCATG
m*Nfkbia*-TB2-forward	GGGGTACCGGCTTCTCAGTGGAGGACGAG

m*Nfkbia*-TB2-reverse	GAAGATCTCGGCGCCCTATAAACGCT
m*Nfkbia*-mutTB2-forward	TGGCTTGGACGGCATCCGC
m*Nfkbia*-mutTB2-reverse	GCGGATGCCGTCCAAGCCA
m*Ctgf*-posTB-forward	GGGGTACCAAGGGGTCAGGATCAATCCGG
m*Ctgf*-posTB-reverse	GAAGATCTCCGGGAGCCGGCT
m*Bmi1*-TB1-forward	GGGGTACCAAATGGTTAAGAGGGAGACTCT
m*Bmi1*-TB1-reverse	GAAGATCTATTTATTCAGGGTACGAT-ACTTTAATAGG
m*Bmi1*-TB2-forward	GGGGTACCATCTTGAGCGTCTTCAAGCCCT
m*Bmi1*-TB2-reverse	GAAGATCTACGCAGGGCAGATGTGC
m*Bmi1*-TB3-forward	GGGGTACCCAGAAGCAGGAGACATGGTGG
m*Bmi1*-TB3-reverse	GAAGATCTTTAGTGTCGGTGTAGTCGGGC
m*Bmi1*-TB4-forward	GGGGTACCGCCCGACTACACCGACACTAA
m*Bmi1*-TB4-reverse	GAAGATCTTGGAAACTGACACCGGCTCCA
m*Bmi1*-mutTB3-forward	GCTGTGGAATGCCGCCTC
m*Bmi1*-mutTB3-reverse	GAGGCGGCATTCCACAGC
m*Bmi1*-mutTB4-forward	CCTAATTCCCAGGCCGCCCTTAAATG-CCGAGGGGAGCACGTGACCCGGCGGA
m*Bmi1*-mutTB4-reverse	GATCTCCGCCGGGTCACGTGCTCCCCTCG-GCATTTAAGGGCGGCCTGGGAATTAGGGTAC

FL: full length; TB: Tead4 binding site; mut: mutant; pos: positive. Primers for m*Bmi1*-mutTB4 were designed to generate double-strand DNA fragment with sticky ends by annealing.

Table 14: Primers for electrophoretic mobility shift assay

Gene	**Sequence (5'→3')**
m*Nfkbia*-F1-forward	GGATACCTCACAGTTACTTTTTTAGC TATGTTTGAG
m*Nfkbia*-F1-reverse	TGCAATGCAGGGACATTTGGC
m*Nfkbia*-F2-forward	GTACCTAGAGGGAGGGGGC
m*Nfkbia*-F2-reverse	CAGGGGATTTCTCAGGGGCG
m*Ctgf*-pos-forward	GAAGGTGGGGAGGAATGTGAGGAA

	TGTCCCTGTTT
m*Ctgf*-pos-reverse	AAACAGGGACATTCCTCACATTCCTC CCCACCTTC
Negative control-forward	CATGGATTACAAGGATGACGACGA TAAGCCACCGTCCA
Negative control-reverse	CCGGTGGACGGTGGCTTATCGTC GTCATCCTTGTAATCCATGGTAC

Primers for m*Ctgf*-positive control and negative control were designed to generate double-strand DNA fragment by annealing.

2.1.11 Cell lines

Table 15: Cell lines

Cell line	**Origin**	**Medium**
Hepa1-6	C57 mouse hepatoma	DMEM complete, 10%FBS
HEK293T	Human embryonic kidney	DMEM complete, 10%FBS
NCTC Clone 1469	C3H mouse liver	DMEM complete, 10%FBS

2.1.12 Software and data analysis

Table 16: Software

Software	**Provider**
Image J	Wayne Rasband (National Institutes of Health)
Flowjo	TreeStar Inc., Ashland, Oregon, USA
GraphPad Prism	GraphPad Software Inc., La Jolla, California, USA
ZEN 2 (blue edition)	Carl Zeiss Microscopy GmbH, Jena, Germany
Snapgene	GSL Biotech LLC, La Jolla, California, USA

GSEA software	UC San Diego and Broad Institute
R, R-studio	R Core Team, RStudio, Inc.

ImageJ software was used to process high resolution images. RFP- and GFP-positive cells were quantified by flow cytometry. Reanalysis of gene expression omnibus data GSE69590, GSE83148, GSE65359 and GSE84429, Gene Set Enrichment Analysis (gsea-3.0) and R project (Version 3.6.1) were utilized. Data analysis, linear models and differential expression was processed via limma package version 3.9. Student's *t*-test was used to statistically compare differences between two groups. Significance levels were defined as follows: *p-value<0.05, **p-value<0.01, and ***p-value<0.001, ****p-value<0.0001 (Prism7). Representative data from a series of at least three independent experiments carried out in triplicate are presented as the mean ± standard error of the mean (SEM) unless otherwise indicated.

2.2 Molecular biology

2.2.1 Plasmids construction

To construct plasmids, the specific primers for each gene or promoter region were designed with two different restriction enzyme digestion sites at the 5' end of the primers. After double digestion of the PCR products and the vectors, digested DNA fragments and vectors were purified by Gel and PCR product clean-up kit (Omega Bio-tek, Norcross, GA, USA). By ligation of double-digested DNA and vector with T4 ligase, a specific DNA fragment was inserted into the vector. The primers for plasmid constructions are listed in Table 12 and 13.

2.2.2 Transformation of bacteria

To acquire enough plasmid for functional experiments, competent GT116 cells were specifically prepared for psiRNA-h7SK-GFPzeo plasmids transformation according to the manufacture's instruction. Competent TOP10 cells were prepared for the other

plasmid transformations. Competent bacteria were thawed on ice, 50 ng plasmid DNA were added, gently mixed and incubated on ice for 30 min. The reaction was heat-shocked for 45 seconds using a 42°C water bath, followed by 2 min incubation on ice. To active competent bacteria, 500 µl S.O.C. medium was added into the mixture, followed by 1 hour incubation with shaking at 200 rpm/min in a 37°C incubator. Finally, 100 µl transformation mixes were spread on Lysogeny broth (LB) plates supplemented with antibiotics, either ampicillin (100 µg/ml) or kanamycin (30 µg/ml), for positive clone selection by incubating the plate inversely at 37°C overnight.

2.2.3 Clone PCR and agarose gel electrophoresis

To identify positive clones, separate colonies were picked from the plates using filter tips, transferred to 1 ml LB medium including antibiotics, and incubated for 2 hours at 37°C with shaking at 200 rpm/min. Standard PCR amplification (KAPA Taq ReadyMix PCR Kit, Kapa Biosystems, Basel, Switzerland) was performed, directly using 0.5 µl of bacterial suspension. During the PCR reaction, 1% agarose gel was prepared with 1× TBE buffer for analysing the clone PCR products. Once the PCR reaction finished, PCR products were mixed with the DNA loading dye. 10 µl of the mixture were loaded into the gel carefully. The gel was run at 130V (80~150V) until the dye line reached approximately 75%~80% of the way down the gel. The gel was analysed by E-box VX2 Gel Documentation Imaging machine (Vilber, Collégien, France).

2.2.4 Expansion of plasmids

The remaining bacteria suspension of positive clones were expanded in 5 ml LB medium supplemented with antibiotics and incubated in the shaking incubator at 37°C, 250 rpm/min overnight. To prepare plasmids in small-scale, 5–10 ml overnight cultures are appropriate to produce approximately 20 µg of plasmids using the E.Z.N.A.® Endo-Free Plasmid Mini Kit I (Omega Bio-tek). To prepare plasmid in large-scale, 200 ml overnight cultures are appropriate to produce approximately 10

mg of plasmid using QIAGEN Plasmid Maxi Kit (QIAGEN, Hilden, Germany). All procedures were performed according to the manufacturer's instructions.

2.2.5 Genomic DNA extraction

To extract genomic DNA from cell lines or primary mouse hepatocytes, DNeasy Blood & Tissue kit (QIAGEN) was used according to the manufacturer's instruction.

2.2.6 Total mRNA isolation and reverse transcription

To prepare total mRNAs, QIAzol Lysis Reagent (QIAGEN) was used to lyse and homogenize samples based on the manufacturer's instructions. To analyse mRNA levels, 2 μg of total RNA was reverse transcribed with SMART® MMLV Reverse Transcriptase (TaKaRa, Kusatsu, Japan).

2.2.7 Quantitative real-time PCR (qPCR)

The cDNA was diluted to 10 ng/μl and mixed with 2×FS Universal SYBR Green Master (Roche, Mannheim, Germany) and gene-specific primers (5 nM) (Table 10). PCR was performed with a CFX96 Touch™ Real-Time PCR Detection System (Bio-Rad, Hercules, USA) with the following parameters: 1) 95°C for 10 min to activate FastStar Taq DNA polymerase; 2) 95°C for 10 sec to denature dsDNA followed by 60°C for 30 sec to allow primer annealing and elongation to finally collect SYBR green signals; 3) step 2 was repeated for 40 times; and 4) a final melt-curve analysis step was performed. The PCR results were analyzed with CFX Manager™ Software (Bio-Rad, Hercules, USA).

2.2.8 Dual-luciferase reporter assay

Dual-luciferase reporter assay is widely used to study eukaryotic gene expression and cellular physiology. Applications include the study of receptor activity, transcription factors, intracellular signalling, mRNA processing and protein folding. Dual reporters are commonly used to improve experimental accuracy. The term "dual reporter" refers to the simultaneous expression and measurement of two individual

reporter enzymes within a single system. Typically, the “experimental” reporter is correlated with the effect of specific experimental conditions, while the activity of the co-transfected “control” reporter provides an internal control that serves as the baseline response. Normalizing the activity of the experimental reporter to the activity of the internal control minimizes experimental variability caused by differences in cell viability or transfection efficiency.

Assays were performed with pGL3-basic reporter plasmid (Promega, Madison, USA) and pRL-TK control plasmid (Promega). *Nfkbia* promoter region (-977–+34, NM_010907), *Bmi1* promoter region (-979–+417, NM_007552), truncated promoter regions and mutant TEAD4-binding site fragments were cloned into the multiple cloning site through restriction enzymes. To visualise *Nfkbia*-driven and *Bmi1*-driven activity, luciferase reporter open reading frame was substituted with red fluorescent protein (RFP) open reading frame (pRFP-Nfkbia and pRFP-Bmi1). Cells of 80% confluence were transfected with reporter plasmids and/or overexpression plasmids as indicated. The Dual-Luciferase® Reporter (DLR) Assay System (Promega) was used to detect Firefly and Renilla (control signal) luciferase activities with a FLUOstar Omega microplate reader (BMG LABTECH, Ortenberg, Germany) 48 hours after transfection. The shRNA-GFP-positive Hepa1-6 clones were transfected with pRFP-Nfkbia or pRFP-Bmi1 reporter assays for additional 48 hours in chamber slides. The slides were fixed with 4% PFA (paraformaldehyde) at room temperature for 15 min. The RFP signals were directly visualised with a BX53 upright Microscope (Olympus, Shinjuku City, Tokyo, Japan) or an AxioObserver. Z1 inverted microscope (Zeiss, Jena, Germany). In addition, RFP-positive cells were counted with a CytoFLEX S flow cytometer (Beckman, Brea, USA).

2.2.9 Chromatin immunoprecipitation (ChIP)

ChIP is a widely used method to identify specific proteins associated with a region of the genome, or in reverse, to identify regions of the genome associated with specific

proteins. The ChIP assay was performed with an EZ ChIP kit (Merck, Darmstadt, Germany) following the user guide as described previously[166]. Briefly, 1×10^7 Hepa1-6 and NCTC Clone 1469 cells were fixed with formaldehyde (final concentration 1%) at room temperature for 10 min to covalently crosslink proteins to DNA. To generate 200–1000bp length of DNA fragments, harvested cells were sonicated (Ultrasonic homogenizers, BANDELIN electronic GmbH, Berlin, Germany) to shear the chromatin to the manageable size through the following operating parameters: 40% amplitude, 15 seconds-on and 50 seconds-off for sonication, 10 cycles were needed. Gel electrophoresis was performed to confirm the DNA fragment size. TEAD4 antibody and Mouse IgG antibody (negative control) were linked to agarose beads and incubated with sheared chromatin at 4°C with rotation overnight. During the incubation, TEAD4 antibody might bind to TEAD4/DNA complex to form the agarose beads/TEAD4 antibody/TEAD4/DNA fragment complex. After a low speed centrifuge at 4°C (1000 rpm, 1 min), the agarose beads complex was collected. After purification of associated DNA, the detection of specific DNA sequences is performed by quantitative real time PCR with the specific primers (Table11). If the DNA fragment is associated with TEAD4, the relative representation of that DNA sequence will be enriched by the immunoprecipitation process.

2.2.10 Electrophoretic mobility shift assay (EMSA)

EMSA was performed as described previously[167]. To facilitate the assay, the radioisotope was replaced with GelRed (Biotium, Fremont, USA). To prepare 20 ml 5% polyacrylamide gel, 15.6 ml dH_2O, 1 ml 10× TBE, 3.36 ml 30% acrylamide stock (19:1), 200 µl 10% Ammonium persulphate solution were mixed well while minimizing bubble formation. The mixture was added with 20 µl TEMED, mixed well and poured into the gel maker. To set the reaction system, 10–40 µg TEAD4 protein and 100 ng DNA fragment was mixed in 5× binding buffer supplemented with 0.1 µl 100×BSA. After 30 min incubation at room temperature, 6× green gel loading dye was added into the reaction mix. The mixture was loaded into 5% polyacrylamide gel that was pre-run without sample at 150 V for30 min with 0.5× TBE buffer. After running the gel

for about 2 hours at 150 V, the gel was stained in 0.5× TBE buffer with GelRed dye for 30 min at room temperature. The gel was put in the E-box VX2 Gel Documentation Imaging machine (Vilber, Collégien, France), UV light was used to visualise DNA or DNA/protein complex bands.

2.3 Cell biology

2.3.1 Cultivation of cell lines

The Hepa1-6, NCTC clone 1469 and HEK293T cell lines were maintained in DMEM (Gibco, Paisley, UK) containing 1% L-Glutamine and supplemented with 10% FBS (Millipore, Darmstadt, Germany) and 1% penicillin/streptomycin (Millipore) at 37°C in a 5% CO_2 incubator.

2.3.2 Primary murine hepatocyte isolation

Primary murine hepatocytes (PMHs) were prepared from wild-type (WT) C57BL/6 (6 to 9-months-old, male) mice, *Irak4*$^{-/-}$ mice and *Myd88*$^{-/-}$/*Trif*$^{-/-}$ mice and HBsAg-transgenic mice by *in-situ* collagenase type IV (Worthington, Lakewood, USA) perfusion, as described previously[168]. Briefly, the mouse was sacrificed by cervical dislocation and secured on the working platform with ventral side up. The abdomen/chest region was thoroughly cleaned with 70% ethanol, from low abdomen region to chest region, the fur and muscle layer were cut through and the liver, portal vein and inferior vena cava were exposed; a butterfly cannula (22G) was inserted into the portal vein carefully. The cannula was connected with the pump tube, the pump was started to perfuse the liver with 50 ml prewarmed (42°C) Hank's buffered salt solution without magnesium or calcium, including 0.5 mM ethylene glycol tetraacetic acid (EGTA). Prewarmed Hank's buffered salt solution (100 ml) including type IV collagenase (100 units/ml) was further perfused to digest the liver tissue. The digested liver was cut out and transferred into a 10 cm dish with 10 ml culture medium (Ham’s F12 medium; 10% active FBS, 1% L-Glutamine, 1%

penicillin/streptomycin). The liver was torn apart with two pair of forceps. Once torn apart, the cell suspension was triturated three times with a 10 ml pipette. The suspension was filtered through a 100 µm cell strainer and centrifuged at 4°C, 30×g for 5 min. The centrifugation was repeated twice to remove debris and non-parenchymal cells. After resuspension, total hepatocytes were counted and diluted to 3×10^5 cells/ml. Due to TLR2/4 context, in the following the *Myd88*$^{-/-}$/*Trif*$^{-/-}$ mice are termed *Myd88*$^{-/-}$ mice. Knockout mice were kindly provided by Prof. Carsten Kirschning. PMHs were seeded on collagen I-coated culture plates or coverslips. One day after preparation, PMHs were stimulated with cell culture-derived HBV (multiplicity of infection [MOI] > 1,000) or a non-particle control. HBV particle preparation and stimulation were performed as previously described[89]. Briefly, the cell line HepG2.117, stably transfected with an HBV-coding plasmid, was cultured for HBV particles production. HBV particles were prepared from cell culture supernatants by overnight precipitation with 6% polyethylene glycol 8000 (PEG8000; Sigma, Darmstadt, Germany) at 4°C, concentrated by centrifugation (12,000g for 60 min at 4°C) and stored at -80°C. A mock control was produced by precipitating supernatants of HepG2 cells under the same conditions. For the infection and immune induction experiments, a total of five different HBV preparations with 10^9 genome equivalents/ml were used.

2.3.3 Primary human hepatocyte isolation

Primary human hepatocytes (PHHs) were prepared from non-tumorous tissue obtained from freshly resected livers of four different donors, as previously described[169]. Briefly, the liver specimens were placed in a 14 cm petri dish, and a cannula was positioned in an accessible hepatic vessel. The cannula was fixed, and remaining vessels were sealed with Histoacryl (Braun, Melsungen, Germany). The liver tissues were rinsed with perfusion solution (Ca^{2+}- and Mg^{2+}-free Hank's balanced salt solution supplemented with 0.02 mg/ml gentamycin and 20 mM HEPES) prewarmed to 37°C. After nearly all blood had been flushed out, the livers

were equilibrated with perfusion solution containing 0.5 mM EGTA for 10 to 20 min in a recirculation approach. Collagenase type IV [0.6 mg/ml] from *Clostridium histolyticum* (Sigma, Seelze, Germany) was dissolved in perfusion solution containing 5 mM $CaCl_2$, and the solution was sterilized using a 0.45 µm membrane filter. The duration of collagenase perfusion depended on tissue size and quality but did not exceed 20 min. The obtained cell suspension was filtered through a 230 µm-meshed cell strainer. PHHs were pelleted by low-speed centrifugation at gradually increasing rates (30×g, 40×g, and 50×g, for 10 min). PHHs were seeded on collagen I-coated culture plates or coverslips and stimulated with cell culture-derived HBV (MOI > 1,000) or a non-particle control, one day after preparation[89]. All patients provided written documentation of their informed consent. The study conformed to the ethical guidelines of the 1975 Declaration of Helsinki and was approved by the Institutional Review Board (Ethics Committee) of the medical faculty at the University Duisburg-Essen. Samples were acquired by the *Westdeutsche Biobank Essen*.

2.3.4 Flow cytometry

Flow cytometry was performed for DNA content and cell cycle analysis. For these assays, 1×10^6 cells were spun down at 300×g for 5 min and resuspended with 200 µl PBS. For DNA content analysis, Hoechst 33342 (10 µg/ml) was added to the cell suspension and incubated at 37°C for 15 min avoiding light. After staining, cells were washed with PBS two times and resuspended with 300 µl PBS for flow cytometry analysis using the CytoFLEX S. For quantifying RFG signals 1×10^6 cells were spun down at 300×g for 5 min, resuspended with 200 µl PBS and directly measured in the CytoFLEX S analyser.

2.3.5 LPS and Pam3CSK4 stimulation

Hepa1-6 cells or NCTC Clone 1469 cells were seeded on 96-flat well plates or 24-well plates, and stimulated with LPS (10 µg/ml, Invivogen, San Diego, USA) or synthetic palmitoylated lipopeptide (Pam3CSK4, 500 ng/ml, Invivogen) for different lengths of time (0, 6, 12, 24, 48 and 72 hours) depending on the different methods.

2.3.6 Inhibitor treatment

PMHs were isolated and seeded on collagen-I coated plates or coverslips, and were treated with C29 (50 μM) or XMU-MP-1 (1 μM) for different lengths of time before the HBV exposure. For DNA content analysis, WT PMHs were isolated and seeded on collagen-I coated 12-well plates, and were treated with XMU-MP-1 (5 μM) for 48 hours. After the treatment, PMHs were collected and stained with Hoechst 33342 for flow cytometry analysis.

2.3.7 Hematoxylin and eosin staining

Hematoxylin and eosin (HE) staining was performed to observe cell morphology and liver histopathologic conditions. For PHHs or PMHs seeded on collagen I-coated coverslips, cells were fixed with 4% PFA at room temperature for 15 min. After PBS washes, cells were stained with the HE Fast Staining Kit (Roth, Karlsruhe, Germany) according to the instruction manual. After HE staining dehydration in 100% ethanol and clearance in xylene was performed and cells were mounted with Canada balsam (Sigma-Aldrich, Darmstadt, Germany). For liver tissue sections, sections were stained with the HE Fast Staining Kit after deparaffination and rehydration. After HE staining dehydration in 100% ethanol and clearance in xylene was performed, sections were mounted with Canada balsam.

2.3.8 Immunohistochemical staining

Immunohistochemical staining was performed with paraffin-embedded tissue sections. Deparaffinization and rehydration of the section was achieved by the following processes: slides were incubated at 65°C for 30 min, followed by 2 × 5 min xylene; 2 × 3 min 100% ethanol; 3 min 95% ethanol; 3 min 70% ethanol; 3 min 50% ethanol and 3 min PBS. Endogenous peroxidase was quenched by incubating slides at room temperature for 10 min with 3% H_2O_2. After washing 2 times with PBS, citrate buffer was applied to unmask the antigen by incubating sections in the buffer for 45 min at 95°C, avoiding bubbles. After additionally washing with PBS, sections

were blocked with 10% normal serum (same species with the secondary antibody) at room temperature for 10-20 min. After removing blocking serum from sections, diluted primary antibody was added onto the sections. The sections were incubated at 4°C, overnight in a wet box. Sections were washed twice with PBS and incubated with diluted biotinylated secondary antibody at room temperature for 1 hour in a wet box. After incubation, sections were washed twice with PBS and incubated with VECTASTAIN ABC reagent (tertiary antibody) at room temperature for 45 min in a wet box. After washing twice with PBS, sections were incubated with peroxidase substrate solution until desired staining intensity develops. Sections were rinsed under tap water and counterstained with hematoxylin for 2 min at room temperature. After washing under tap water, sections were dehydrated gradually with 70% ethanol, 90% ethanol and 2 times 100% ethanol for 5 min each, and were cleared with xylene twice for 5 min. Finally, slides were mounted with Canada balsam.

2.3.9 Immunofluorescent staining

Cover slips were washed 3 times with PBS and fixed for 10 min at room temperature with 4% PFA. Cells were additionally washed with PBS, after which immunocytochemical (ICC) staining was conducted. Fixed cells were incubated for 10 min on ice with 0.2% Triton X-100 (Sigma-Aldrich, Steinheim, Germany) and 0.2% BSA (Carl Roth, Karlsruhe, Germany) in PBS. Following permeabilization, the cells were blocked by incubation for 1 hour at room temperature with 0.02% Triton X-100 and 5% BSA in PBS. Primary antibodies were applied overnight at 4°C. Cells were washed with PBS three times and incubated with secondary antibodies at room temperature for 1 hour without light exposure. Finally, the cells were washed three times with PBS and covered with Fluoroshield™ mounting medium, including DAPI (Sigma-Aldrich). Tissue specimens were fixed and paraffin embedded. Slides were deparaffinized, unmasked and blocked with 5% BSA in PBS. Staining was proceeded as described for cover slips.

2.4 Protein biochemistry

2.4.1 Preparation of protein lysate

To prepare total protein lysates, RIPA buffer (150 mM NaCl, 1% Nonidet P-40, 0.5% sodium deoxycholate, 0.1% SDS, 25 mM Tris) supplemented with protease and phosphatase inhibitor cocktail (Thermo Scientific, USA) was used. Lysates were centrifuged for 15 min at 14,400×g and 4°C. The protein concentration was determined with BCA Protein Assay Kit (Pierce, Rockford, USA).

2.4.2 Protein quantification via Bicinchoninic acid (BCA) assay

The BCA protein assay is a well-known copper-based method for colorimetric detection and quantitation of total protein. Before quantitation, total protein was diluted at 1:5 (1 µl sample plus 4 µl water) with deionized water in flat-bottom transparent 96-well plate. BCA working reagent was prepared according to the manufacture's instruction. The 5 µl standard sample was added in the same plate. 100 µl BCA working reagent were added into standard samples and diluted samples. The plate was incubated in a 37°C incubator with shaking for 30 min. The plate was placed into the FLUOstar Omega microplate reader and absorbance was determined at 562 nm wave length. Finally, the concentration of diluted samples was calculated according to the standard curve.

2.4.3 Western blot

Samples were prepared in 5 × loading buffer and incubated at 95°C for 5min. Twenty micrograms of total protein was loaded on 10% resolving and 5% stacking gel and resolved with a Mini-PROTEAN® Tetra Cell (Bio-Rad) and transferred onto PVDF membranes (Trans-Blot® Turbo™, BioRad). Primary and secondary antibodies used are listed in Table 6. Amersham ECL Prime Western Blotting Detection Reagent (GE Healthcare, Chicago, USA) and an ADVANCED Fluorescence and ECL Imager (INTAS, Göttingen, Germany) were used to visualise light signals.

2.4.4 Protein expression and purification

The murine *Tead4* sequence (NM_001080979) was cloned into the His-GST-TEV-pET(2G-T) vector, producing hexahistidine (His_6)-GST-tagged proteins. Recombinant TEAD4 was expressed in *E. coli* strain BL21 (DE3). The protein was bound to high-capacity Glutathione Sepharose 4B GST-tagged protein purification resin (GE Healthcare) according to the manufacturer's instructions. Recombinant TEAD4 was eluted (50 mM Tris, 10 mM reduced glutathione, pH 8.0) from the resin and stored at 4°C.

2.5 Mouse experiments

Mouse experiments were performed according to the Institutional Animal Care and Use Committee guidelines of the Animal Core Facility of University Hospital Essen. Mice were bred at University Hospital Essen and given humane care according to the criteria outlined in the Guide for the Care and Use of Laboratory Animals prepared by the Society for Laboratory Animal Science.

2.5.1 LPS and Pam3CSK4 injection

Ultrapure LPS (2.5 mg/kg bodyweight) or Pam3CSK4 (1 mg/kg bodyweight) were diluted in PBS and injected by intraperitoneal or intravenous injection, respectively. Mice were sacrificed 0-6 hours after injection. Mice livers were divided into four parts according to the natural structure of the murine liver. The biggest lobe was fixed with 10% neutrally buffered formaldehyde overnight and embedded in paraffin for histochemical staining. The remaining liver lobes were sliced into small pieces and stored in RNAlater and cryotubes directly at -80°C for RNA and protein extraction, respectively. Six-month-old transgenic mice were used for the treatment with TLR ligands, three mice were administered for each group.

2.5.2 Verteporfin treatment

HBsAg-transgenic mice were intraperitoneally administered with DMSO or verteporfin at a dose of 100 mg/kg for three days and sacrificed at day 7. Mice liver samples were prepared as described in 2.5.1. Six-month-old transgenic mice were used for the treatment and three mice were administered for each group.

3. Results

3.1 Toll-like receptor signalling activates the Hippo pathway to regulate the innate immune response against Hepatitis B virus

3.1.1 Characterisation of gene expression patterns after HBV exposure in PHHs

To date, only a few studies have indicated that HBV particles can be recognised by TLRs, triggering an innate immune response in hepatocytes. To evaluate gene expression patterns and the potential role played by the Hippo signalling pathway in HBV-induced innate immunity, microarray data (GSE69590)[90] from PHHs that were infected with HBV for 40 hours were reanalysed using GSEA. As shown in Figure 6A, chemokines, including *CXCL6*, *CCL2*, *CXCL3*, *CXCL2,* and *CCL20,* were significantly upregulated after 40 hours of exposure to HBV particles in PHHs. Interestingly, no differences in *IL6* and *IL1B* were observed between the control group and the HBV-infected group, which suggested that 40 hours after HBV exposure was not a proper time point for the detection of *IL6* and *IL1B* expression. Furthermore, *NFKB1* was upregulated in the HBV-infected group compared with the control group, whereas *NFKBIA* and *RELA* were downregulated. NFKB1 and RELA are associated with the activation of the NF-κB signalling pathway, forming a complex that is subsequently translocated into the nucleus to target the promoter regions of *IL6*, *IL1B,* and *TNF*, resulting in the upregulation of IL6, IL1B and TNF. IκBα (coded by *NFKBIA*) is an inhibitor of NF-κB signalling, binding to the NFKB1 and RELA complex to suppress nuclear translocation. Here, the upregulation of *NFKBIA* and *NFKB1* suggested that an innate immune response balancing mechanism was activated following HBV infection. Consistent with our previous work[89], NF-κB signalling was enriched (Figure 6B) in the HBV-exposed group, which suggested that NF-κB signalling could be induced by TLR2-mediated downstream effector activation. The Hippo signalling pathway plays an important role in the rapid, innate immune response[99]. Because YAP is the downstream effector of Hippo signalling, YAP target

genes were also reanalysed in this dataset. In contrast, YAP target genes were enriched in the control group compared with the HBV-exposed group (Figure 6B), which implied that YAP was inactivated after HBV exposure.

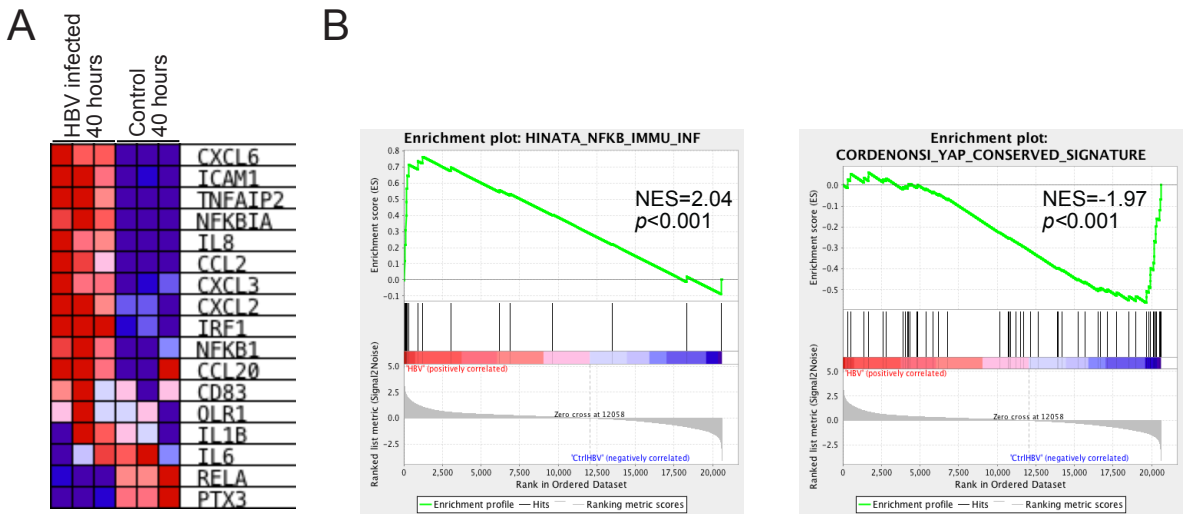

Figure 6. NF-κB signalling and Hippo signalling are activated after exposure to HBV particles for 40 hours in PHHs.

A. Heatmap visualisation of gene expression in the HINATA_NF-κB_IMMU_INF gene set after GSEA analysis of GSE69590 microarray data. **B**. GSEA analysis indicated correlations among NF-κB signalling, Hippo signalling, and HBV exposure in PHHs. GSEA computed four key statistics for the GSEA report: enrichment score (ES), normalised enrichment score (NES), false discovery rate (FDR), and nominal p-value. ES reflects the degree to which a gene set is overrepresented at the top or bottom of a ranked list of genes. NES is the primary statistic for examining gene set enrichment results. By normalising the enrichment score, GSEA accounts for differences in the gene set size and correlations between gene sets and the expression dataset. FDR is the estimated probability that a gene set with a given NES represents a false-positive finding. The nominal p-value estimates the statistical significance of the enrichment score for a single gene set. The top portion of the plot shows the running ES for the gene set, as the analysis walks down the ranked list. The score at the peak of the plot (the score furthest from 0.0) represents the ES for the gene set. Gene sets that feature a distinct peak at the beginning or end of the ranked list are generally the most interesting. The middle portion of the plot shows where the members of the gene set appear on the ranked list of genes. The leading-edge subset of a gene set is the subset of members that contribute the most to the ES. For a positive ES, the leading-edge subset represents the set of members that appear on the ranked list prior to the peak score. For a negative ES, this subset represents the set of members that appear subsequent to the peak score. The bottom portion of the plot shows the value of the ranking metric, moving down the list of ranked genes. The ranking metric measures a given gene's correlation with a phenotype. The value of the ranking metric moves from positive (left) to negative (right), going down the ranking list. A positive value indicates a correlation with the first phenotype, whereas a negative value indicates a correlation with the second phenotype. For a

continuous phenotype (a time series or a gene of interest), a positive value indicates a correlation with the phenotype profile, whereas a negative value indicates no correlation or an inverse correlation with the profile.

3.1.2 GSEA results could be verified in HBV-exposed PMHs

Our previous work showed that HBV particles were able to induce innate immune responses in PHHs and primary murine hepatocytes (PMHs)[89,125]. Here, PMHs were exposed to cell-culture-derived HBV particles [multiplicity of infection (MOI) > 1,000] or non-particle control vehicle (at an equivalent volume), for different lengths of time. A marked increase in *Il6*, *Il1β,* and *Tnf* expression was observed 1 hour after HBV exposure, which peaked after 6 hours (Figure 7A). YAP is a critical downstream effector of the Hippo signalling pathway, and its transcription level was only slightly affected by exposure to HBV particles; however, the expression of a YAP target gene, *Ctgf*, was significantly induced. Because *NFKBIA* expression was upregulated in the GSEA results, we confirmed that *Nfkbia* was also upregulated in PMHs after HBV exposure. Moreover, *Nfkbia* displayed a similar expression profile as *Ctgf*, which suggested that *Nfkbia* might represent another target gene of YAP. To confirm the quantitative PCR results, a western blot analysis was performed. Figure 7B shows that phosphorylated YAP levels decreased after HBV exposure, whereas the total YAP levels did not change, which indicated that YAP phosphorylation was inhibited, resulting in the increased translocation into the nuclear compartment in the HBV-exposed group compared with the non-particle treated and untreated control groups. Simultaneously, HBV exposure increased the levels of phosphorylated NF-κB and decreased the levels of total IκBα.

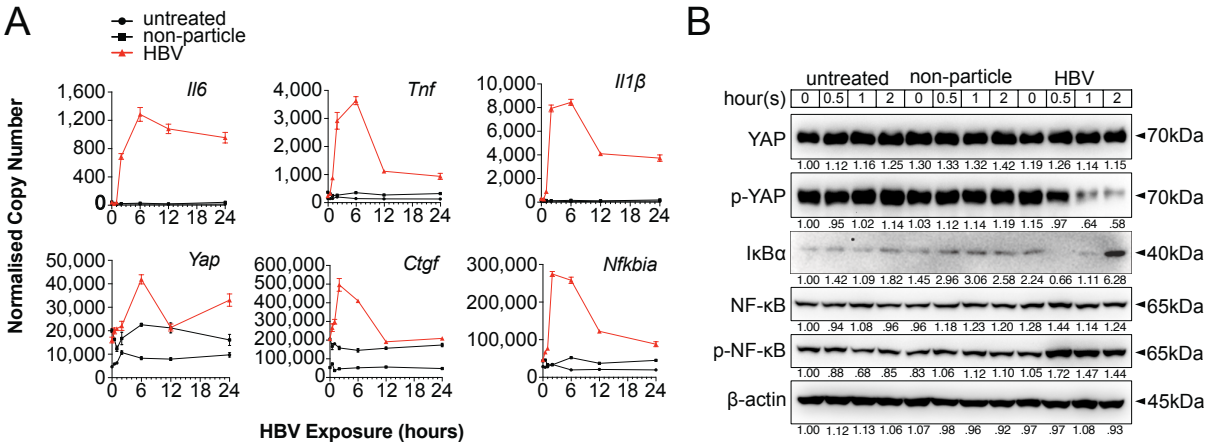

Figure 7. HBV exposure activate NF-κB signalling and YAP target genes.
Primary murine hepatocytes (PMHs) were treated with cell culture-derived HBV (MOI of 1000) or non-particle control for different time points (0, 0.5, 1, 2, 6, and 12 hours). **A**. The gene expression levels of *Il6*, *Tnf*, *Il1β, Yap*, *Ctgf,* and *Nfkbia* were determined by quantitative PCR (normalised against *Actb*, mean ± SEM). **B**. Western blotting was performed to detect YAP, phosphorylated YAP, IκBα, NF-κB, and phosphorylated NF-κB in HBV-exposed PMHs. Data sets are representatives of at least three independent experiments. kDa, kilodalton.

3.1.3 YAP and NF-κB are translocated into the nucleus after HBV exposure in PMHs

To visualise intercellular YAP and NF-κB, immunocytochemistry was performed. As shown in Figure 8, YAP and NF-κB were translocated into nucleus 1–2 hours after HBV exposure. Consistent with the western blot results, the exposure of PMHs to HBV not only activated NF-κB signalling but also affected the Hippo signalling pathway.

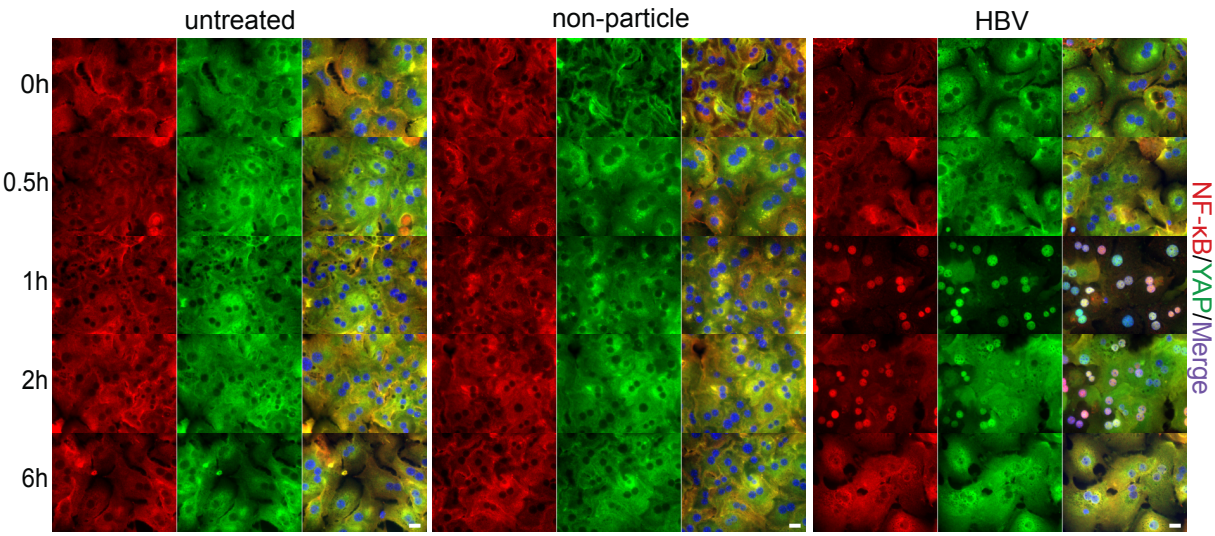

Figure 8. Immunocytochemical (ICC) staining visualises the nuclear translocation of YAP and NF-κB.

Primary murine hepatocytes (PMHs) were treated with cell-culture-derived HBV (MOI of 1000) or non-particle control for different time points (0, 0.5, 1, 2, and 6 hours). PMHs were fixed with 4% paraformaldehyde (PFA), at room temperature for 10 min, and subsequently permeabilised and blocked on coverslips. After PBS washes, immunocytochemical staining was performed, by applying primary and secondary, fluorophore-conjugated antibodies, to visualise YAP (green) and NF-κB (red) localisation. Data sets are representatives of at least three independent experiments. Scale bar, 20 μm.

3.1.4 TLR2 mediates the activation of the Hippo signalling pathway during HBV exposure in PMHs

To investigate the effects of HBV exposure on Hippo signalling in PMHs, the activation of the TLR-Myeloid differentiation primary response protein 88 (MyD88)-IL-1 receptor-associated kinase 4 (IRAK4) cascade was investigated, which occurs upstream of NF-κB signalling. Our previous study showed that HBV infections can induce the activation of TLR2 in PHHs[89]. To verify whether TLR2 is required for the HBV exposure-induced activation of NF-κB and YAP in PMHs, a TLR2 inhibitor (50 μM C29) was administered to PMHs, 2 hours before 6 hours of HBV exposure. HBV-induced TLR2 signalling was obstructed by C29 treatment compared with the dimethyl sulfoxide (DMSO) vehicle-treated and untreated groups, as indicated by the decreased expression of *Il6* and *Tnf* (Figure 9A). The TLR2 blockade decreased the HBV-mediated phosphorylation of MST1/2, YAP, and NF-κB (Figure 9B) compared

with DMSO-treated cells exposed to HBV. These results implied that TLR2 is essential for the recognition of HBV particles and the activation of Hippo signalling.

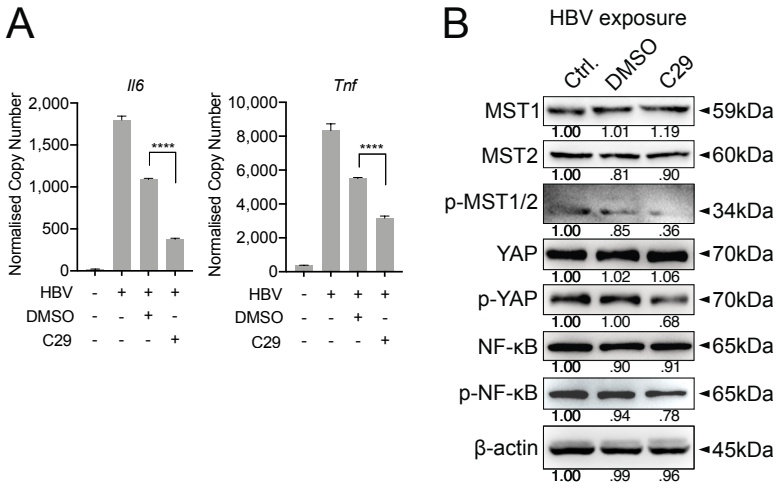

Figure 9. TLR2 inhibitor obstructs the HBV-mediated activation of NF-κB and Hippo signalling.

A. PMHs were treated with the TLR2 inhibitor C29 (50 μM), for 1 hour, prior to HBV exposure for an additional 2-6 hours. After 6 hours, quantitative PCR was performed, to detect *Il6* and *Tnf* expression. **B**. Western blotting was performed to detect MST1/2, phosphorylated MST1/2, YAP, phosphorylated YAP, NF-κB, and phosphorylated NF-κB in C29-pretreated PMHs, 2 hours after HBV exposure. Data sets are representative of at least three independent experiments. ****p-value< 0.0001. kDa, kilodalton.

To investigate whether Hippo signalling affected NF-κB activation, XMU-MP-1 (1 μM), an MST1/2 inhibitor, was applied to PMHs, 1 hour prior to HBV exposure. Similarly, diminished levels of phosphorylated MST1/2 impeded the intensity of HBV-induced innate immune responses, as demonstrated by decreased *Il6* and *Tnf* expression (Figure 10A). Furthermore, decreased levels of phosphorylated MST1/2, YAP, and NF-κB were observed in XMU-MP-1-pretreated PMHs following HBV exposure compared with PMHs exposed to HBV without pretreatment. (Figure 10B).

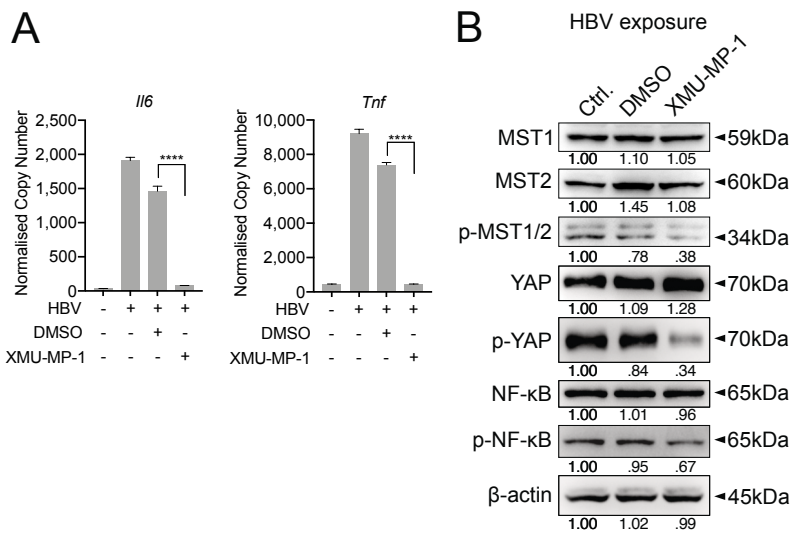

Figure 10. XMU-MP-1 suppresses HBV-mediated Hippo signalling and NF-κB signalling.
A. PMHs were treated with XUM-MP-1 (1 μM), 1 hour prior to HBV exposure, for an additional 2-6 hours. After 6 hours, quantitative PCR was performed to detect *Il6* and *Tnf* expression levels. **B**. Western blotting was performed to detect MST1/2, phosphorylated MST1/2, YAP, phosphorylated YAP, NF-κB, and phosphorylated NF-κB in XMU-MP-1-pretreated PMHs, 2 hours after HBV exposure. Data sets are representative of at least three independent experiments. ****p-value< 0.0001. kDa, kilodalton.

ICC staining demonstrated that C29 (50 μM) and XMU-MP-1 (1 μM) pretreatment blocked the HBV-induced nuclear translocation of NF-κB, whereas the nuclear amount of YAP increased compared with PMHs exposed to HBV without pretreatment (Figure 11). Therefore, HBV-induced TLR2 signalling simultaneously activates NF-κB and Hippo signalling.

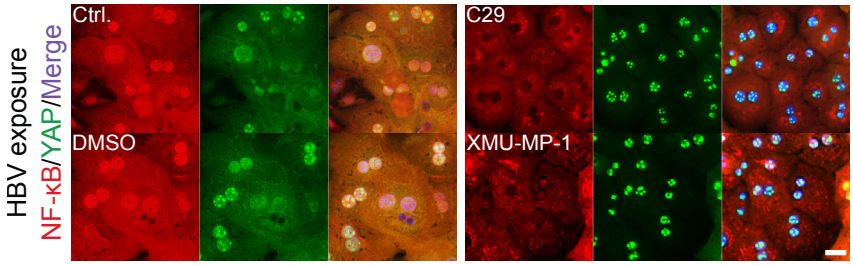

Figure 11. C29 and XMU-MP-1 suppresses the nuclear translocation of YAP and NF-κB in HBV-exposed PMHs.
ICC staining was performed 2 hours after HBV exposure, to visualise YAP (green) and NF-κB (red) localisation in PMHs pretreated with C29 (50 μM) and XMU-MP-1 (1 μM). Scale bar, 20 μm. Data sets are representative of at least three independent experiments.

3.1.5 IRAK4 activates MST1/2 by phosphorylating and inducing the degradation of PP2A

In the Hippo signalling pathway, protein phosphatase 2A (PP2A) functions as a key upstream regulator of MST1/2[99]. After determining that TLR2 activated the Hippo signalling pathway following HBV exposure in PMHs, the specific mechanism through which TLR2 mediates MST1/2 phosphorylation was not yet explored. We hypothesised that IRAK4 could increase the phosphorylation of MST1/2 by dephosphorylating and degrading PP2A. PMHs were isolated from WT, *Irak4*$^{-/-}$, and *Myd88*$^{-/-}$ mice and exposed to HBV particles, for different lengths of time. Western blot analysis of uncultured PMHs indicated that total PP2A level was slightly elevated, whereas the levels of phosphorylated PP2A decreased in PMHs isolated from *Irak4*$^{-/-}$ and *Myd88*$^{-/-}$ mice (Figure 12A). These findings suggested a close interaction between IRAK4, MyD88 and PP2A. Moreover, the levels of phosphorylated MST1/2, phosphorylated YAP, and phosphorylated NF-κB were decreased, whereas IκBα levels increased in PMHs isolated from *Irak4*$^{-/-}$ and *Myd88*$^{-/-}$ mice compared with those in WT PMHs (Figure 12A). Quantitative PCR was also performed to determine *Il6, Tnf* and *Il1β* expression levels after HBV exposure. The unchanged expression levels of *Il6*, *Il1β* and *Tnf* indicated that NF-κB signalling was not activated in *Irak4*$^{-/-}$ and *Myd88*$^{-/-}$ PMHs after HBV exposure compared with the WT PMHs (Figure 12B). ICC staining confirmed that the TLR-MyD88-IRAK4 axis is critical and necessary for Hippo signalling activation, as illustrated by the continuous nuclear transition of YAP and nuclear exclusion of NF-κB in *Irak4*$^{-/-}$ and *Myd88*$^{-/-}$ PMHs after HBV exposure (Figure 12C). Taken together, these results indicate that the TLR-MyD88-IRAK4 axis might be required for the regulation of Hippo pathway activity, mediated by regulation of PP2A.

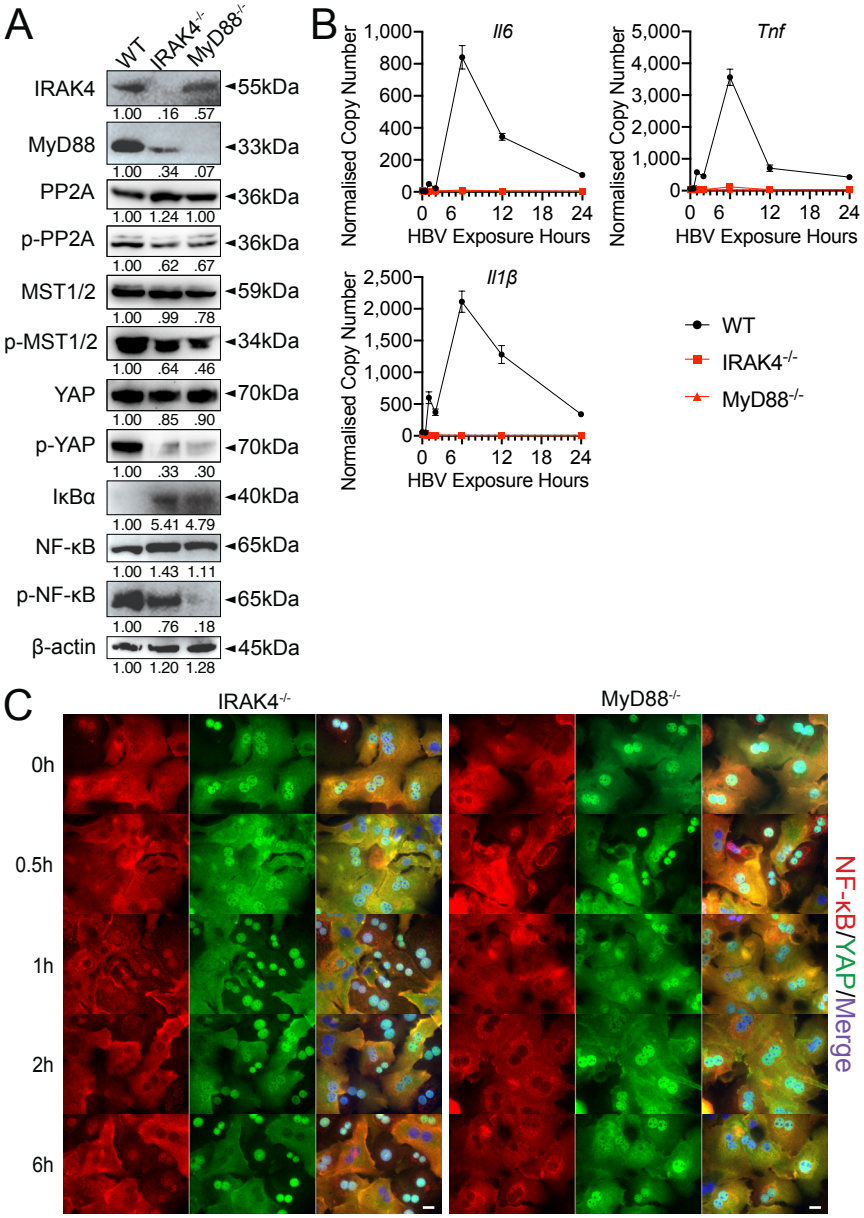

Figure 12. The IRAK4/MyD88 pathway activates MST1/2 by phosphorylating and inducing the degradation of PP2A.

A. Western blotting was performed to detect the abundance of IRAK4, MyD88, PP2A, phosphorylated PP2A, MST1/2, phosphorylated MST1/2, YAP, phosphorylated YAP, IκBα, NF-κB, and phosphorylated NF-κB in uncultured PMHs derived from wild-type (WT), *Irak4*$^{-/-}$, and *Myd88*$^{-/-}$ male mice. **B**. Quantitative PCR was performed to detect *Il6*, *Tnf,* and *Il1β* expression, at different time points after the exposure of PMHs, isolated from WT, *Irak4*$^{-/-}$, and *Myd88*$^{-/-}$ mice, to HBV, at an MOI of 1000 (gene expression levels were normalised against *Actb*, mean ± SEM). **C**. ICC staining was performed to visualise the intracellular localisation of YAP (green) and NF-κB (red) in PMHs derived from *Irak4*$^{-/-}$ and *Myd88*$^{-/-}$ mice after HBV exposure for 0-6 hours. Data sets are representatives of two independent PMH cultures, used in triplicate experiments. Scale bar, 20 μm; kDa, kilodalton.

3.1.6 Hippo signalling regulates the rapid immune response by suppressing YAP/TEAD4-mediated transcription

The YAP/TEAD4 transcription factor complex is an effector of the Hippo signalling pathway, playing a vital role in the regulation of gene transcription by recognising the TEAD4-binding motif in the promoter regions of target genes. Because *Nfkbia* and *Ctgf* had similar expression profiles after HBV exposure in PMHs, *Nfkbia* was hypothesised to be a potential target gene of YAP/TEAD4. The overexpression of YAP in Hepa1-6 cells and PMHs resulted in the upregulation of IκBα (the protein product of *Nfkbia*) expression compared with control cells (Figure 13A), indicating that *Nfkbia* might be a target gene for YAP. To confirm this result, we knocked down YAP and TEAD4 in PMHs, using specific small-interfering RNAs (siRNAs). HBV exposure for 2 hours increased the level of phosphorylated NF-κB and decreased IκBα levels in PMHs with suppressed YAP or TEAD4 expression compared with control PMH cells (Figure 13B). These gain- and loss-of-function experiments suggested that *Nfkbia* may be a target gene of the YAP/TEAD4 transcription factor complex.

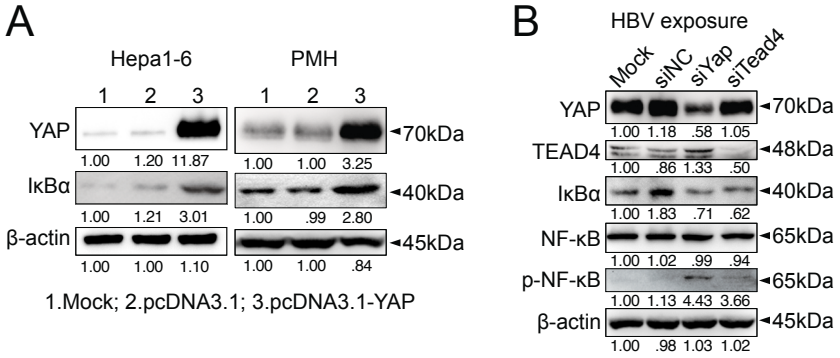

Figure 13. The gain- and loss-of-function of YAP and TEAD4 directly affect IκBα expression.

A. Western blotting revealed the expression levels of YAP and IκBα in Hepa1-6 cells and PMHs 48 hours after the overexpression of YAP. **B**. Western blot analysis detected the expression of YAP, TEAD4, IκBα, NF-κB, and phosphorylated NF-κB in PMHs treated with siYap (50 nM) or siTead4 (50 nM) for 48 hours, followed by HBV exposure for 2 hours. Data sets are representative of at least three independent experiments. kDa, kilodalton.

To confirm that *Nfkbia* transcription was regulated by YAP/TEAD4, the *Nfkbia* promoter region was cloned into an RFP reporter vector, which was transfected into Hepa1-6 clones that were stably transfected with GFP-fused small-hairpin RNA (shRNAs: Scramble, shYap, and shTead4). The knockdown efficiencies of the chosen clones are presented in Figure 14. As shown in Figure 15, the RFP expression levels were clearly suppressed in YAP- and TEAD4-knockdown cells compared with control cells, which was confirmed by using flow cytometry to count RFP-positive cells. These results suggested that the YAP/TEAD4 transcription factor complex might affect NF-κB signalling by promoting *Nfkbia* expression.

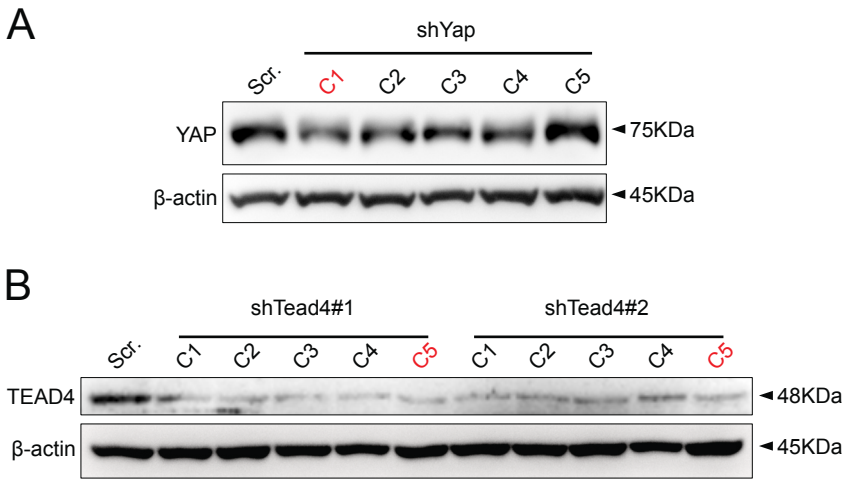

Figure 14. Effective knockdown subclones are selected after the transfection of shRNA-overexpressing vectors in Hepa1-6 cells.

psiRNA-shYap and psiRNA-shTead4#1/#2 plasmids were separately transfected into Hepa1-6 cells, and the culture medium was supplemented with Zeocin (1000 μg/ml), 24 hours after transfection. Selection pressure was maintained for one week, then selected Hepa1-6 were diluted and seeded into 96-well plates to obtain subclones. **A**. The downregulation of YAP was detected by Western blots. The shYap-C1 subclone was selected for further experiments. **B**. The downregulation of TEAD4 was detected by Western blots. The shTead4 #1C5 and shTead4 #2C5 subclones were selected for further experiments. kDa, kilodalton.

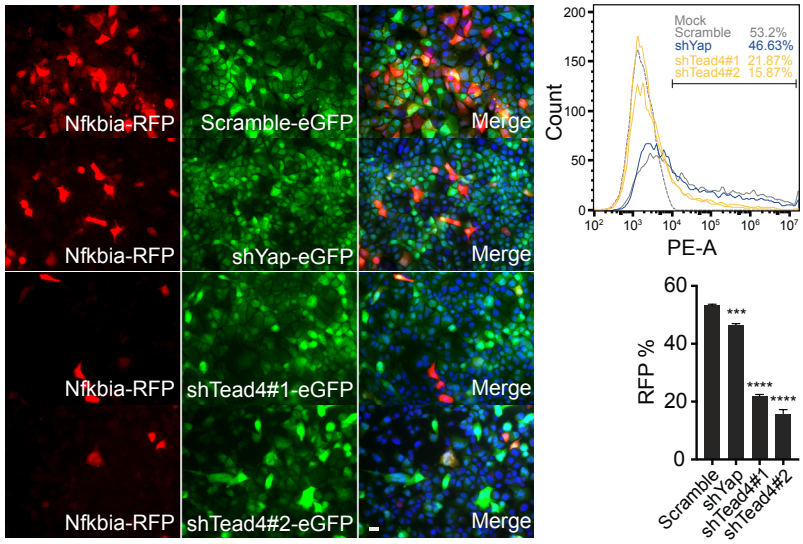

Figure 15. The YAP/TEAD4 complex might interact with the *Nfkbia* promoter.
Hepa1-6 cells, stably transfected with GFP-inducing shRNA plasmids (Scramble, Yap, Tead4), were co-transfected with an RFP reporter plasmid containing the *Nfkbia* promoter, to assess *Nfkbia* promoter activity. Immunocytochemistry and flow cytometry were utilised to determine *Nfkbia* promoter-driven RFP expression. Scale bar, 20 μm. Data sets are representative of at least three independent experiments. ***p-value<0.001, ****p-value<0.0001.

To further confirm this mechanism of regulation, we selected a stable YAP-overexpressing Hepa1-6 clone and confirmed the overexpression of YAP by examining the GFP signal. After transfecting these cells with the *Nfkbia*-driven RFP reporter plasmid, we observed more substantial RFP signals in cells exhibiting high levels of YAP than in cells expressing low levels of YAP (Figure 16). Taken together, these results demonstrate that the Hippo signalling pathway may regulate the rapid, innate immune response by subduing YAP/TEAD4, to affect *Nfkbia* expression.

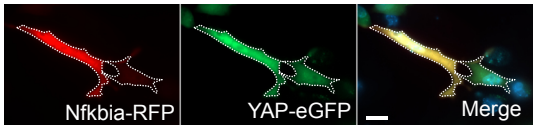

Figure 16. YAP gain-of-function increases *Nfkbia*-driven RFP intensity.
The *Nfkbia*-driven RFP reporter plasmid was transfected into a stable YAP-overexpressing Hepa1-6 clone. After 48 hours of transfection, the fluorescent imaging of Hepa1-6 cells showed the *Nfkbia* promoter-driven RFP intensity in cells overexpressing eGFP-associated YAP. Scale bar, 20 μm. Data sets are representative of at least three independent experiments.
.

3.1.7 *Nfkbia* is a direct target gene of the YAP/TEAD4 transcription factor complex

Using an open-source transcription factor-binding site prediction platform (http://jaspar2016.genereg.net), we identified several TEAD4-binding sites in the *Nfkbia* promoter region (-977–+34; Figure 17), assembled into two clusters.

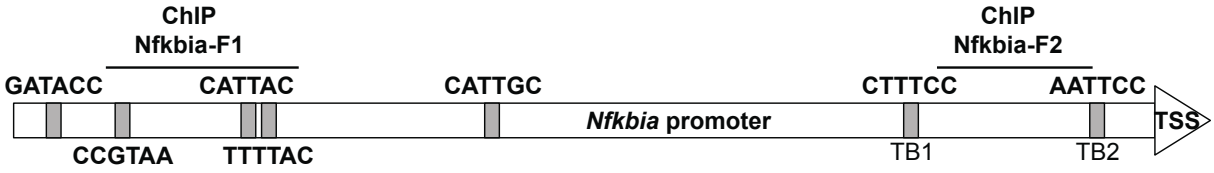

Figure 17. Scheme showing the YAP/TEAD4 binding sites in the *Nfkbia* promoter region (-977–+34, NM_010907).

Grey boxes represent the predicted TEAD4 binding sites, and the upper two lines show the ChIP-qPCR products, representing the different fragments (F1 and F2) in the ChIP primers. Two proximal binding sites were identified, named TB1 and TB2.

The promoter region was cloned into the pGL3-basic luciferase reporter vector, combining with the pRL-TK control luciferase vector, DLR assays were performed after TLR activation in Hepa1-6 and NCTC clone 1469 cell lines, following LPS treatment (10 μg/ml) that was supposed to induce TLR4-mediated innate immune response and YAP-mediated transcription of *Nfkbia*. For these mechanistic studies, LPS was used in place of HBV particles because the LPS-induced immune responses are comparable to that induced by HBV particles, as previously described[125]. After LPS treatment, the luciferase activity in both cell lines increased significantly compared with untreated cells (Figure 18A). To further investigate how the loss or gain of YAP function affects *Nfkbia*-driven luciferase activity, we first knocked down YAP with siRNA in Hepa1-6 cells, followed by transfection with the luciferase reporter vector. Luciferase activity decreased with increasing doses of siRNA (Figure 18B). Although the basal YAP level was quite high in the Hepa1-6 cell line, YAP was undetectable in the NCTC clone 1469 cell line (Figure 19); therefore, we decided to overexpress YAP in NCTC clone 1469 cells. Luciferase activity was

upregulated with increasing YAP expression (Figure 18B). To accomplish transcriptional activation, YAP must be able to form a transcription factor complex with TEAD4. VGLL4 is a competitive inhibitor of YAP that binds to TEAD, via the Tondu domain[170]. YAP, TEAD4, and VGLL4 were overexpressed together in the HEK293T cell line. Similar to the results observed in the NCTC clone 1469 cell line, the overexpression of YAP in the HEK293T cell line increased luciferase activity compared with the control group; however, luciferase activity did not increase when TEAD4 was overexpressed, which suggested that YAP is the limiting factor in YAP/TEAD4-mediated transcriptional activation. However, the combined overexpression of YAP and TEAD4 increased luciferase activity compared with the control group (Figure 18C). In contrast, luciferase activity was significantly decreased when either YAP or TEAD4 was overexpressed together with VGLL4 compared with the control group. Luciferase activity was particularly reduced, in a dose-dependent manner, when YAP and TEAD4 were overexpressed together with VGLL4 (Figure 18C). These results suggested that the YAP/TEAD4 transcription factor complex can promote *Nfkbia* expression by regulating its promoter activity.

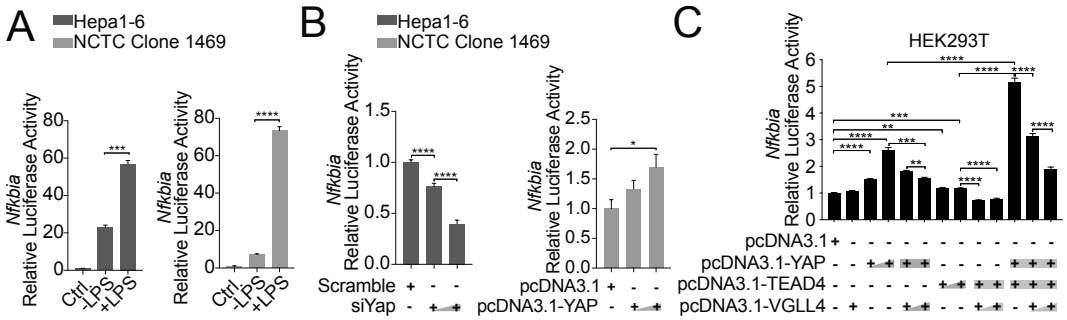

Figure 18. YAP/TEAD4 complex targets the *Nfkbia* promoter.

A. The luciferase reporter plasmid pGL3-Nfkbia was transfected into Hepa1-6 or NCTC clone 1469 cells for 12 hours, followed by LPS (10 μg/ml) treatment for 24 hours, and luciferase activity was measured. **B**. A dual-luciferase reporter (DLR) assay was performed to detect luciferase activity 48 hours after the knockdown of Yap (siYap) in Hepa1-6 cells or the overexpression of YAP (pcDNA3.1-YAP) in NCTC clone 1469 cells. **C**. A DLR assay was performed after the co-transfection of YAP, TEAD4, or VGLL4 overexpression plasmids and pGL3-Nfkbia in HEK293T reporter cells. Data sets are representative of at least three independent experiments. *p-value<0.05, **p-value<0.01, ***p-value<0.001, ****p-value<0.0001.

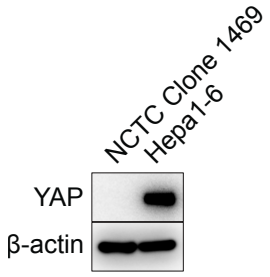

Figure 19. YAP expression levels in Hepa1-6 cells and NCTC Clone 1469 cells.
YAP expression levels in NCTC Clone 1469 and Hepa1-6 cell lysates were detected by Western blot. The YAP expression level is high in Hepa1-6 cells but extremely low in NCTC Clone 1469 cells.

ChIP assay was performed to determine whether the YAP/TEAD4 transcription factor complex interacts directly with the promoter region of *Nfkbia* and to identify which part of the promoter is bound by the complex. The entire promoter region was divided into two different clusters, fragment 1 and fragment 2, according to the distribution of TEAD4-binding sites (Figure 17). Two pairs of ChIP-qPCR primers for *Nfkbia* and control primers for *Ctgf,* which is a well-known YAP/TEAD4 target gene, were designed (Table 11). Hepa1-6 cells and NCTC Clone 1469 cells (1×10^7 cells) were harvested and fixed. Chromatin fragments of 200–1000 bp were generated by shearing with sonication. The TEAD4 antibody and Mouse-IgG antibody were incubated with the sheared chromatin fragments, to form agarose/TEAD4 antibody/TEAD4 protein/DNA fragment complexes, which were collected by a brief centrifugation step. Finally, the DNA fragments were purified and detected by quantitative PCR. The ChIP results, using *Ctgf* primers as a positive control and negative control primers that target to the coding region of *Nfkbia*, showed that TEAD4 was able to specifically bind to the *Ctgf* promoter in Hepa1-6 cells expressing high levels of YAP but not in NCTC 1469 cells expressing low levels of YAP (Figure 20A). The results of the ChIP assay performed with the negative control primers and a mock antibody (IgG) confirmed the quality of the ChIP assay results. When using specific primers for the *Nfkbia* promoter, the ChIP assay results indicated that

fragment 2 (F2) represents the primary segment of the promoter sequence that is responsible for complex regulation (Figure 20B).

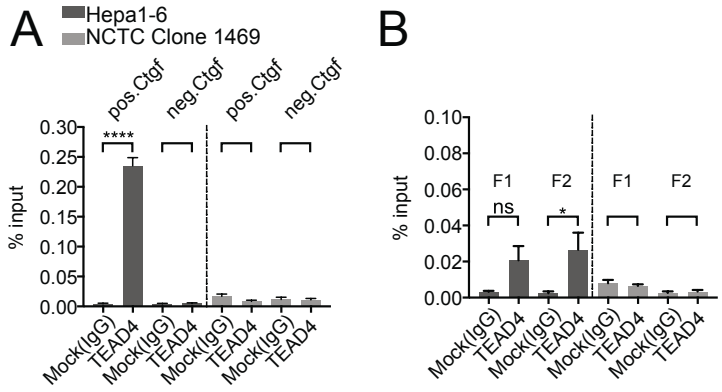

Figure 20. YAP/TEAD4 directly binds to the fragment 2 region of the *Nfkbia* promoter. Chromatin immunoprecipitation assay was performed to determine the interaction between TEAD4 and the *Nfkbia* promoter, using agarose-TEAD4 antibody and sonicated chromatin (200–1000 bp). By incubating agarose-conjugated antibody with sonicated chromatin, the TEAD4 antibody could bind to chromatin fragments cross-linked with TEAD4 proteins. The pulled-down chromatin fragments were purified and detected by quantitative PCR, using specific primers (Table 11). **A**. *Ctgf* positive and negative control primers were used for quality control of the ChIP assay. **B**. Specific primers targeting *Nfkbia* promoter were used for quantifying the pulled-down DNA fragments. Data sets are representative of at least three independent experiments. *p-value< 0.05, ****p-value< 0.0001, ns, not significant.

To confirm the interaction between the transcription factor complex and fragment 2, the TEAD4 protein was overexpressed and purified. EMSA indicated that no TEAD4-DNA complex formed with the negative control DNA fragment, which did not contain a TEAD4-binding site. *Nfkbia* fragment 2 and the *Ctgf* positive control fragment formed a complex with the TEAD4 protein, in a dose-dependent manner (Figure 21). The EMSA results confirmed the direct interaction between TEAD4 and the *Nfkbia* promoter.

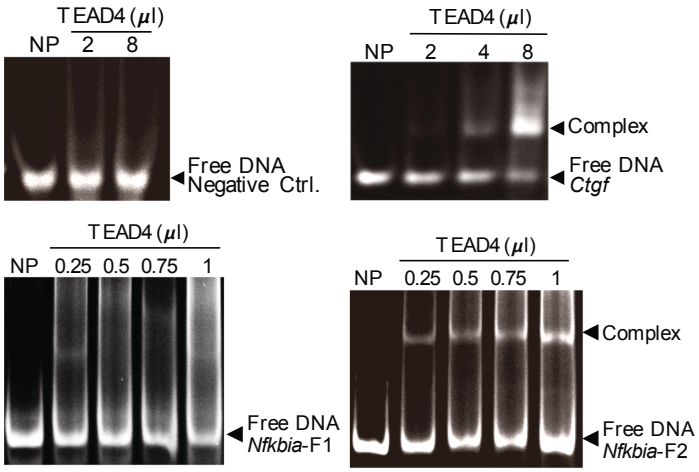

Figure 21. TEAD4 forms a protein/DNA complex with *Nfkbia*-F2.
Electrophoretic mobility shift assay was performed to show the direct interaction of the YAP/TEAD4 complex and *Nfkbia* promoter by incubating TEAD4 (10-40 μg) with PCR-generated DNA fragments (Table 14) and subsequently performing gel electrophoresis.

Because *Nfkbia* fragment 2 includes two TEAD4-binding sites, TB1 and TB2 (Figure 17), we further attempted to determine which binding site was responsible for binding with the YAP/TEAD4 complex. Each TEAD4-binding motif, along with a 50 bp flanking sequence on each side, was cloned into a pGL3-basic luciferase reporter vector, in addition to the *Ctgf* promoter binding sites that was also cloned into luciferase reporter vector as a positive control. A DLR assay demonstrated that TB2 is the dominant TEAD4-binding site in the *Nfkbia* promoter (Figure 22A). Furthermore, the luciferase activity of base substitution-mediated mutation of TB2 (mTB2) (Figure 22B) was significantly decreased compared with that of TB2 (Figure 22A). To further confirm this result, the sequences of TB2 and mTB2 were cloned into the RFP reporter vector. When YAP-GFP-overexpressing Hepa1-6 cells were transfected with the RFP reporter vectors, RFP expression was markedly decreased in the mTB2-expressing group compared with the TB2-expressing group (Figure 22C). RFP-positive cells were counted by flow cytometry, as shown in Figure 22D. The percentages of RFP-positive cells were 11.03% ± 4.37% in the mTB2 group and 38.97% ± 11.24% in the TB2 group. Taken together, these results illustrated that the YAP/TEAD4 transcription factor complex can directly bind to the TB2 TEAD4-binding

site, which is located proximal to the transcription start site, to promote *Nfkbia* expression.

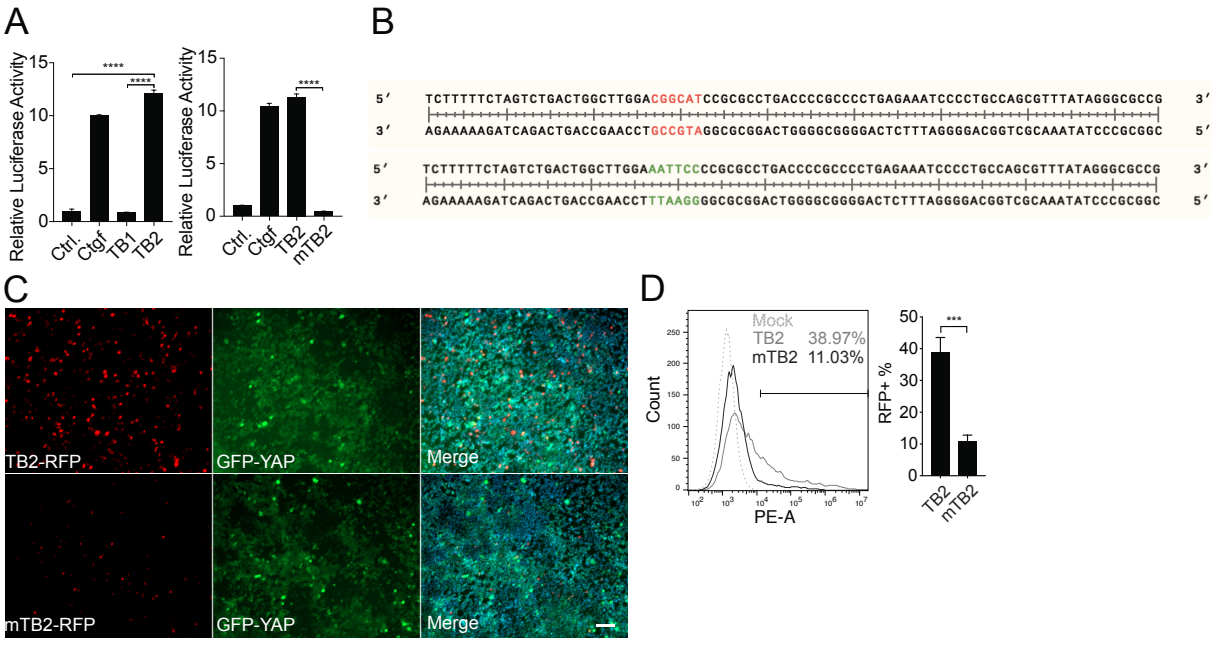

Figure 22. The YAP/TEAD4 complex directly binds to the TB2 binding site within *Nfkbia*-F2. **A**. Dual luciferase reporter assay was performed after cloning the TB1, TB2, and mutated TB2 (mTB2) binding sites into the reporter plasmid. **B**. WT TB2 and mutant TB2 sequence information. Location of mutation (-26 to -21) in the *Nfkbia* promoter region (-977 to +34). Red letters show the mutant TB2. Green letters show the wildtype TB2. **C**. The mutated TB2 binding site led to weak RFP signals in YAP-GFP-overexpressed Hepa1-6 cells. TB2 or mTB2 were cloned into an RFP reporter plasmid. Plasmids were transfected into YAP-GFP-overexpressing Hepa1-6 cells. After 48 hours, photos were obtained with an AxioObserver.Z1 Inverted Microscope (ZEISS). **D**. Flow cytometry was performed to detect RFP-positive cells, following the transfection of TB2- or mTB2-specific RFP reporter plasmids into YAP-overexpressing Hepa1-6 cells. Data sets are representative of at least three independent experiments. Scale bar is 100 μm. ***p-value<0.001, ****p-value<0.0001; TB, TEAD-binding site.

3.1.8 The TLR-MyD88-IRAK4-Hippo axis plays an important role in mouse liver immunity, *in vivo*

Our previous study indicated that hepatic immune induction occurs at barely detectable levels in humanised liver-chimeric mice infected with HBV[89]. To investigate the hepatic TLR-MyD88-IRAK4-Hippo axis, *in vivo*, HBV-induced innate immune responses were mimicked by the TLR2 ligand Pam3CSK4 (1 mg/kg bodyweight, intravenous injection), which was administered to 2-month-old mice for

different lengths of time (0, 1, 2, and 6 hours). After mouse liver collection and appropriate sample preparation, qPCR, Western blotting, and ICC staining were performed to validate the previous findings, *in vivo*. Quantitative PCR analysis demonstrated that the rapid immune response in the mouse liver occurred immediately following Pam3CSK4 injection, as indicated by sharp increases in *Il6*, *Tnf,* and *Il1β* expression levels (Figure 23A). Western blot analysis of whole-liver tissue lysates (Figure 23B) indicated that Pam3CSK4 treatment suppressed the phosphorylation of PP2A, 6 hours after treatment. The suppressed phosphorylation of MST1/2 was observed in two of three animals. However, YAP phosphorylation did not appear to be affected, whereas the phosphorylation of NF-κB was observed 6 hours after treatment. Interestingly, the initial downregulation of IκBα levels, followed by the subsequent further increase of these levels, 1-2 hours after treatment, was observed, which was consistent with the *in vitro* findings. The nuclear translocation of YAP and NF-κB was observed in fixed liver tissues, one hour after Pam3CSK4 administration, as assessed by ICC staining. After the first hour, both YAP and NF-κB were gradually excluded from the nucleus over time (Figure 23C).

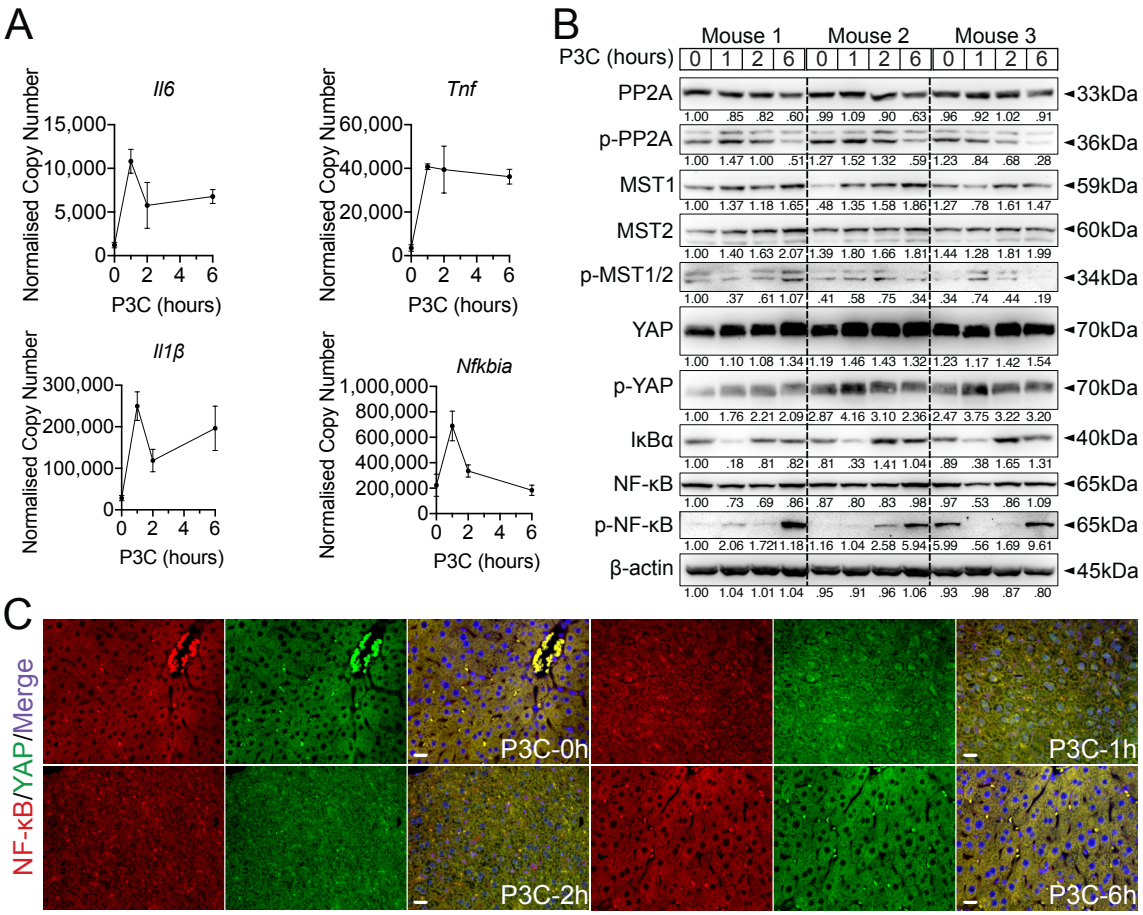

Figure 23. The Pam3CSK4-induced TLR-MyD88-IRAK4-Hippo axis plays an important role in innate immunity in the mouse liver.

A. Quantitative PCR was performed to detect hepatic *Il6*, *Tnf*, *Il1β,* and *Nfkbia* expression levels 0, 1, 2 and 6 hours after the injection of Pam3CSK4 (1 mg/kg body weight, i.v.) in 2-month-old male mice (group size n = 3). **B**. PP2A, phosphorylated PP2A, MyD88, MST1/2, phosphorylated MST1/2, YAP, phosphorylated YAP, IκBα, NF-κB, and phosphorylated NF-κB were analysed by Western blotting after Pam3CSK4 treatment. **C**. Immunocytochemical staining was performed to visualise the intracellular localisation of YAP (green) and NF-κB (red) at 0, 1, 2, and 6 hours after Pam3CSK4 treatment. Data sets are representative of at least three independent experiments. Scale bar, 20 μm. kDa, kilodalton.

In addition, LPS (2.5 mg/kg body weight, intraperitoneal injection) was also administered to 2-month-old mice, for different lengths of time. The qPCR data and the ICC staining results were consistent with those observed following Pam3CSK4 treatment, whereas the western blot results were not that clear to show the change of phosphorylated NF-κB (Figure 24A-C).

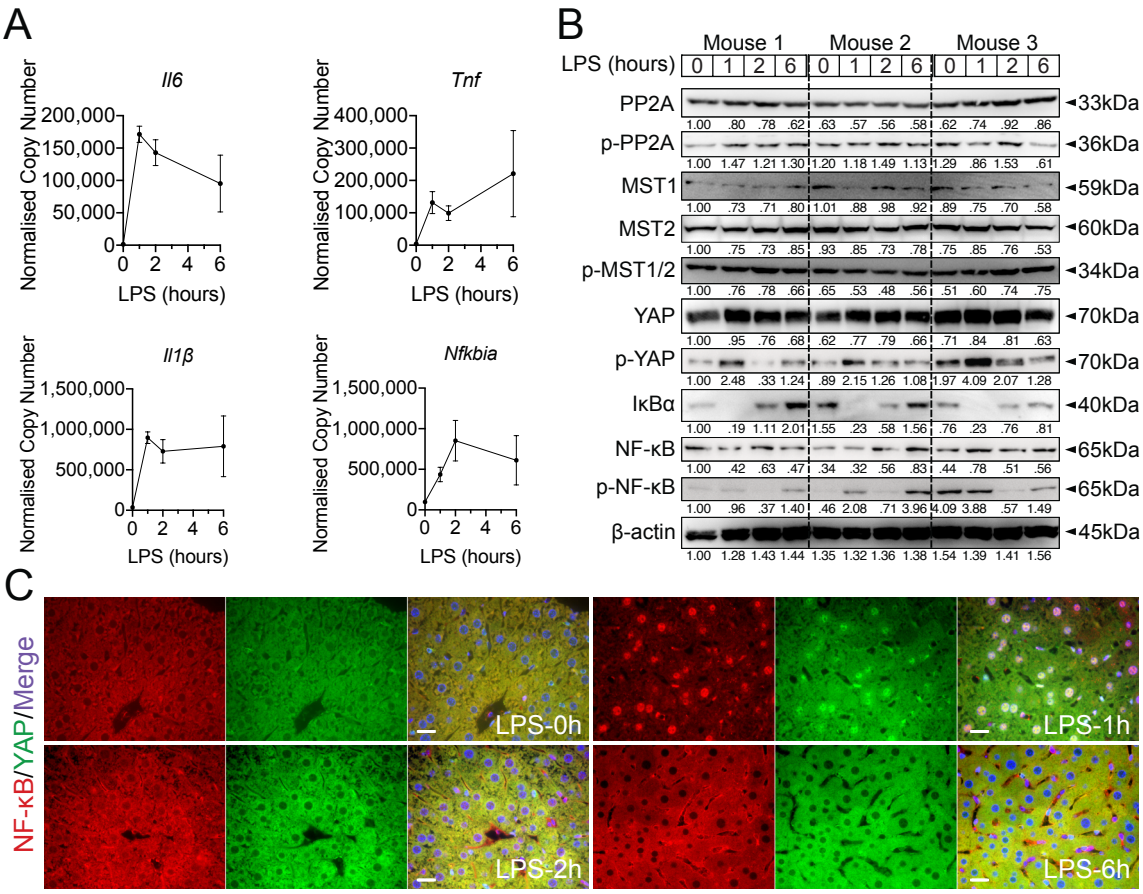

Figure 24. The LPS-induced TLR-MyD88-IRAK4-Hippo axis plays an important role in innate immunity in the mouse liver.

A. Quantitative PCR was performed to detect hepatic *Il6*, *Tnf*, *Il1β,* and *Nfkbia* expression levels 0, 1, 2, and 6 hours after the injection of LPS (2.5 mg/kg body weight, i.p.) in 2-month-old male mice (group size n = 3). **B**. PP2A, phosphorylated PP2A, MyD88, MST1/2, phosphorylated MST1/2, YAP, phosphorylated YAP, IκBα, NF-κB, and phosphorylated NF-κB were analysed by Western blotting, after LPS treatment. **C**. Immunocytochemical staining was performed to visualise the intracellular localisation of YAP (green) and NF-κB (red) at 0, 1, 2, and 6 hours after LPS treatment. Data sets are representative of at least three independent experiments. Scale bar, 20 μm. kDa, kilodalton.

The early nuclear translocation of both NF-κB and YAP was clearly indicated by ICC staining, 1 hour after both Pam3CSK4 and LPS treatment; however, cytosolic protein fractions could still be detected (Figures 23C and 24C). This subcellular distribution and the possibility that not 100% of liver cells were fully activated after the i.v. injection of TLR ligands might explain the weak changes observed during the western blot analysis of total liver tissue. However, the obtained *in vivo* results

supported our hypothesis that the TLR-MyD88-IRAK4-Hippo axis is important for the rapid, innate immune response in the liver.

3.1.9 TLR-MyD88-IRAK4-Hippo axis is important in PHHs

To validate whether these findings in mice are also applicable to humans, we isolated PHHs from resected human livers. The PHHs were exposed to HBV particles or non-particle control vehicle, for different lengths of time. Compared with those in the untreated group and the non-particle control group, the *IL6*, *TNF*, *IL1B*, *CTGF,* and *NFKBIA* gene expression levels increased after HBV particle exposure, at the very early stage (Figure 25A). Western blotting confirmed a slight decline in PP2A and MST1/2 expression levels, 2 hours after HBV infection. Phosphorylated YAP sharply declined after 1 hour, and phosphorylated NF-κB appeared as early as 30 min after treatment with HBV particles (Figure 25B). Similar to the results obtained in PMHs, in PHHs, the very early disappearance of IκBα and its immediate rebound indicated rapid immune regulation. The mechanism that mediates this instant disappearance of IκBα remains an open question that requires further investigation.

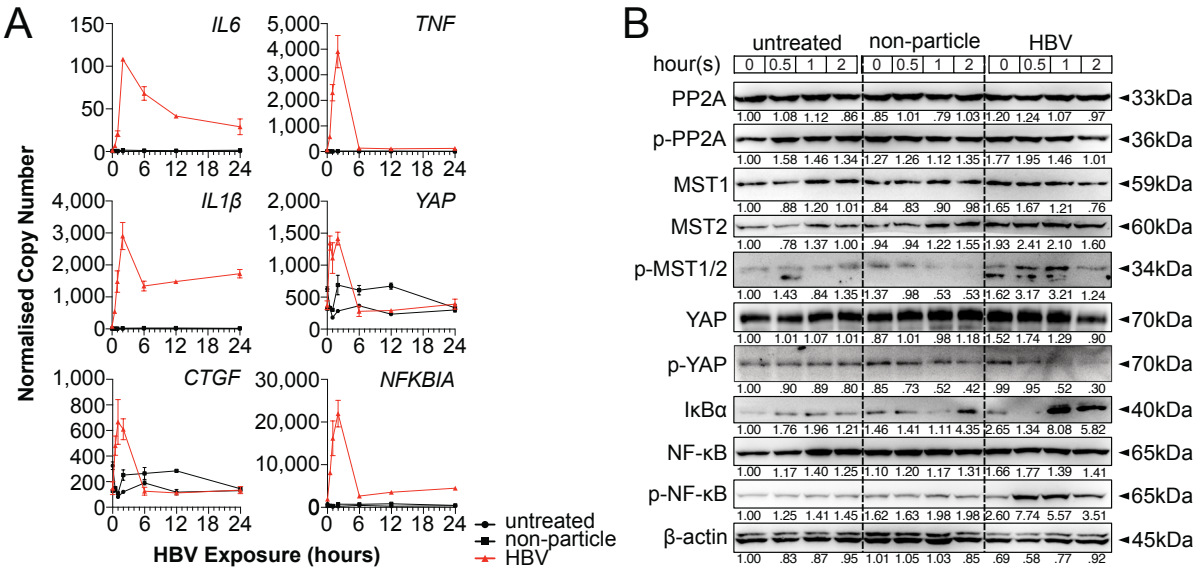

Figure 25. HBV particle exposure induces the activation of the TLR2-MyD88-IRAK4-Hippo axis in PHHs.

Primary human hepatocytes (PHHs) from four different donors were treated with cell culture-derived HBV (MOI of 1000), for different lengths of time. **A**. The gene expression of *IL6*, *TNF*, *IL1B*, *YAP*, *CTGF,* and *NFKBIA* was determined by quantitative PCR (normalised against *ACTB*, mean ± SEM). **B**. Western blotting was performed to determine the expression levels of PP2A, phosphorylated PP2A, MyD88, MST1/2, phosphorylated MST1/2, YAP, phosphorylated YAP, IκBα, NF-κB, and phosphorylated NF-κB after the exposure of PHHs to HBV. Data sets are representative of at least three independent experiments. kDa, kilodalton.

Finally, ICC staining illustrated that HBV particles were recognised by PHHs and induced YAP and NF-κB nuclear translocation to regulate the rapid, innate immune response, after 1 hour of HBV exposure (Figure 26). These results further indicated that the TLR-MyD88-IRAK4-Hippo axis also plays an important role in the recognition of HBV particles in human hepatocytes and regulates the rapid, innate immune response by activating NF-κB and Hippo signalling.

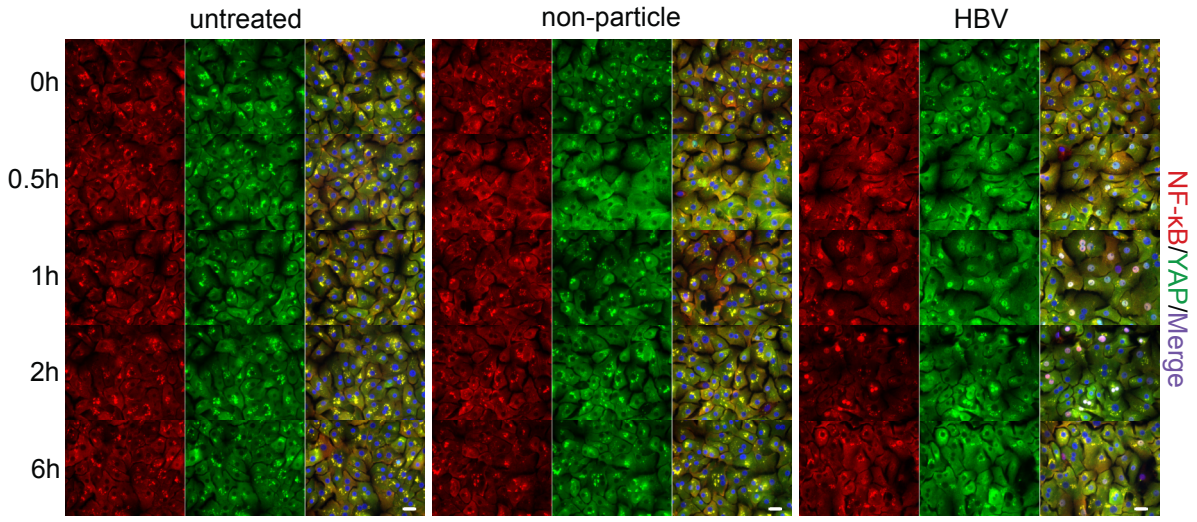

Figure 26. HBV particle exposure induces the nuclear translocation of YAP and NF-κB in PHHs.

Primary human hepatocytes (PHHs) from four different donors were treated with cell culture-derived HBV (MOI of 1000), for different lengths of time, on collagen I-coated coverslips. After fixation and permeabilisation, immunocytochemical staining was performed, using primary and fluorophore-conjugated secondary antibodies, to visualise the intracellular localisation of YAP (green) and NF-κB (red). Data sets are representative of at least three independent experiments. Scale bar, 20 μm.

3.1.10 TLR-MyD88-IRAK4-Hippo axis activation partially explains the situation in chronic HBV-infected patients

The above findings were performed in models mimicking acute HBV infection. Next, the relevance of the TLR2-MyD88-IRAK4-Hippo axis was investigated in CHB patients. The ChIP dataset GSE83148[171], which included liver biopsy samples from 122 CHB patients and 6 uninfected controls, was reanalysed by GSEA, using hallmark, Kyoto Encyclopedia of Genes and Genomes (KEGG), and oncogenic gene sets from the Molecular Signatures Database (v7.0), which indicated significant alterations in TLR signalling, NF-κB signalling, the inflammatory response, and YAP signalling (Figure 27A). The gene expression levels of factors associated with the TLR2-MyD88-IRAK4-Hippo axis were compared between CHB and control samples (Figure 27B). Interestingly, hepatic *TLR2* but not *TLR4* was upregulated in CHB patients. Moreover, the expression level of *STK4* (the gene encoding MST1) was significantly correlated with the expression levels of *TLR2*, *NFKB1,* and *IL1B* (Figure 27C). An intracellular effector of TLR2 signalling, *MYD88,* was upregulated in CHB patients, although *IRAK4* was not. The relative expression levels of *NFKB1*, *RELA, IL6,* and *IL1B* also increased in the CHB group. The expression level of *STK4* (the gene encoding MST1) was upregulated, whereas the expression levels of *PPP2CA* (the gene encoding PP2A), *STK3* (the gene encoding MST2), and *YAP* were not affected. The expression levels of the YAP/TEAD response genes *CTGF* and *NFKBIA* also did not differ between CHB and control patients (Figure 27B). These

findings suggested that hepatic TLR2 activation and NF-κB signalling may occur in CHB patients.

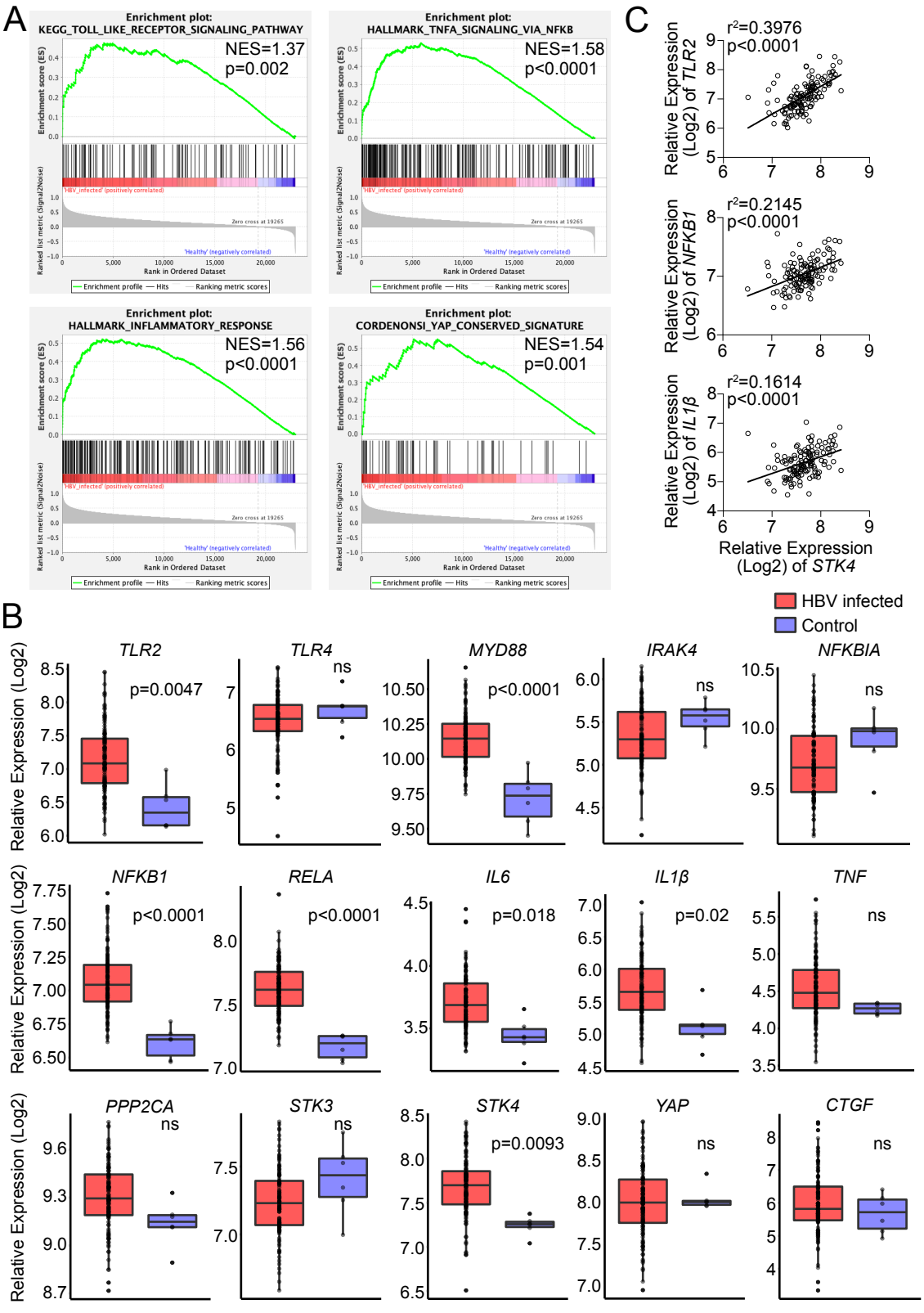

Figure 27. Hepatic gene expression signatures in chronic HBV-infected patients support the relevance of the TLR2-MyD88-IRAK4-Hippo axis during HBV infection.
A. The GSE83148 data set (122 HBV-infected, 6 controls) was reanalysed to perform GSEA. Significant gene enrichment could be shown for TLR signalling (KEGG), NF-κB signalling, inflammatory responses (Hallmark), and the YAP signature (CORDENOSI). **B**. In addition, the relative expression levels of genes associated with TLR signalling (*TLR2, TLR4, MYD88, IRAK4, NFKBIA NFKB1, RELA, IL6, IL1B,* and *TNF)* and Hippo signalling (*PPP2CA, STK3, STK4, YAP,* and *CTGF*) were compared between these two groups. **C**. Correlation analysis between the *STK4* expression level (Spearman's) and the *TLR2*, *NFKB1,* and *IL1B* expression levels was performed. ns, not significant.

To further examine the role played by the TLR2-MyD88-IRAK4-Hippo axis during different phases of CHB, another GEO data set, GSE65359[172], was analysed, comparing the different phases of chronic HBV infection. The *TLR2*, *MyD88*, *IL1B,* and *STK4* expression levels were significantly elevated during the immune-clearance phase compared with those in the immune-tolerant phase and the inactive-carrier phase (Figure 28). These data indicated that the TLR2-MyD88-IRAK4-Hippo axis was activated during the immune-clearance phase. Although GSEA of GSE83148[171] showed the enrichment of Hippo/YAP-associated genes in CHB patients (Figure 27A), Hippo pathway activity, as indicated by *CTGF* and *NFKBIA* gene expression, was not observed in GSE65359. This finding might be explained by the significantly elevated expression of *STK4* (MST1), as MST1 cytoplasmic activity can inhibit YAP/TEAD transcriptional activity. Interestingly, the expression level of *STK4* was significantly correlated with those of *TLR2*, *NFKB1,* and *IL1B* (Figure 27C). This observation indicated that although TLR2 activation appears to occur during the immune-active phase of HBV infection, additional regulatory mechanisms may control the TLR2-MyD88-IRAK4-Hippo axis, *in vivo*, preventing inopportune Hippo pathway activity. As increasingly advanced tissue culture systems are developed, microtome slices from biopsies or resections could be utilised to perform HBV-related *ex vivo* studies in the future.

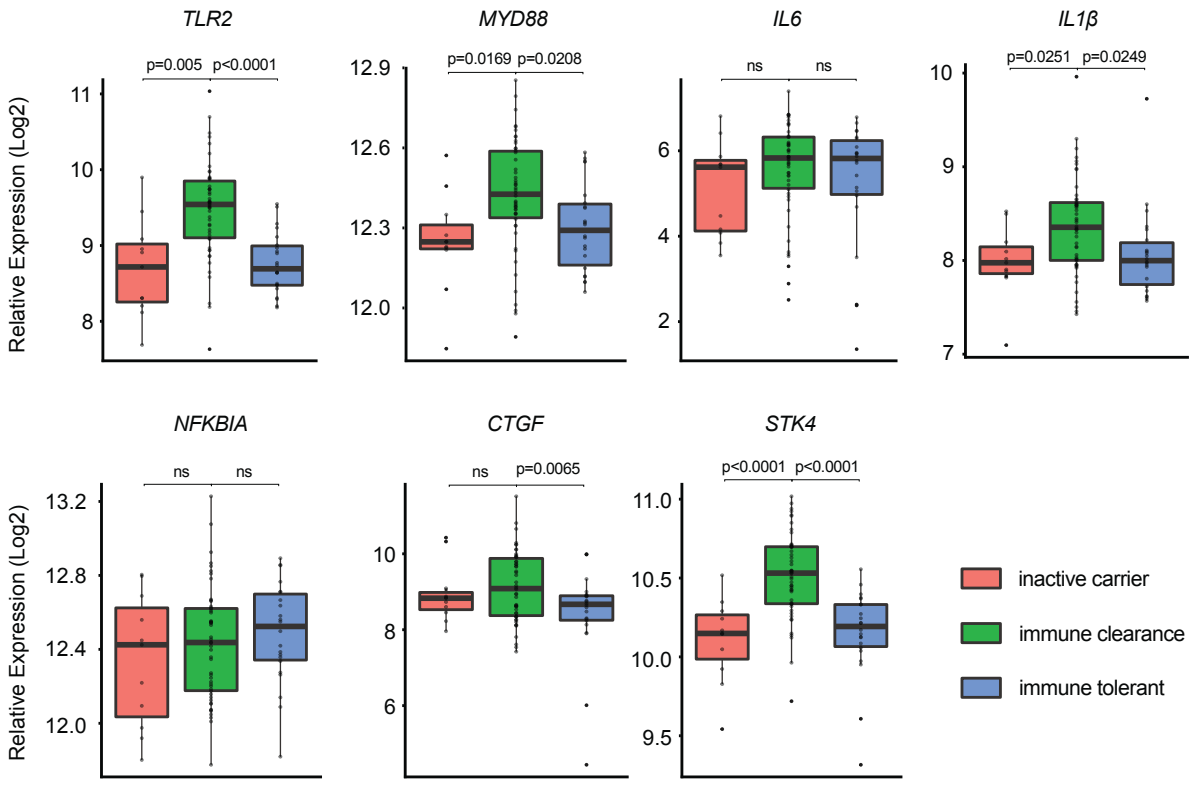

Figure 28. The *TLR2-MYD88-STK4* axis is activated during the immune-clearance phase of chronic HBV infection.

The GSE65359 data set was reanalysed to examine the relative expression levels of genes. The data set included 83 chronic hepatitis B patients (22 immune-tolerant, 50 immune-clearance, and 11 inactive-carrier state). The *TLR2*, *MYD88*, *IL6*, *IL1B*, *NFKBIA*, *CTGF,* and *STK4* mRNA levels were determined for each group. ns, not significant.

Whether HBV activates innate immunity or represses innate host defences continues to be debated. The Hippo pathway, which is known for growth control, has been suggested to play a vital role in immune regulation. Here, we comprehensively investigated the interaction between HBV-triggered innate immunity and Hippo signalling. The reanalysis of the GSE69590[90] gene array of HBV-infected PHH samples identified HBV-related changes in Hippo and NF-κB signalling. Immunocytochemical staining and Western blot analysis revealed the time-dependent nuclear translocation of YAP and NF-κB in HBV-exposed PMHs. The inhibition of TLR2 and MST1/2 highlighted a potential role for TLR2 and Hippo signalling in HBV-induced immunity. The results of loss- and gain-of-function experiments implied that YAP directly regulated IκBα expression. Functional investigations confirmed the regulation of *Nfkbia* promoter activity by the YAP/TEAD4

transcription factor complex. Furthermore, the administration of Pam3CSK4 to mice and the exposure of PHHs to HBV demonstrated the relevance of the TLR2-MyD88-IRAK4-Hippo axis for the activation of HBV-induced innate immunity. Interestingly, the reanalysis of GSE83148[171] indicated the hepatic activation of TLR2; however, Hippo activity in patients with chronic HBV infections appeared to be controlled by an additional, so far unknown mechanism.

3.2 HBsAg-mediated inactivation of Hippo signalling results in the accumulation of YAP and BMI1, contributing to HCC development by affecting the cell cycle and chromosomal instability

3.2.1 HBsAg-transgenic mice develop hepatocellular carcinoma

Transgenic mice expressing HBsAg (Tg[Alb-1HBV]Bri44; Alb/HBs) overexpress all HBV envelope proteins, as described elsewhere[136]. The overproduction of the HBV envelope polypeptide and the accumulation of toxic HBsAg in hepatocytes results in severe and prolonged hepatocellular injury, which triggers a programmed response within the liver[136]. This hepatocellular injury is characterised by inflammation, regenerative hyperplasia, transcriptional dysregulation, and aneuploidy[136]. The incidence of HCC in this transgenic mouse model is associated with sex, as almost 100% of male transgenic mice develop HCC starting at the age of 8 months[136]. Numerous tumours can be observed on the livers of HBsAg-transgenic mice at 12 months (Figure 29).

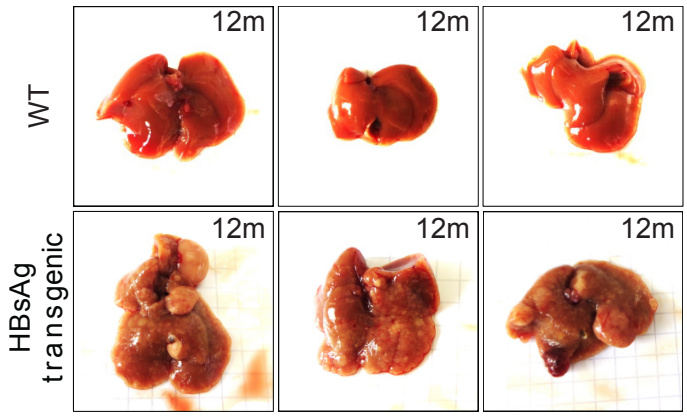

Figure 29. Hepatocarcinogenesis occurs in HBsAg-transgenic mice.
Mouse livers were harvested from 12-month-old WT and HBsAg-transgenic mice, and washed in PBS several times to remove blood. Cleaned livers were transferred into a 10 cm petri dish for imaging.

3.2.2 Characterisation of abnormal gene expression patterns in HBsAg-transgenic mice

To determine the abnormal gene expression pattern that correlates with HBsAg overexpression, microarray data (GSE84429, Liang K., 2012), generated from WT and HBsAg-transgenic mouse liver samples, were reanalysed by GSEA. The significant enrichment of YAP-associated genes, DNA repair-associated genes, protein serine-threonine kinase activity-associated genes, cell cycle-associated genes, DNA replication-associated genes, and centrosome-associated genes were observed for HBsAg-transgenic mice compared with WT mice (Figure 30). The enrichment results suggested that YAP target genes were upregulated in HBsAg-transgenic mice compared with WT mice, which implied the inactivation of Hippo signalling. Furthermore, DNA replication- and cell cycle-associated gene enrichment suggested increased cell proliferation, whereas DNA repair- and centrosome-associated gene enrichment suggested the existence of DNA damage and chromosomal instability. Interestingly, protein serine-threonine kinase activity-associated gene enrichment indicated the frequent protein phosphorylation.

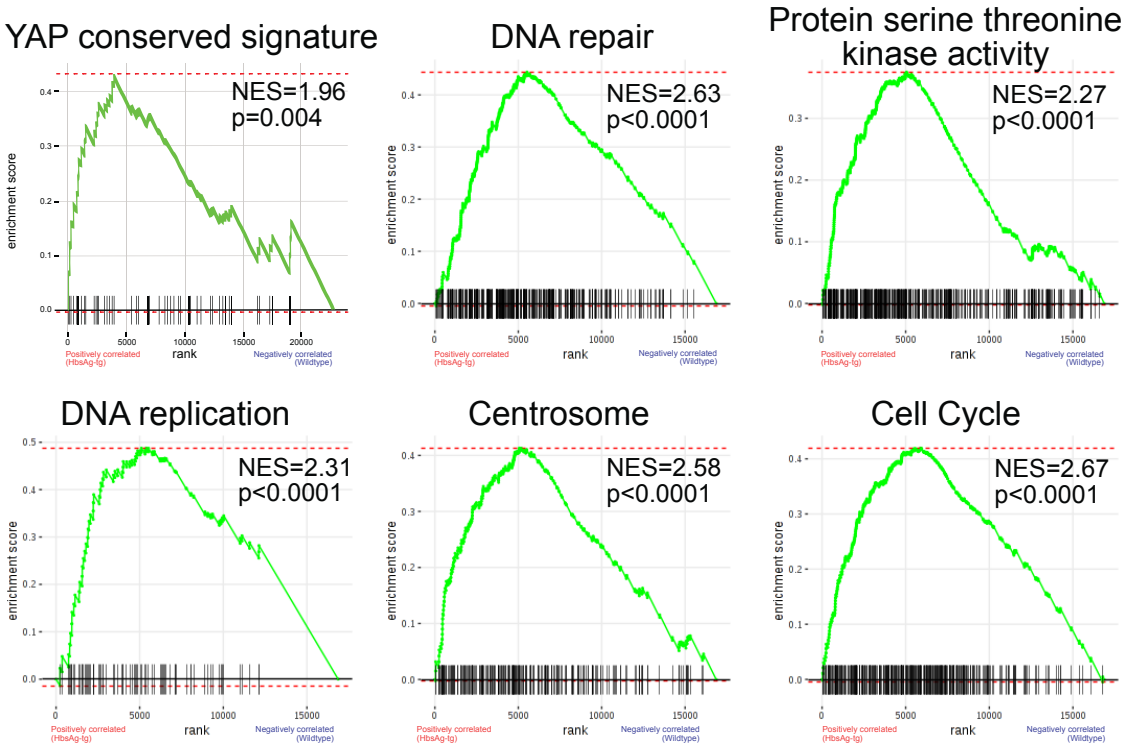

Figure 30. GSEA reanalysis of GSE84429 microarray data.
GSEA analysis was performed, comparing WT and HBsAg-transgenic mice. The results indicated that YAP-associated genes, DNA repair-associated genes, protein serine-threonine kinase activity-associated genes, cell cycle-associated genes, DNA replication-associated genes, and centrosome-associated genes were enriched in HBsAg-transgenic mice. All enrichment plots suggested correlations among HBsAg overexpression and YAP activation, cell proliferation, DNA damage, and chromosomal instability.

3.2.3 The Hippo signalling pathway is inactivated in HBsAg-transgenic mice

YAP is a crucial effector, downstream of the Hippo signalling pathway. Because YAP-associated genes were upregulated in HBsAg-transgenic mice, the key components of the Hippo signalling pathway might be expressed abnormally in these mice. Therefore, the *Stk3* and *Stk4* expression levels (code for MST2 and MST1) were determined in WT mice (n = 19) and HBsAg-transgenic mice (n = 27), by qPCR. Both of these genes were downregulated in transgenic mouse livers (Figure 31), which indicated that the Hippo signalling pathway was suppressed, by a yet unknown mechanism in these transgenic mice.

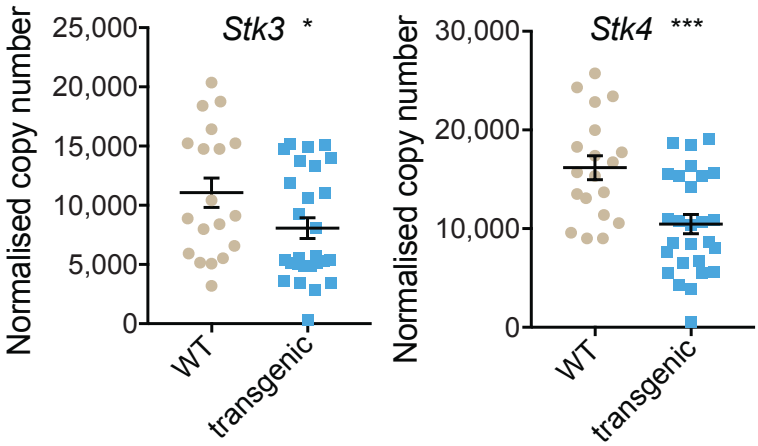

Figure 31. *Stk3* and *Stk4* expression levels are decreased in transgenic mice.
Mouse liver samples were collected from 19 WT and 27 transgenic mice. Total RNA isolation was performed immediately after sample collection, with Qiazol reagent. After reverse transcription was performed, quantitative PCR was performed to detect the mRNA levels of *Stk3* and *Stk4* in WT and transgenic mice. *p-value< 0.05, ***p-value< 0.001.

To further examine the pathogenesis in HBsAg-transgenic mice, the expression patterns of HBsAg and YAP were examined in transgenic mouse livers using HE and

immunohistochemical staining, to visualise all of the changes that occur during different stage of hepatocarcinogenesis. HE staining revealed changes in nuclear morphology, which included the increased incidence of nuclear inclusion in transgenic mice, which has been reported to be strongly associated with tumorigenesis[173]. The IHC staining of HBsAg and YAP showed that transgenic mice continued to produce HBsAg and upregulate YAP expression, over time (Figure 32). These staining results suggested that YAP activation might be linked to abnormal nuclear morphology.

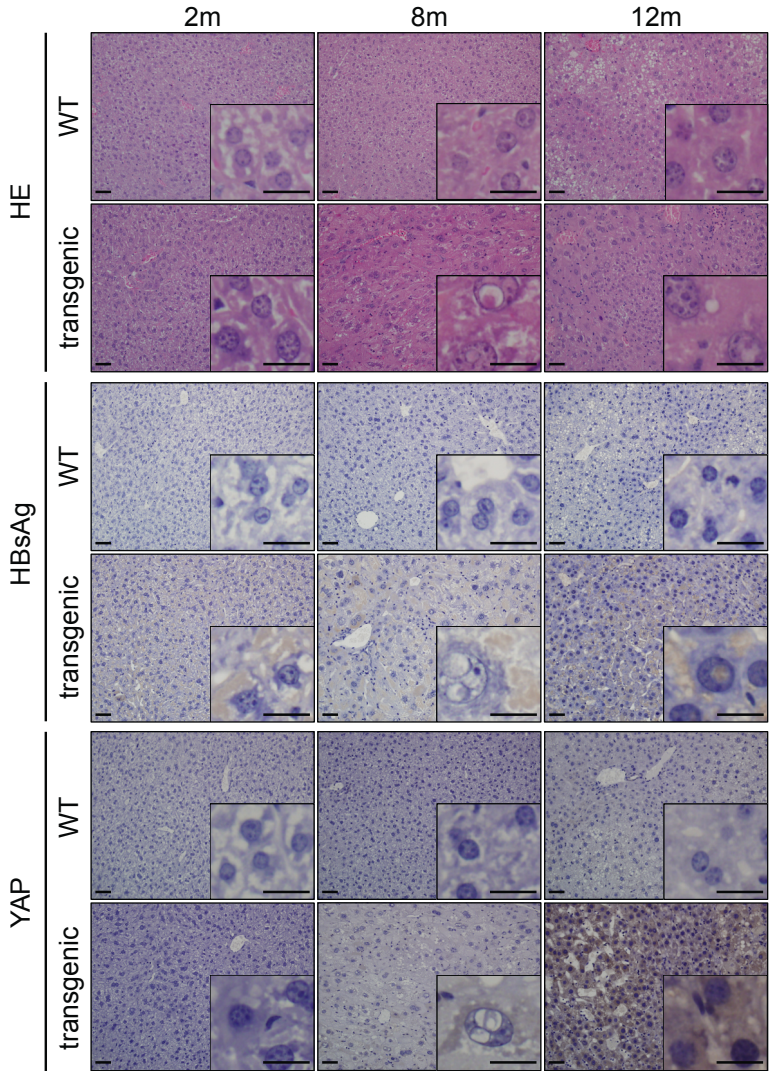

Figure 32. Pathological changes and YAP expression changes could be observed during different stage of hepatocarcinogenesis in HBsAg-transgenic mice.

Mouse liver samples from WT and transgenic mice were collected and embedded in paraffin, at 2 months, 8 months, and 12 months. HE staining was performed, to demonstrate the pathological

changes that occur in the transgenic mouse liver, particularly changes to nuclear morphology. The IHC staining of HBsAg showed that transgenic mice continually overexpress HBsAg in the liver. The IHC staining of YAP showed that YAP was upregulated during the mouse growth. Scale bar, 20 μm.

To further study the nuclear structure in hepatocytes, immunofluorescence staining with Ki67 was performed in WT and transgenic liver sections, to visualise cell proliferation and cell division. As shown in Figure 33A, abnormal chromatid separation during mitosis was observed in transgenic mice, which was indicated by the observation of unpaired chromatids and centrosomes, suggesting the generation of aneuploidy. Therefore, PMHs were isolated from WT and transgenic mice, and DNA content analysis was performed by flow cytometry. As shown in Figure 33B, polyploidy and aneuploidy were markedly increased in transgenic mice compared with WT mice. Taken together, the inactivation of the Hippo signalling pathway promoted the increased nuclear translocation of YAP, which might play certain roles in the formation of polyploidy and aneuploidy in transgenic mice.

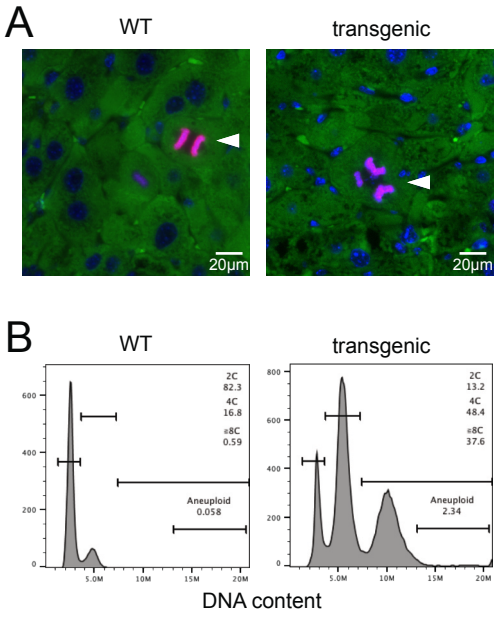

Figure 33. Polyploidy and aneuploidy are increased in transgenic mice.
A. Immunofluorescence staining was performed in moue liver sections, using the Ki67 antibody to visualise the nucleus, which revealed unpaired chromatids and centrosomes. **B**. PMHs were isolated from WT and HBsAg-transgenic mice and stained with Hoechst 33342 (10 μg/ml), for 20 min at 37°C. Flow cytometry was subsequently performed to analyse the DNA content of PMHs.

3.2.4 The inactivation of Hippo signalling results in the nuclear accumulation of YAP and BMI1, leading to cell aneuploidy, chromosomal instability, and cell proliferation

Our previous work showed that BMI1 is upregulated in HBsAg-transgenic mice[125]. As an oncogene, BMI1 has been shown to silence tumour suppressor genes, protect cells from apoptosis, by suppressing $p16^{INK4a}$ and $p19^{ARF}$, promote the epithelial-mesenchymal transition, and induce telomerase activity[174]. BMI1 has also been associated with DNA damage and repair processes[174]. Based on these known functions, IHC staining was performed against BMI1, Ki67, and alpha-fetoprotein (AFP), in both WT and transgenic mouse sections. As shown in Figure 34, BMI1 was upregulated in transgenic mouse liver with mice growth, as well as Ki67. The liver tumour marker AFP was upregulated significantly through the age of 12 months in transgenic mice. The inactivation of the Hippo signalling pathway plays a crucial role in the cell cycle, tumorigenesis, and chromosome instability[175]. The inhibition of MST1/2, which are key components of the Hippo pathway, has been hypothesised to induce cell polyploidy and aneuploidy in hepatocytes. Therefore, PMHs were isolated from WT mice and treated with XMU-MP-1 (an MST1/2 inhibitor, 5 μM), for 48 hours. After treatment, DNA content analysis was performed. As shown in Figure 35, consistent with the hypothesis, the inactivation of the Hippo signalling pathway induced both polyploidy and aneuploidy.

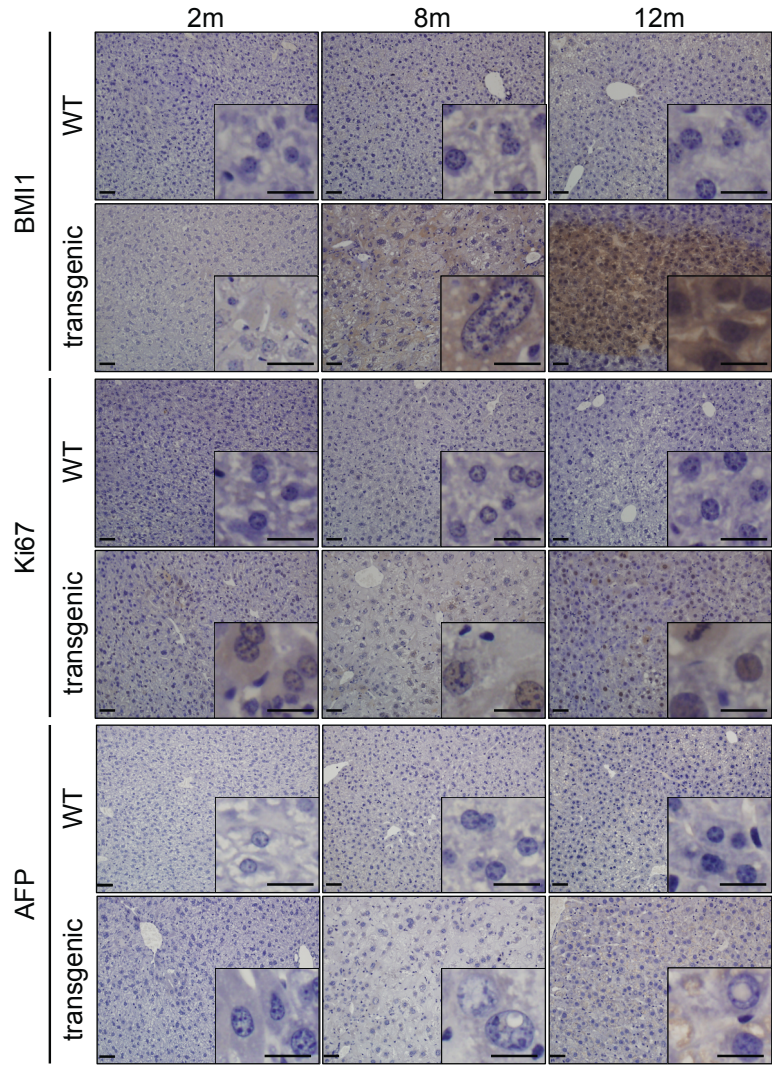

Figure 34. BMI1 is upregulated and associated with cell proliferation and hepatocarcinogenesis.

Mouse liver samples from WT and HBsAg-transgenic mice were collected and embedded in paraffin, at 2 months, 8 months, and 12 months. IHC staining of BMI1, Ki67, and AFP showed changes in their expression patterns at different time points during hepatocarcinogenesis.

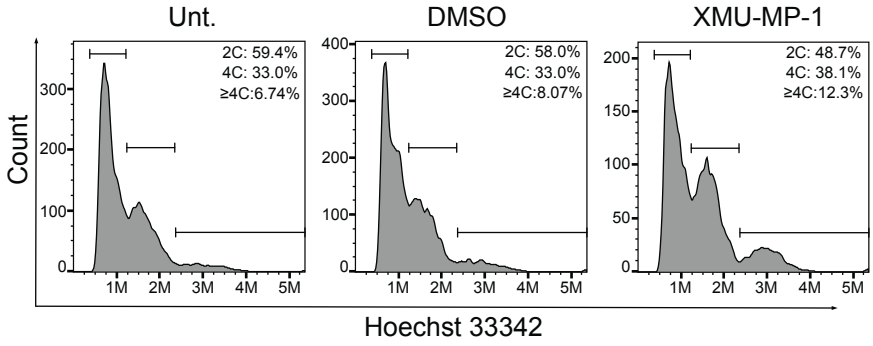

Figure 35. XMU-MP-1 induces polyploidy and aneuploidy.
PMHs isolated from a WT mouse were treated with XMU-MP-1 (5 μM) or the same volume of DMSO, for two days. After treatment, PMHs were collected and stained with Hoechst 33342 (10 μg/ml), for 20 min at 37°C, to perform DNA content analysis.

To confirm the above findings, proteins associated with Hippo signalling, BMI signalling, the cell cycle, DNA damage, and cell proliferation were analysed in WT and HBsAg-transgenic PMHs. PMH lysates from WT and transgenic mice were investigated by western blot analysis. As shown in Figure 36A three forms of HBsAg were expressed in HBsAg-transgenic mice. MST1/2 and MOB1 were suppressed in transgenic mice, whereas phosphorylated YAP was markedly downregulated and total YAP was slightly upregulated (Figure 36B). Here, cleaved MST1/2 indicated the MST activity, these forms were totally lacking in HBsAg-transgenic mice. All of these changes in the Hippo signalling pathway indicated the inactivation of Hippo signalling, resulting in the nuclear translocation of YAP. Interestingly, the molecular weights of LATS1/2 differed between WT and transgenic mice, which suggested that LATS1/2 might interact with other proteins and form a complex. Because the presence of HBsAg was the only difference between WT and transgenic mice, LATS1/2 has been hypothesised to interact with HBsAg, forming a complex associated with the dysfunction of LATS1/2 and the phosphorylation of YAP. BMI1 was upregulated in transgenic mice compared with WT mice, which was consistent with the IHC staining results (Figure 34), whereas $p16^{INK4a}$ and $p19^{ARF}$, which are downstream of BMI1, were both downregulated. Without the functions of $p16^{INK4a}$ and $p19^{ARF}$, p53 was further downregulated, whereas cyclin D1 was upregulated, to promote cell proliferation, which was further confirmed by the decreased expression of Caspase 3 in transgenic mice relative to WT mice (Figure 36C). The histone γH2AX is a maker of DNA damage[176] and was found to be induced in transgenic mice (Figure 36C). All of these results suggested that the HBsAg-mediated inactivation of the Hippo signalling pathway resulted in the accumulation of YAP and BMI1 in the nucleus, which might associate with cell polyploidy and aneuploidy, chromosome instability and cell proliferation.

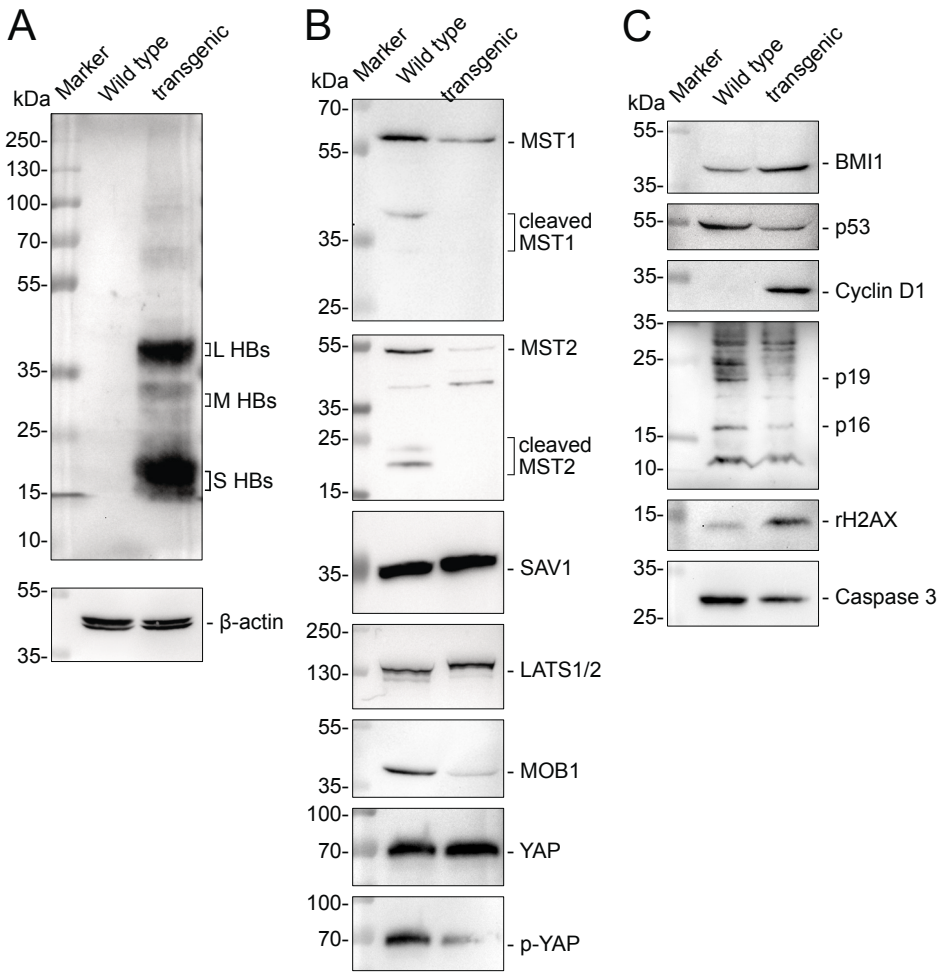

Figure 36. The nuclear accumulation of YAP and BMI1 lead to cell proliferation and DNA damage.

Primary murine hepatocytes were isolated from WT and HBsAg-transgenic mice and lysed with RIPA buffer. Western blot was performed to detect the expression levels of **A**. HBsAg; **B**. Hippo signalling components (MST1/2, cleaved MST1/2, SAV1, LATS1/2, MOB, YAP and phosphorylated YAP); **C**. BMI1 and its downstream effectors (p53, p16, p19, Cyclin D1), γH2AX and Caspase 3.

3.2.5 YAP-induced BMI1 promotes cell proliferation.

Because YAP and BMI1 were synchronistical upregulated in HbsAg-transgenic mice and the YAP/TEAD4 transcription factor complex is an effector of the Hippo signalling pathway, *Bmi1* has been suggested to be a potential target gene of YAP. The overexpression or knockdown of YAP in Hepa1-6 cells was associated with the respective up- or downregulation of BMI1 expression (Figure 37A and B), which indicated the regulation of *Bmi1* by YAP. To further study the functions of BMI1, the BMI1 overexpression plasmids that overproduce GFP-fused BMI1 were transfected

in Hepa1-6 cells for 48 hours. As shown in Figure 37C, upregulated BMI1 increased the expression of Cyclin D1 which is a marker for transition between G1 and S phase.

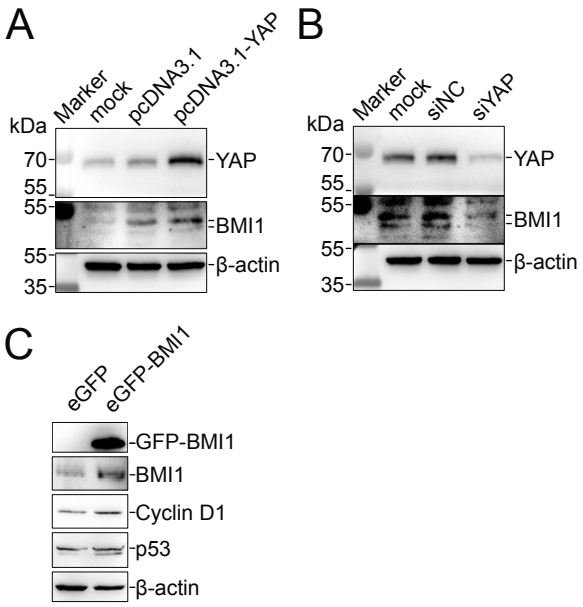

Figure 37. The gain- and loss-of-function of YAP regulate BMI1 expression.
YAP was either overexpressed or knocked down in Hepa1-6 cells by the transfection of overexpression plasmids or siRNAs targeting YAP, respectively. After 48 hours of transfection, cells were collected for western blot analysis. **A**. YAP and BMI1 expression levels were detected in Hepa1-6 cells after the overexpression of YAP. **B**. YAP and BMI1 expression levels were detected in Hepa1-6 cells after the knockdown of YAP. **C**. GFP-fused BMI1 was overexpressed in Hepa1-6 cells, to validate the effects of BMI1 on the cell cycle. The data sets are representative of at least three independent experiments. kDa, kilodalton.

To confirm this transcriptional regulation of the *Bmi1* promoter, the same shRNA subclones and analysis methods described in section 3.1.6 were used for the following experiments. As shown by fluorescent imaging (Figure 38A), the RFP expression levels, indicating *Bmi1* promoter activity (red), were clearly suppressed in YAP- and TEAD4-knockdown cells (green), which was confirmed by counting RFP-positive cells through flow cytometry (Figure 38B). These results suggested that the YAP/TEAD4 transcription factor complex might regulate *Bmi1* expression to promote cell proliferation.

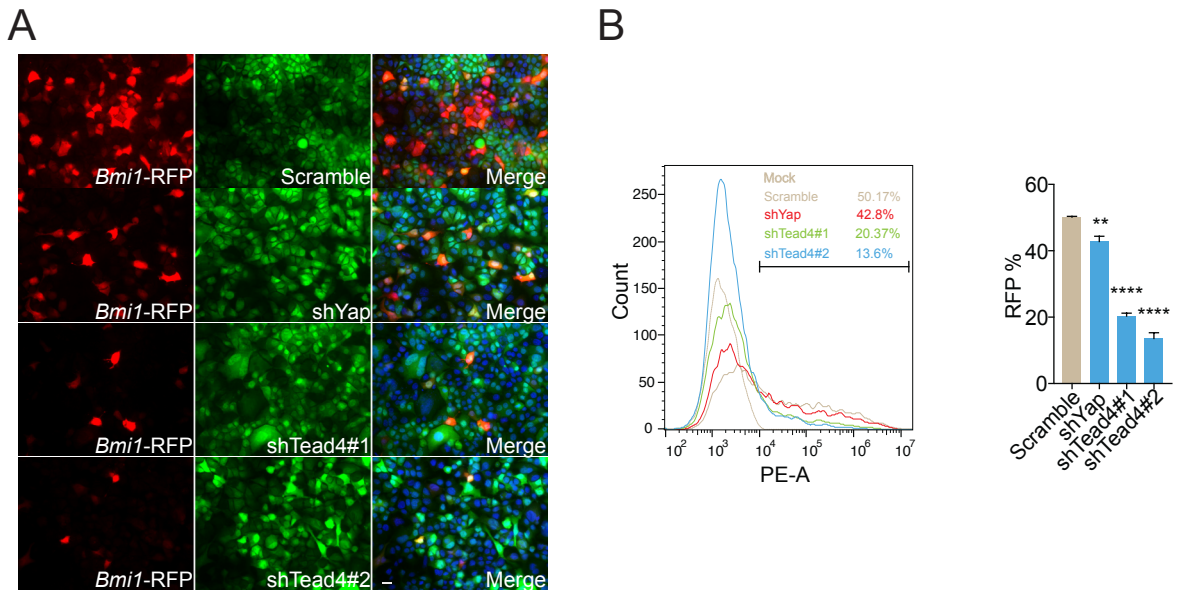

Figure 38. The YAP/TEAD4 complex might interact with the *Bmi1* promoter.
Hepa1-6 cells that were stably transfected with GFP-expressing shRNA plasmids (Scramble, Yap, and Tead4) were co-transfected with the RFP reporter plasmid, to assess *Bmi1* promoter activity. **A**. Immunocytochemistry and **B**. flow cytometry were utilised to determine the *Bmi1* promoter-driven RFP expression. Data sets are representative of at least three independent experiments. Scale bar, 20 μm. **p-value< 0.01, ****p-value< 0.0001.

3.2.6 *Bmi1* is a direct target gene of the YAP/TEAD4 transcription factor complex

To study whether the *Bmi1* promoter region is bound by the YAP/TEAD4 complex, the same prediction platform described in section 3.1.7 was used for bioinformatics analysis. Several TEAD4-binding sites were identified in the *Bmi1* promoter region (–979 to +417, Figure 39), which were assembled into three clusters.

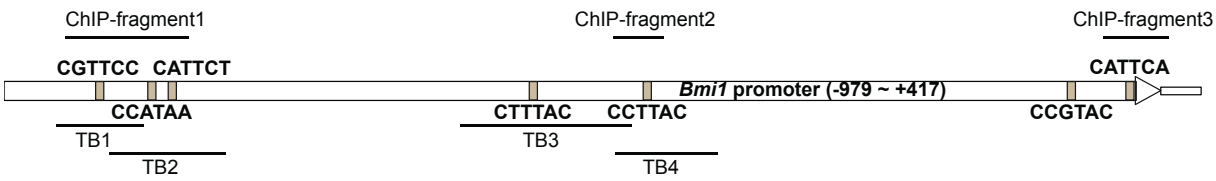

Figure 39. Scheme showing the YAP/TEAD4-binding sites in the *Bmi1* promoter region (–979 to +417, NM_007552).
Yellow boxes represent the predicted TEAD4-binding sites, whereas the upper three lines show the ChIP-qPCR products, which represent the different fragment (F1, F2, and F3) in the ChIP

primers. Four binding sites were located in fragments 1 and 2, which were named TB1, TB2, TB3, and TB4.

The promoter region was cloned into the pGL3-basic luciferase reporter vector, for use in the DLR assay. To investigate how the loss- or gain-of-function of YAP affects the *Bmi1*-driven luciferase activity, similar methods to those described in section 3.1.7 were used for the luciferase reporter assay. After YAP was knocked down using siRNA in Hepa1-6 cells, the luciferase activity was found to decrease with an increasing dose of siRNA (Figure 40A). The overexpression of YAP in NCTC clone 1469 cells was associated with the upregulation of luciferase activity (Figure 40A). By overexpressing YAP, TEAD4, and VGLL4 together in HEK293T cell lines, similar to the results observed in the NCTC clone 1469 cell line, the overexpression of YAP alone increased luciferase activity compared with that in the control group but not the overexpression of TEAD4 alone. Interestingly, the combined overexpression of YAP and TEAD4 markedly increased luciferase activity (Figure 40B). In contrast, luciferase activity was significantly decreased when either YAP or TEAD4 was overexpressed together with VGLL4. Luciferase activity was reduced, in a dose-dependent manner, when YAP and TEAD4 were co-overexpressed with VGLL4 (Figure 40B). These results suggested that the YAP/TEAD4 transcription factor complex can promote *Bmi1* expression by regulating its promoter activity.

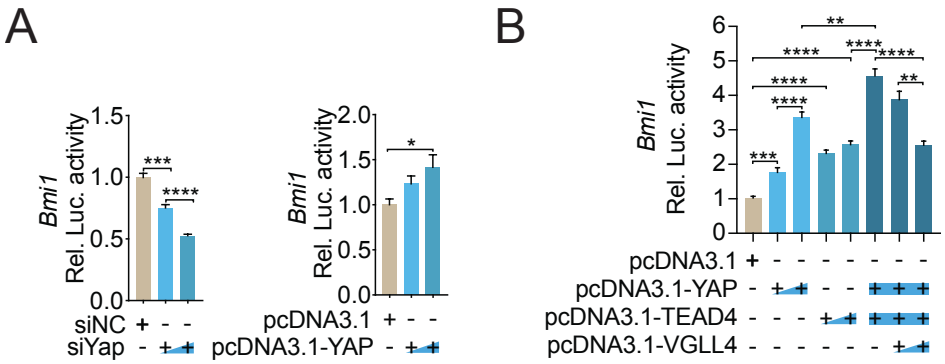

Figure 40. The YAP/TEAD4 complex targets the *Bmi1* promoter.
A. A dual-luciferase reporter (DLR) assay was performed to detect luciferase activity, 48 hours after the knockdown of Yap (siYap) in Hepa1-6 cells or the overexpression of YAP (pcDNA3.1-YAP) in NCTC clone 1469 cells. **B**. A DLR assay was performed after the co-transfection of YAP,

TEAD4 and VGLL4 overexpression plasmids in pGL3-Bmi1 and HEK293T reporter cells. Data sets are representative of at least three independent experiments. *p-value<0.05, **p-value<0.01, ***p-value<0.001, ****p-value<0.0001.

To determine whether the regulation of *Bmi1* by YAP/TEAD4 occurs in a direct manner, similar methods (ChIP) to those described in section 3.1.7 were performed. The entire promoter region was divided into three different clusters, fragment 1, fragment 2, and fragment 3, according to the distribution of TEAD4-binding sites (Figure 39). Three pairs of ChIP-qPCR primers and control primers for *Ctgf,* were designed (Table 11). The ChIP results, using the positive control *Ctgf* primers and negative control primers, showed that TEAD4 was able to specifically bind to the *Ctgf* promoter in Hepa1-6 cells, which express high levels of YAP but not in NCTC 1469 cells, which express low levels of YAP (Figure 41A). The negative control results confirmed the quality of the ChIP assay. The ChIP results, using specific primers for the *Bmi1* promoter, indicated that fragment 2 (F2) represents the primary area of the promoter region that is responsible for complex regulation (Figure 41B).

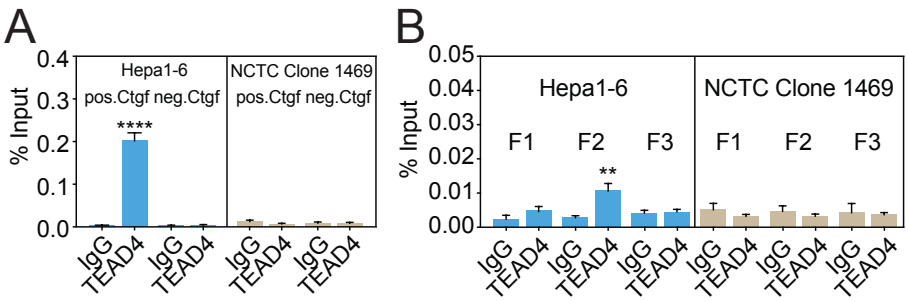

Figure 41. YAP/TEAD4 binds directly to the fragment 2 region of the *Bmi1* promoter.
Chromatin immunoprecipitation assay was performed to determine the interaction between TEAD4 and the *Bmi1* promoter, using and agarose-TEAD4 antibody and sonicated chromatin (200 bp–1000 bp). **A**. *Ctgf* positive and negative control primers were used for quality control of the ChIP assay. **B**. Specific primers targeting *Bmi1* promoter were used for quantifying the pulled-down DNA fragments. Data sets are representative of at least three independent experiments. **p-value< 0.01, ****p-value< 0.0001.

Because *Bmi1* fragment 2 includes two TEAD4-binding sites, TB3 and TB4 (Figure 39), further experiments were performed to determine which binding site was responsible for TEAD4 binding. Including TB1 and TB2, each TEAD4-binding motif,

plus a 50 bp flanking sequence on each side, was cloned into the pGL3-basic luciferase reporter vector, in addition to the *Ctgf* promoter binding sites which was also cloned into the luciferase reporter vector as a positive control. A DLR assay demonstrated that both TB3 and TB4 were the main TEAD4-binding sites in the *Bmi1* promoter (Figure 42A). Furthermore, the luciferase activities of bases-substitution-mediated mutation of TB3 (mTB3) and TB4 (mTB4) were significantly decreased compared with those of TB3 and TB4 (Figure 42B). Taken together, these results illustrated that the YAP/TEAD4 transcription factor complex can directly bind to the TEAD4-binding regions of fragment 2, to promote *Bmi1* expression.

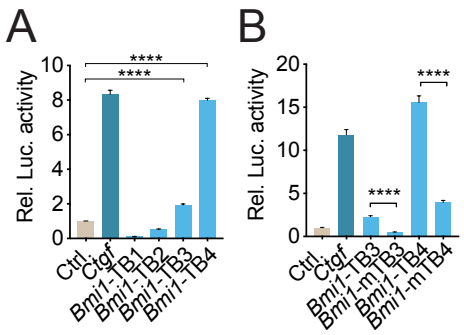

Figure 42. The YAP/TEAD4 complex directly binds to the TB3 and TB4 binding sites of *Bmi1*-F2.

Dual luciferase reporter assay was performed after cloning the TB1, TB2, TB3, TB4, and mutated TB3 (mTB3) and TB4 (mTB4) binding sites into the reporter plasmid, in HEK293 cells. **A**. DLR assay was performed after cloning the TB1, TB2, TB3 and TB4 binding sites into the reporter plasmid. **B**. DLR assay was performed after cloning the mutated TB3 (mTB3) and mutated TB4 (mTB4) binding sites into the reporter plasmid. Data sets are representative of at least three independent experiments. ****p-value< 0.0001.

3.2.7 The disruptions of the YAP/TEAD complex suppresses BMI1 in HBsAg-transgenic mice

Because YAP-induced BMI1 was associated with DNA damage, chromosomal instability, and cell proliferation, *in vivo* experiments were performed in 6-month-old HBsAg-transgenic mice. The transgenic mice were treated with Verteporfin (YAP/TEAD4 inhibitor, 100 mg/kg) or the same volume of DMSO. The mice were injected on days 1, 2, and 3, by i.p. injection. On day 7, the mouse livers were

collected for experiments. The western blot results showed that Verteporfin treatment decreased YAP and BMI1 expression levels, which suggested that the downregulation of YAP in transgenic mice might control the development of HCC by decreasing the expression of BMI1.

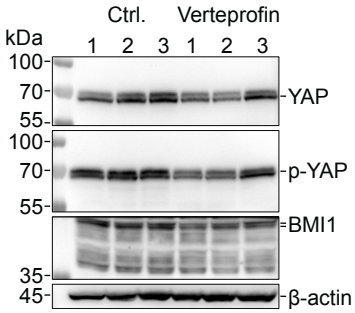

Figure 43. Downregulated YAP decreases BMI1 expression in transgenic mice.
Transgenic mice were treated with Verteporfin (100 mg/kg) (n = 3) or the same volume of DMSO (n = 3), for 3 days. On day 7, mouse livers were collected for total protein isolation. Western blot was performed to detect YAP, phosphorylated YAP, and BMI1 expression levels. kDa, kilodalton.

Chronic HBV infection is a key risk factor associated with the development of HCC. Our previous work showed that BMI1 is upregulated in (I) the livers HBsAg-transgenic mice, (II) HBV-exposed PMHs, and (III) HBV-related HCC tissue sections[125]. Here, we investigated the relationship between Hippo signalling and BMI1 expression in HBsAg-mediated hepatocarcinogenesis. The reanalysis of a ChIP dataset showed that genes associated with Hippo signalling, cell cycle, centrosomal function, and DNA repair/replication were altered in HBsAg-transgenic mouse liver samples. Quantitative PCR and western blot results confirmed that the downregulation of MST1/2 was accompanied by the loss of YAP phosphorylation and the induction of BMI1 expression. The immunohistochemical staining of HBsAg-transgenic mice liver sections further indicated that the expression of HBsAg induced the increased expression of YAP and BMI1, which resulted in cell proliferation and abnormal nuclear morphology. Flow cytometry revealed that polyploidy and aneuploidy also occurred in PMHs isolated from HBsAg-transgenic mice. The bioinformatics analysis of the *Bmi1* promoter indicated the presence of several

TEAD4 bind sites. The ChIP assay results and the analysis of binding site mutations in DLR assays confirmed that the YAP/TEAD4 transcription factor complex was able to bind and activate the *Bmi1* promoter. The Hepa1-6 cell line was transfected with an RFP-reporter plasmid containing the Bmi1 promoter region, and the knockdown of *Yap* or *Tead4* resulted in decreased RFP signals. The Hippo signalling pathway plays a vital role in cell homeostasis. Our findings suggested that the HBsAg-mediated inactivation of the Hippo pathway resulted in increased BMI1 expression, possibly promoting hepatocarcinogenesis through alterations in the cell cycle and chromosomal stability.

4. Discussion

4.1 HBV is recognised by TLR2 and activates the Hippo signalling pathway

Chronic HBV infection is a high-risk factor for HCC. Current therapies for CHB remain limited to either pegylated interferon-α, or one of the five approved nucleoside analogue (NA) treatments[177]. Although viral suppression can be achieved in the majority of patients when treated with high-barrier-to-resistance new-generation NAs, HBsAg loss is only achieved in approximately 10% of patients for both classes of drugs after a follow-up of 5 years[178]. Whether HBV activates the innate immune response or represses innate host defences continues to be debated. Investigations examining the mechanisms through which HBV evades innate immune monitoring are urgently needed. The present study showed that (I) acute HBV infections concordantly induced TLR2 and Hippo signalling activity in primary hepatocytes, (II) Hippo pathway activation counter regulated innate immune responses by controlling *NFKBIA* expression, both *in vitro* and *in vivo,* and (III) hepatic gene expression signatures associated with TLR2/MyD88/NF-κB signalling could be detected in CHB patients.

Many studies in HBV-infected patients and primate models have reported that HBV infections are unable to induce an innate immune response[70,75,179]. However, these studies either focused on interferon responses or generally assessed HBV exposure for longer than 6 hours, after which it is difficult to detect a rapid, innate cytokine response. Yoneda *et al.* showed artefacts of inflammatory immune responses in PHHs treated with HBV for 40 hours[90]. However, the 40-hour exposure of HBV particles did not affect *IL6* and *IL1B* production (Figure 6A), which suggested that the production of *IL6* and *IL1B* peaked earlier and returned to a normal level before the examined 40 hour time point. In the present study, we chose 0.5, 1, and 2 hours as our main time points. We observed a rapid, innate immune response as soon as 30 min after HBV exposure, which peaked between 1-2 hours after treatment, as assessed by the ICC staining of NF-κB. However, after 6 hours of HBV exposure, we

observed the return of these inflammatory factors to basal levels, which suggested that the active suppression of innate immunity occurred after 6 hours. These findings were further confirmed by the observed changes of IκBα after HBV exposure. After a 0.5-hour exposure to HBV particles, IκBα disappeared and was restored gradually, between 1 and 2 hours (exemplarily, Figure 7B). Usually, the transcriptional and translational processes cannot regulate IκBα levels so quickly, except through modifications by protein kinases. However, the restoration of IκBα, the dephosphorylation of YAP, and the subsequent expression of *Il6*, *Il1β,* and *Tnf* were the focus of this study, and the mechanisms underlying the rapid disappearance of IκBα remains an open question for future studies. Here, we characterised the essential role played by Hippo signalling in the innate immune response to HBV infection. The activation of MST1/2 was important for the rapid innate immune response. In addition, YAP, the primary effector for Hippo signalling, was found to be crucial for balancing the overactivation of innate immunity with reduced tissue injury. The Hippo signalling pathway was originally defined as an intracellular kinase cascade that coupled organ size control and tumorigenesis. Therefore, this field has expressed a long-term interest in understanding how Hippo signalling activity is controlled during homeostasis. In *Drosophila*, Hpo and Wts are key components that are indispensable for toll receptor-induced innate immunity, via PII (an IRAK homolog) and MyD88[99]. However, the innate immunity in mammals is much more complicated than that in *Drosophila*. In this study, we utilised a TLR2 inhibitor and an MST1/2 inhibitor to pretreat PMHs, prior to HBV exposure. When either TLR or Hippo signalling was inhibited, downstream NF-κB signalling was also substantially suppressed. Liu and Zheng *et al*. reported that MyD88/IRAK4, a downstream effector of TLRs, downregulates PP2A levels, to activate Hippo signalling during the innate immune response[99,180]. Here, we isolated PMHs from *Myd88*$^{-/-}$ or *Irak4*$^{-/-}$ mouse livers and exposed them to HBV. Interestingly, more YAP was observed to translocate into the nucleus, even without HBV exposure; moreover, no NF-κB was observed to translocate into the nucleus, even with HBV exposure. These findings suggested that the TLR2-IRAK4-MyD88 axis is likely required for HBV particle recognition and to

activate the innate immune response. MST1/2 has been shown to be activated by TLR2-IRAK1/4 and to regulate the expression of CXCL1 and CXCL2 during *Mycobacterium tuberculosis* infection[122]. Consistent with the results of previous studies, *Irak4* or *Myd88* knockout increased PP2A levels and decreased phosphorylated MST1/2 levels, further inducing YAP translocation into the nucleus and promoting IκBα expression, which repressed NF-κB nuclear translocation[99]. The present study is the first to report that the YAP/TEAD4 complex directly binds to the proximal binding site of the *Nfkbia* promoter region, to regulate IκBα expression. This fundamentally explains how the YAP/TEAD4 complex can balance the rapid innate immune response.

4.2 Humanised mouse model for HBV infection study

Mouse hepatocytes do not express the NTCP receptor, which is the cellular factor required for HBV entry[165], and are, therefore, not susceptible to HBV infection. In this study, TLR2 expressed in PMHs recognised HBV particles as pathogens, without the process of infection. Our previous work demonstrated that HBV particles could facilitate TLR2 activation when binding to NTCP in PHHs[89]. Even after HBV particles were UV-irradiated, they remained able to activate the innate immune response in PHHs[89]. Moreover, although Kupffer cells are not thought to express NTCP, they are able to detect HBV particles and patient-derived HBsAg, through TLR2[165]. Importantly, our previous work[125] showed that HBV exposure induces *Il6*, *Tnf* and *Il1β* expression in PMHs as well. Therefore, PMHs were initially chosen for the *in vitro* experiments performed in this study. PMH cultures are homogeneous and highly reproducible. To simulate HBV infections in mice, we treated mice with the TLR2 agonist Pam3CSK4, by i.v. injection. Although this method does not sufficiently represent a real HBV infection, this model was useful for exploring the significance of the TLR2-MyD88-IRAK4-Hippo axis during rapid, innate immunity in the liver. Future studies might utilise a humanised mouse model, to develop an *in vivo* model for HBV-induced innate immunity. The initial approaches that examined early immune responses in HBV-infected liver-chimeric mice were unable to demonstrate or to

exclude hepatic immune-associated gene induction[89]. This model must be adopted towards immune induction, rather than stable HBV infection, to enable investigations of TLR and Hippo pathway activation, in the future. However, we also studied PHH cultures, with similar results, indicating that our findings are also relevant in humans. As tissue culture systems continue to be developed, more advanced liver biopsy culture methods have been established[181-183]. A tissue culture model could provide a growth environment more similar to the natural situation. In future studies, additional exploratory experiments will be performed, to facilitate the development of an HBV infection model. Highlighting the relevance of our study, a very recent publication reported that monocytes from CHB patients express higher levels of inflammatory cytokines than those from healthy donors. Furthermore, HBV induces the production of inflammatory cytokines, *in vitro,* via TLR2/MyD88/NF-κB signalling in monocytes[165].The reanalysis of large-scale gene expression data[171] from liver biopsies suggested increased hepatic TLR2/MyD88/NF-κB signalling in CHB patients. The role played by Hippo signalling during long-term, persistent HBV-infections was less pronounced in these datasets. However, our findings may have implications for the development of novel HBV treatment strategies. Immunotherapeutic strategies that are currently in clinical development include TLR7, TLR8, and RIG-I agonists (SB9200)[184]. Whether and how these ligands affect the Hippo pathway and contribute to immune control and tumorigenesis remains an important open question.

4.3 HBsAg is a tumour inciter

The results of the present study illustrated the kinetics and the magnitude of the effects associated with HBsAg overexpression-induced hepatocarcinogenesis in the HBsAg-transgenic mouse model. In this study, the HBsAg-associated findings indicated that the overproduction of HBV surface antigens initiates a series of events, characterised by polyploidy, aneuploidy, DNA damage/repair, cell proliferation, and inflammation responses to the development of HCC in transgenic mice. HBsAg is expressed as three differently sized polypeptides: the large surface polypeptides, the medium surface polypeptides, and the small surface polypeptides. Although the

HBsAg-transgenic mouse was first established decades ago, the mechanisms through which HBsAg induces the development of HCC remain still unclear. During the past decade, HBx has been a focus of research and has been reported to act as a coactivator that forms a complex with other transcription factors to promote tumorigenesis[139,185-188]. The small surface polypeptides are approximately 17 kDa in size, with a similar molecular weight as the HBx protein. In this study, LATS1/2 proteins were found to be characterised at different molecular weights between WT and transgenic mice, which suggested that LATS1/2 might interact with HBsAg to form a complex, shifting the protein band on the western blot membrane. Unfortunately, associated experiments to confirm this hypothesis were not performed in this study. However, the direct-IP and Co-IP assays have been designed for the further analysis of potential interactions between HBsAg and LATS1/2. This study represents the first time that HBsAg might act as a suppressor of the Hippo signalling pathway, by decreasing and inactivating the expression of MST1/2 and MOB1 and potentially by forming a complex with LATS1/2. These changes resulted in increasing amounts of ungoverned YAP, which translocated into the nucleus to promote BMI1 expression, leading to DNA damage, cell proliferation, aneuploidy, and chromosomal instability.

The preS1/preS2/S sequence has been reported to encode a transcriptional activator, with potentially transforming properties[189-191]. These transcriptional effects can activate the protein kinase C-dependent c-Raf-1/MAP1-kinase signalling pathway, promoting transcription factors and increasing the proliferation rate of hepatocytes[191]. A truncated version of the large surface antigen has also been shown to promote the development of HCC in transgenic mice[192]. The medium surface antigens can bind to the promoter regions of oncogenes, to promote oncogene expression, including c-myc, c-fos, and c-Ha-ras[193,194]. In HBsAg-transgenic mice, an interaction between HBsAg and Hippo signalling was observed; however, further studies remain necessary to determine the mechanisms through which Hippo signalling is suppressed. The Hippo signalling pathway regulates organ size, cell fate, cell

proliferation, and innate immunity. The inactivation of Hippo signalling has been associated with tumorigenesis, by allowing the nuclear translocation of dephosphorylated YAP. Here, HBsAg was found to suppress the Hippo signalling pathway, resulting in the accumulation of YAP in the nucleus, supporting the development of HCC.

In HBsAg-transgenic mice, the overproduced HBsAg induces hepatocellular injury; however, HBsAg has also been shown to be retained in the endoplasmic reticulum (ER), causing ER-stress[136,195]. Overproduced HBsAg is folded and assembled into higher-order complexes, through covalent modifications. Because protein folding is a complex and error-prone process, the protein-folding capacity of the ER can easily be saturated, following various types of physiological and pathological insults, such as viral infection, mutant protein expression, ageing, and simple increases in the secretory protein synthesis[196]. Wu *et al*. reported that Hippo signalling plays a critical role in the ER stress-induced unfolded protein response (UPR)[197]. *Mst1/2*- or *WW45*-deficient livers exhibited greatly enhanced UPRs, resulting in the gradually increasing levels of YAP, which was dependent on the induction of PKR-like ER kinase (PERK) signalling, a pathway that is required for cell survival[197,198]. In HBsAg-transgenic mice, ER stress was induced, whereas Hippo signalling was inactivated, leading to the ungoverned activation of UPRs. Individual UPR pathways have been associated with cancers, arising from diverse tissues[199,200]. In the future, more studies examining the relationships between ER stress and Hippo signalling in HBsAg-transgenic mice should be designed. Many of the mechanisms through which HBsAg promote the development of HCC remain poorly understood. Understanding these mechanisms will assist with the development of new therapeutic strategies for the treatment of CHB.

4.4 Nuclear accumulation of YAP and BMI1 in the development of HCC

Both YAP and BMI1 are oncoproteins. As the major effector of the Hippo signalling pathway, YAP forms a transcription factor complex with TEADs in the nucleus,

promoting the expression of target genes. BMI1 is a member of the polycomb protein group, and it contains a RING finger domain and a central helix-turn-helix-turn-helix-turn motif[201,202]. BMI1 has various functions, including oncogenic activities, DNA damage protection and developmental activities. In HBsAg-transgenic mice, upregulated BMI1 suppressed $p16^{INK4a}$ and $p19^{ARF}$, which subsequently increased Cyclin D1 and suppressed p53 expression. Cyclin D1 is responsible for the transit from the G1 phase to the S phase, whereas p53 is a gatekeeper of the G2/M phase of the cell cycle[203]. DNA damage had been observed in HBsAg-transgenic mice, as indicated by the upregulation of phosphorylated H2AX. The combination of frequent DNA damage and a bustling cell cycle can result in abnormal mitosis and chromosomal instability. Interestingly, several TEAD4 motifs were found in the *Bmi1* promoter region, which allowed the YAP/TEAD4 complex to directly promote BMI1 expression. In our previous work, BMI1 was found to be upregulated in HBV-related HCC comparing with non-HBV-related HCC, which suggested that HBV infection may be associated with BMI1 upregulation and the development of HCC[125]. Here, we further reported that HBsAg-mediated YAP activation upregulated BMI1 expression, contributing to cell proliferation, abnormal mitosis, and chromosomal instability associated with the development of HCC.

In the present study, Verteporfin, a YAP/TEAD4 inhibitor, was administered in 8-month-old HBsAg-transgenic mice for 7 days, resulting in the downregulation of YAP and BMI1. However, in a first proof-of-principle a 7-day treatment was not sufficient to reduce DNA damage, chromosomal instability, or aneuploidy (data not shown) . In the future, long-term treatment should be tested, to observe the incidence of HCC and changes of markers associated with Hippo signalling, BMI1 signalling, DNA damage, cell cycle, and chromosomal instability. To confirm the YAP-BMI1 axis, *in vivo*, PTC596, a BMI1 inhibitor, should be administered in younger mice for long-term treatment, to observe changes in DNA damage, cell cycle, and chromosomal instability.

In conclusion, these findings directly link HBsAg overproduction with the inactivation of Hippo signalling. In clinical practice, HBV-associated, cirrhosis-free tumour development might be explained by HBsAg-YAP-BMI1-axis-mediated cell proliferation and chromosomal instability.

5. Summary

In summary, we demonstrate that the Hepatitis B virus (HBV) was able to stimulate TLR2, which not only mediated NF-κB signalling but also activated the Hippo pathway, which regulated the innate immune response by producing and controlling inflammatory factors. YAP/TEAD4 functioned as a key regulator and was likely important for balancing the innate immune response through the induction of IκBα. In contrast to previous reports indicating that HBV acts as a "stealth virus", our study showed that a rapid, innate immune response occurred at a very early stage, immediately after HBV exposure, which was subsequently suppressed by IκBα and further unknown mechanisms, which may explain the ability of HBV to evade innate immunity. This rapid, innate immune response is necessary for the host defence but can also induce tissue injury when the activation is too strong. The activation of the Hippo signalling effector YAP accompanied the TLR2-NF-κB-mediated immune response and negatively regulates the activation of NF-κB to reduce tissue injury. Taken together, our data indicated that the Hippo signalling pathway acts as a regulator of the rapid, innate immune response. These findings directly link hepatic inflammation with growth control mechanisms and might explain tumour progression in non-cirrhotic, HBV-infected patients.

In HBsAg-transgenic mice, the overproduction of HBsAg caused the nuclear accumulation of YAP and BMI1, while simultaneously decreasing the expression of MST1/2 and MOB1, which are key components of the Hippo signalling pathway. In addition, the YAP/TEAD4 transcription factor complex promoted BMI1 expression, through directly binding to the promoter region of *Bmi1*. As an inhibitor of $p16^{INK4a}$ and $p19^{ARF}$, BMI1 upregulation induces DNA replication and cell proliferation. DNA damage and unpaired chromatids were observed in transgenic mouse hepatocytes. These characteristic features promote chromosomal instability, leading to the development of hepatocellular carcinoma. HBsAg can be expressed as three different-sized surface polypeptides, and our findings suggested that the small HBsAg may interact with LATS1/2, forming a complex that additionally promotes the

dephosphorylation and subsequent nuclear translocation of YAP. The Hippo signalling pathway plays a vital role during cell homeostasis. Our findings suggested that the HBsAg-mediated Hippo pathway inactivation results in BMI1 accumulation, possibly promoting hepatocarcinogenesis by altering the cell cycle and decreasing chromosomal stability.

6. Zusammenfassung

Zusammenfassend zeigen wir, dass das Hepatitis-B-Virus (HBV) in der Lage war, den TLR2 zu stimulieren, der nicht nur den NF-κB-Signalweg aktivierte, sondern auch den Hippo-Signalweg, welcher die angeborene Immunantwort durch die Produktion und Kontrolle von Entzündungsfaktoren regulierte. Als Transkriptionsfaktor fungierte YAP/TEAD4 wie ein Schlüsselregulator und scheint wichtig, um die angeborene Immunantwort durch die Induktion von IκBα zu kontrollieren. Im Gegensatz zu früheren Berichten, in denen vermutet wird, dass HBV als "heimliches Virus" keine Immunantworten auslöst, zeigte unsere Studie, dass unmittelbar nach der HBV-Exposition eine schnelle, angeborene Immunantwort in einem sehr frühen Stadium auftrat. Diese Immunantwort wurde anschließend durch IκBα und weitere unbekannte Mechanismen unterdrückt, was die Fähigkeit von HBV, sich der angeborenen Immunität zu entziehen, erklären könnte. Diese schnelle, angeborene Immunantwort ist für die Wirtsabwehr notwendig, kann aber auch eine Gewebeschädigung hervorrufen, wenn die Aktivierung zu stark ausfällt. Die Aktivierung des Hippo-Effektors YAP begleitete die TLR2-NF-κB-vermittelte Immunantwort und regulierte die Aktivierung von NF-κB auf negative Weise, was eine anhaltende entzündungsbedingte Gewebeschädigung vermeiden könnte.
Zusammengenommen zeigen unsere Daten, dass der Hippo-Signalweg als Negativ-Regulator der schnellen, angeborenen Immunantwort wirkt. Diese Erkenntnis stellt eine direkte Verbindung zwischen der Leberentzündung und den Wachstumskontrollmechanismen her und könnte die entzündungsassoziierte Tumorprogression bei nicht zirrhotischen, HBV-infizierten Patienten erklären.

Zu dem verursachte die Überproduktion des HBV-Oberflächenantigens (HBsAg) in HBsAg-transgenen Mäusen die nukleäre Akkumulation von YAP und BMI1, während gleichzeitig die Expression von MST1/2 und MOB1, Schlüsselkomponenten des Hippo-Signalwegs, vermindert wurde. Darüber hinaus förderte der YAP/TEAD4-Transkriptionsfaktor-Komplex die BMI1-Expression, indem er direkt an die Promotorregion von *Bmi1* bindet. Als Inhibitor von $p16^{INK4a}$ und $p19^{ARF}$ beeinflusst

BMI1 die DNA-Replikation und Zellproliferation. Entsprechend wurden DNA-Schäden und ungepaarte Chromatiden in HBsAg-transgenen Maushepatozyten beobachtet. Diese charakteristischen Merkmale fördern die chromosomale Instabilität, was die Entwicklung eines Hepatozelluläres Karzinom begünstigt. Das HBsAg kommt in Form von drei unterschiedlich großen Polypeptiden vor. Unsere Ergebnisse legten nahe, dass das kleine HBsAg mit LATS1/2 interagieren und einen Komplex bilden kann, der zusätzlich die Dephosphorylierung und anschließende Translokation von YAP in den Zellkern fördern könnte.

Der Hippo-Signalweg spielt eine wichtige Rolle bei der Zellhomöostase. Unsere Ergebnisse deuten darauf hin, dass die HBsAg-vermittelte Aktivierung des Hippo-Signalwegs zu einer Akkumulation von BMI1 führt, diese fördert möglicherweise die Hepatokarzinogenese durch Veränderung des Zellzyklus und Erhöhung der chromosomalen Instabilität.

7. References

1 Lee, W. M. Hepatitis B virus infection. *N Engl J Med* **337**, 1733-1745, doi:10.1056/NEJM199712113372406 (1997).

2 Tiollais, P., Pourcel, C. & Dejean, A. The hepatitis B virus. *Nature* **317**, 489-495, doi:10.1038/317489a0 (1985).

3 Sa-Nguanmoo, P., Rianthavorn, P., Amornsawadwattana, S. & Poovorawan, Y. Hepatitis B virus infection in non-human primates. *Acta Virol* **53**, 73-82, doi:10.4149/av_2009_02_73 (2009).

4 Patient, R., Hourioux, C. & Roingeard, P. Morphogenesis of hepatitis B virus and its subviral envelope particles. *Cell Microbiol* **11**, 1561-1570, doi:10.1111/j.1462-5822.2009.01363.x (2009).

5 Bruss, V. Hepatitis B virus morphogenesis. *World J Gastroenterol* **13**, 65-73, doi:10.3748/wjg.v13.i1.65 (2007).

6 Datta, S., Chatterjee, S., Veer, V. & Chakravarty, R. Molecular biology of the hepatitis B virus for clinicians. *J Clin Exp Hepatol* **2**, 353-365, doi:10.1016/j.jceh.2012.10.003 (2012).

7 Liang, T. J. Hepatitis B: the virus and disease. *Hepatology* **49**, S13-21, doi:10.1002/hep.22881 (2009).

8 Gilbert, R. J. *et al.* Hepatitis B small surface antigen particles are octahedral. *Proc Natl Acad Sci U S A* **102**, 14783-14788, doi:10.1073/pnas.0505062102 (2005).

9 Ning, X. *et al.* Secretion of genome-free hepatitis B virus--single strand blocking model for virion morphogenesis of para-retrovirus. *PLoS Pathog* **7**, e1002255, doi:10.1371/journal.ppat.1002255 (2011).

10 Venkatakrishnan, B. & Zlotnick, A. The Structural Biology of Hepatitis B Virus: Form and Function. *Annu Rev Virol* **3**, 429-451, doi:10.1146/annurev-virology-110615-042238 (2016).

11 Clark, D. N. & Hu, J. Unveiling the roles of HBV polymerase for new antiviral strategies. *Future Virol* **10**, 283-295, doi:10.2217/fvl.14.113 (2015).

12 Kay, A. & Zoulim, F. Hepatitis B virus genetic variability and evolution. *Virus Res* **127**, 164-176, doi:10.1016/j.virusres.2007.02.021 (2007).

13 Ma, Z., Cao, Q., Xiong, Y., Zhang, E. & Lu, M. Interaction between Hepatitis B Virus and Toll-Like Receptors: Current Status and Potential Therapeutic Use for Chronic Hepatitis B. *Vaccines (Basel)* **6**, doi:10.3390/vaccines6010006 (2018).

14 Zhu, A. *et al.* HBV cccDNA and Its Potential as a Therapeutic Target. *J Clin Transl Hepatol* **7**, 258-262, doi:10.14218/JCTH.2018.00054 (2019).

15 Kramvis, A. Genotypes and genetic variability of hepatitis B virus. *Intervirology* **57**, 141-150, doi:10.1159/000360947 (2014).

16 Pourkarim, M. R., Amini-Bavil-Olyaee, S., Kurbanov, F., Van Ranst, M. & Tacke, F. Molecular identification of hepatitis B virus genotypes/subgenotypes: revised classification hurdles and updated resolutions. *World J Gastroenterol* **20**, 7152-7168, doi:10.3748/wjg.v20.i23.7152 (2014).

17 Andernach, I. E., Hubschen, J. M. & Muller, C. P. Hepatitis B virus: the genotype E puzzle. *Rev Med Virol* **19**, 231-240, doi:10.1002/rmv.618 (2009).
18 Forbi, J. C. *et al.* Disparate distribution of hepatitis B virus genotypes in four sub-Saharan African countries. *J Clin Virol* **58**, 59-66, doi:10.1016/j.jcv.2013.06.028 (2013).
19 Kostaki, E. G. *et al.* Unravelling the history of hepatitis B virus genotypes A and D infection using a full-genome phylogenetic and phylogeographic approach. *Elife* **7**, doi:10.7554/eLife.36709 (2018).
20 Lin, C. L. & Kao, J. H. Hepatitis B virus genotypes and variants. *Cold Spring Harb Perspect Med* **5**, a021436, doi:10.1101/cshperspect.a021436 (2015).
21 Girlanda, R. *et al.* Hepatitis B virus genotype A and D and clinical outcomes of liver transplantation for HBV-related disease. *Liver Transpl* **10**, 58-64, doi:10.1002/lt.20004 (2004).
22 Sengupta, S., Panda, S. K., Acharya, S. K. & Durgapal, H. Role of hepatitis B virus genotype D & its mutants in occult hepatitis B infection. *Indian J Med Res* **138**, 329-339 (2013).
23 Malagnino, V. *et al.* High rates of chronic HBV genotype E infection in a group of migrants in Italy from West Africa: Virological characteristics associated with poor immune clearance. *PLoS One* **13**, e0195045, doi:10.1371/journal.pone.0195045 (2018).
24 Mathet, V. L. *et al.* Detection of hepatitis B virus (HBV) genotype E carried--even in the presence of high titers of anti-HBs antibodies--by an Argentinean patient of African descent who had received vaccination against HBV. *J Clin Microbiol* **44**, 3435-3439, doi:10.1128/JCM.00866-06 (2006).
25 Rajoriya, N., Combet, C., Zoulim, F. & Janssen, H. L. A. How viral genetic variants and genotypes influence disease and treatment outcome of chronic hepatitis B. Time for an individualised approach? *J Hepatol* **67**, 1281-1297, doi:10.1016/j.jhep.2017.07.011 (2017).
26 Chudy, M. *et al.* Hepatitis B virus genotype G monoinfection and its transmission by blood components. *Hepatology* **44**, 99-107, doi:10.1002/hep.21220 (2006).
27 Dao, D. Y. *et al.* Hepatitis B virus genotype G: prevalence and impact in patients co-infected with human immunodeficiency virus. *J Med Virol* **83**, 1551-1558, doi:10.1002/jmv.22160 (2011).
28 Velkov, S., Ott, J. J., Protzer, U. & Michler, T. The Global Hepatitis B Virus Genotype Distribution Approximated from Available Genotyping Data. *Genes (Basel)* **9**, doi:10.3390/genes9100495 (2018).
29 Lavanchy, D. Hepatitis B virus epidemiology, disease burden, treatment, and current and emerging prevention and control measures. *J Viral Hepat* **11**, 97-107, doi:10.1046/j.1365-2893.2003.00487.x (2004).
30 Seto, W. K., Lo, Y. R., Pawlotsky, J. M. & Yuen, M. F. Chronic hepatitis B virus infection. *Lancet* **392**, 2313-2324, doi:10.1016/S0140-6736(18)31865-8 (2018).
31 Yuen, M. F. & Lai, C. L. Treatment of chronic hepatitis B. *Lancet Infect Dis* **1**, 232-241, doi:10.1016/S1473-3099(01)00118-9 (2001).

32 Zamor, P. J., deLemos, A. S. & Russo, M. W. Viral hepatitis and hepatocellular carcinoma: etiology and management. *J Gastrointest Oncol* **8**, 229-242, doi:10.21037/jgo.2017.03.14 (2017).
33 Polaris Observatory, C. Global prevalence, treatment, and prevention of hepatitis B virus infection in 2016: a modelling study. *Lancet Gastroenterol Hepatol* **3**, 383-403, doi:10.1016/S2468-1253(18)30056-6 (2018).
34 Hou, J., Liu, Z. & Gu, F. Epidemiology and Prevention of Hepatitis B Virus Infection. *Int J Med Sci* **2**, 50-57, doi:10.7150/ijms.2.50 (2005).
35 MacLachlan, J. H. & Cowie, B. C. Hepatitis B virus epidemiology. *Cold Spring Harb Perspect Med* **5**, a021410, doi:10.1101/cshperspect.a021410 (2015).
36 Gerlich, W. H. Prophylactic vaccination against hepatitis B: achievements, challenges and perspectives. *Med Microbiol Immunol* **204**, 39-55, doi:10.1007/s00430-014-0373-y (2015).
37 Lemoine, M. & Thursz, M. R. Battlefield against hepatitis B infection and HCC in Africa. *J Hepatol* **66**, 645-654, doi:10.1016/j.jhep.2016.10.013 (2017).
38 Romano, L. *et al.* Hepatitis B vaccination. *Hum Vaccin Immunother* **11**, 53-57, doi:10.4161/hv.34306 (2015).
39 Cornberg, M., Lok, A. S., Terrault, N. A., Zoulim, F. & Faculty, E.-A. H. T. E. C. Guidance for design and endpoints of clinical trials in chronic hepatitis B - Report from the 2019 EASL-AASLD HBV Treatment Endpoints Conference(double dagger). *J Hepatol* **72**, 539-557, doi:10.1016/j.jhep.2019.11.003 (2020).
40 Rogers, M. & Davis, G. L. Serology of acute and chronic type B hepatitis. *Dig Dis* **7**, 255-264, doi:10.1159/000171225 (1989).
41 Nelson, N. P., Easterbrook, P. J. & McMahon, B. J. Epidemiology of Hepatitis B Virus Infection and Impact of Vaccination on Disease. *Clin Liver Dis* **20**, 607-628, doi:10.1016/j.cld.2016.06.006 (2016).
42 Komatsu, H., Inui, A. & Fujisawa, T. Pediatric hepatitis B treatment. *Ann Transl Med* **5**, 37, doi:10.21037/atm.2016.11.52 (2017).
43 Mahoney, F. J. Update on diagnosis, management, and prevention of hepatitis B virus infection. *Clin Microbiol Rev* **12**, 351-366 (1999).
44 Liu, D. *et al.* Hepatitis B e antigen and its precursors promote the progress of hepatocellular carcinoma by interacting with NUMB and decreasing p53 activity. *Hepatology* **64**, 390-404, doi:10.1002/hep.28594 (2016).
45 Liaw, Y. F. & Chu, C. M. Hepatitis B virus infection. *Lancet* **373**, 582-592, doi:10.1016/S0140-6736(09)60207-5 (2009).
46 Goyal, A., Ribeiro, R. M. & Perelson, A. S. The Role of Infected Cell Proliferation in the Clearance of Acute HBV Infection in Humans. *Viruses* **9**, doi:10.3390/v9110350 (2017).
47 Tan, A., Koh, S. & Bertoletti, A. Immune Response in Hepatitis B Virus Infection. *Cold Spring Harb Perspect Med* **5**, a021428, doi:10.1101/cshperspect.a021428 (2015).
48 Chisari, F. V. Cytotoxic T cells and viral hepatitis. *J Clin Invest* **99**, 1472-1477, doi:10.1172/JCI119308 (1997).

49 Alberti, A., Diana, S., Sculard, G. H., Eddleston, A. L. & Williams, R. Detection of a new antibody system reacting with Dane particles in hepatitis B virus infection. *Br Med J* **2**, 1056-1058, doi:10.1136/bmj.2.6144.1056 (1978).
50 European Association for the Study of the Liver. Electronic address, e. e. e. & European Association for the Study of the, L. EASL 2017 Clinical Practice Guidelines on the management of hepatitis B virus infection. *J Hepatol* **67**, 370-398, doi:10.1016/j.jhep.2017.03.021 (2017).
51 Papatheodoridis, G. V., Manolakopoulos, S., Liaw, Y. F. & Lok, A. Follow-up and indications for liver biopsy in HBeAg-negative chronic hepatitis B virus infection with persistently normal ALT: a systematic review. *J Hepatol* **57**, 196-202, doi:10.1016/j.jhep.2011.11.030 (2012).
52 Zeisel, M. B. *et al.* Towards an HBV cure: state-of-the-art and unresolved questions--report of the ANRS workshop on HBV cure. *Gut* **64**, 1314-1326, doi:10.1136/gutjnl-2014-308943 (2015).
53 Yuen, M. F. *et al.* HBsAg Seroclearance in chronic hepatitis B in Asian patients: replicative level and risk of hepatocellular carcinoma. *Gastroenterology* **135**, 1192-1199, doi:10.1053/j.gastro.2008.07.008 (2008).
54 Park, J. S. & Pan, C. Q. Viral factors for HBV mother-to-child transmission. *Hepatol Int* **11**, 476-480, doi:10.1007/s12072-017-9825-y (2017).
55 Pawlowska, M., Pniewska, A., Pilarczyk, M., Kozielewicz, D. & Domagalski, K. Prophylaxis of vertical HBV infection. *Expert Opin Drug Saf* **15**, 1361-1368, doi:10.1080/14740338.2016.1211106 (2016).
56 Tsai, K. N., Kuo, C. F. & Ou, J. J. Mechanisms of Hepatitis B Virus Persistence. *Trends Microbiol* **26**, 33-42, doi:10.1016/j.tim.2017.07.006 (2018).
57 Favero, M. S., Bond, W. W., Petersen, N. J., Berquist, K. R. & Maynard, J. E. Detection methods for study of the stability of hepatitis B antigen on surfaces. *J Infect Dis* **129**, 210-212, doi:10.1093/infdis/129.2.210 (1974).
58 Bond, W. W. *et al.* Survival of hepatitis B virus after drying and storage for one week. *Lancet* **1**, 550-551, doi:10.1016/s0140-6736(81)92877-4 (1981).
59 Mysore, K. R. & Leung, D. H. Hepatitis B and C. *Clin Liver Dis* **22**, 703-722, doi:10.1016/j.cld.2018.06.002 (2018).
60 Yuen, M. F. *et al.* Hepatitis B virus infection. *Nat Rev Dis Primers* **4**, 18035, doi:10.1038/nrdp.2018.35 (2018).
61 Wu, J., Han, M., Li, J., Yang, X. & Yang, D. Immunopathogenesis of HBV Infection. *Adv Exp Med Biol* **1179**, 71-107, doi:10.1007/978-981-13-9151-4_4 (2020).
62 Ferrari, C. HBV and the immune response. *Liver Int* **35 Suppl 1**, 121-128, doi:10.1111/liv.12749 (2015).
63 Seeger, C. & Mason, W. S. Molecular biology of hepatitis B virus infection. *Virology* **479-480**, 672-686, doi:10.1016/j.virol.2015.02.031 (2015).
64 Bertoletti, A., Maini, M. & Williams, R. Role of hepatitis B virus specific cytotoxic T cells in liver damage and viral control. *Antiviral Res* **60**, 61-66, doi:10.1016/j.antiviral.2003.08.012 (2003).

65 Sprengers, D. *et al.* Analysis of intrahepatic HBV-specific cytotoxic T-cells during and after acute HBV infection in humans. *J Hepatol* **45**, 182-189, doi:10.1016/j.jhep.2005.12.022 (2006).
66 Wieland, S., Thimme, R., Purcell, R. H. & Chisari, F. V. Genomic analysis of the host response to hepatitis B virus infection. *Proc Natl Acad Sci U S A* **101**, 6669-6674, doi:10.1073/pnas.0401771101 (2004).
67 Fletcher, S. P. *et al.* Identification of an intrahepatic transcriptional signature associated with self-limiting infection in the woodchuck model of hepatitis B. *Hepatology* **57**, 13-22, doi:10.1002/hep.25954 (2013).
68 Giersch, K. *et al.* Hepatitis Delta co-infection in humanized mice leads to pronounced induction of innate immune responses in comparison to HBV mono-infection. *J Hepatol* **63**, 346-353, doi:10.1016/j.jhep.2015.03.011 (2015).
69 Sato, S. *et al.* The RNA sensor RIG-I dually functions as an innate sensor and direct antiviral factor for hepatitis B virus. *Immunity* **42**, 123-132, doi:10.1016/j.immuni.2014.12.016 (2015).
70 Cheng, X. *et al.* Hepatitis B virus evades innate immunity of hepatocytes but activates cytokine production by macrophages. *Hepatology* **66**, 1779-1793, doi:10.1002/hep.29348 (2017).
71 Stacey, A. R. *et al.* Induction of a striking systemic cytokine cascade prior to peak viremia in acute human immunodeficiency virus type 1 infection, in contrast to more modest and delayed responses in acute hepatitis B and C virus infections. *J Virol* **83**, 3719-3733, doi:10.1128/JVI.01844-08 (2009).
72 Dunn, C. *et al.* Temporal analysis of early immune responses in patients with acute hepatitis B virus infection. *Gastroenterology* **137**, 1289-1300, doi:10.1053/j.gastro.2009.06.054 (2009).
73 Lucifora, J. *et al.* Control of hepatitis B virus replication by innate response of HepaRG cells. *Hepatology* **51**, 63-72, doi:10.1002/hep.23230 (2010).
74 Luangsay, S. *et al.* Early inhibition of hepatocyte innate responses by hepatitis B virus. *J Hepatol* **63**, 1314-1322, doi:10.1016/j.jhep.2015.07.014 (2015).
75 Mutz, P. *et al.* HBV Bypasses the Innate Immune Response and Does Not Protect HCV From Antiviral Activity of Interferon. *Gastroenterology* **154**, 1791-1804 e1722, doi:10.1053/j.gastro.2018.01.044 (2018).
76 Suslov, A., Boldanova, T., Wang, X., Wieland, S. & Heim, M. H. Hepatitis B Virus Does Not Interfere With Innate Immune Responses in the Human Liver. *Gastroenterology* **154**, 1778-1790, doi:10.1053/j.gastro.2018.01.034 (2018).
77 Wieland, S. F. & Chisari, F. V. Stealth and cunning: hepatitis B and hepatitis C viruses. *J Virol* **79**, 9369-9380, doi:10.1128/JVI.79.15.9369-9380.2005 (2005).
78 Kawai, T. & Akira, S. Toll-like receptors and their crosstalk with other innate receptors in infection and immunity. *Immunity* **34**, 637-650, doi:10.1016/j.immuni.2011.05.006 (2011).
79 Goubau, D., Deddouche, S. & Reis e Sousa, C. Cytosolic sensing of viruses. *Immunity* **38**, 855-869, doi:10.1016/j.immuni.2013.05.007 (2013).

80 Isogawa, M., Robek, M. D., Furuichi, Y. & Chisari, F. V. Toll-like receptor signaling inhibits hepatitis B virus replication in vivo. *J Virol* **79**, 7269-7272, doi:10.1128/JVI.79.11.7269-7272.2005 (2005).
81 Thompson, A. J. *et al.* Stimulation of the interleukin-1 receptor and Toll-like receptor 2 inhibits hepatitis B virus replication in hepatoma cell lines in vitro. *Antivir Ther* **14**, 797-808, doi:10.3851/IMP1294 (2009).
82 Reuven, E. M., Fink, A. & Shai, Y. Regulation of innate immune responses by transmembrane interactions: lessons from the TLR family. *Biochim Biophys Acta* **1838**, 1586-1593, doi:10.1016/j.bbamem.2014.01.020 (2014).
83 Chaturvedi, A. & Pierce, S. K. How location governs toll-like receptor signaling. *Traffic* **10**, 621-628, doi:10.1111/j.1600-0854.2009.00899.x (2009).
84 Ohto, U. & Shimizu, T. Structural aspects of nucleic acid-sensing Toll-like receptors. *Biophys Rev* **8**, 33-43, doi:10.1007/s12551-015-0187-1 (2016).
85 Takeuchi, O. & Akira, S. Pattern recognition receptors and inflammation. *Cell* **140**, 805-820, doi:10.1016/j.cell.2010.01.022 (2010).
86 Rubio, D. *et al.* Crosstalk between the type 1 interferon and nuclear factor kappa B pathways confers resistance to a lethal virus infection. *Cell Host Microbe* **13**, 701-710, doi:10.1016/j.chom.2013.04.015 (2013).
87 Kawasaki, T. & Kawai, T. Toll-like receptor signaling pathways. *Front Immunol* **5**, 461, doi:10.3389/fimmu.2014.00461 (2014).
88 Park, S. H. *et al.* Type I interferons and the cytokine TNF cooperatively reprogram the macrophage epigenome to promote inflammatory activation. *Nat Immunol* **18**, 1104-1116, doi:10.1038/ni.3818 (2017).
89 Zhang, Z. *et al.* Hepatitis B Virus Particles Activate Toll-Like Receptor 2 Signaling Initially Upon Infection of Primary Human Hepatocytes. *Hepatology*, doi:10.1002/hep.31112 (2020).
90 Yoneda, M. *et al.* Hepatitis B Virus and DNA Stimulation Trigger a Rapid Innate Immune Response through NF-kappaB. *J Immunol* **197**, 630-643, doi:10.4049/jimmunol.1502677 (2016).
91 MacDonald, D. M., Holmes, E. C., Lewis, J. C. & Simmonds, P. Detection of hepatitis B virus infection in wild-born chimpanzees (Pan troglodytes verus): phylogenetic relationships with human and other primate genotypes. *J Virol* **74**, 4253-4257, doi:10.1128/jvi.74.9.4253-4257.2000 (2000).
92 Wieland, S. F. The chimpanzee model for hepatitis B virus infection. *Cold Spring Harb Perspect Med* **5**, doi:10.1101/cshperspect.a021469 (2015).
93 Durantel, D. & Zoulim, F. Innate response to hepatitis B virus infection: observations challenging the concept of a stealth virus. *Hepatology* **50**, 1692-1695, doi:10.1002/hep.23361 (2009).
94 Chen, Z. *et al.* Expression profiles and function of Toll-like receptors 2 and 4 in peripheral blood mononuclear cells of chronic hepatitis B patients. *Clin Immunol* **128**, 400-408, doi:10.1016/j.clim.2008.04.006 (2008).
95 Momeni, M. *et al.* Decreased expression of toll like receptor signaling molecules in chronic HBV infected patients. *Hum Immunol* **75**, 15-19, doi:10.1016/j.humimm.2013.09.015 (2014).

96 Nikbakht Dastjerdi, M. *et al.* The effect of depression and anxiety on expression levels of toll like receptor signaling molecules in chronic HBV infected patients. *Med J Islam Repub Iran* **29**, 180 (2015).
97 Visvanathan, K. *et al.* Regulation of Toll-like receptor-2 expression in chronic hepatitis B by the precore protein. *Hepatology* **45**, 102-110, doi:10.1002/hep.21482 (2007).
98 Yu, F. X., Zhao, B. & Guan, K. L. Hippo Pathway in Organ Size Control, Tissue Homeostasis, and Cancer. *Cell* **163**, 811-828, doi:10.1016/j.cell.2015.10.044 (2015).
99 Liu, B. *et al.* Toll Receptor-Mediated Hippo Signaling Controls Innate Immunity in Drosophila. *Cell* **164**, 406-419, doi:10.1016/j.cell.2015.12.029 (2016).
100 Zhao, B., Lei, Q. & Guan, K. L. Mst out and HCC in. *Cancer Cell* **16**, 363-364, doi:10.1016/j.ccr.2009.10.008 (2009).
101 Zhou, D. *et al.* Mst1 and Mst2 maintain hepatocyte quiescence and suppress hepatocellular carcinoma development through inactivation of the Yap1 oncogene. *Cancer Cell* **16**, 425-438, doi:10.1016/j.ccr.2009.09.026 (2009).
102 Jiang, K. *et al.* SASH1 suppresses triple-negative breast cancer cell invasion through YAP-ARHGAP42-actin axis. *Oncogene* **39**, 5015-5030, doi:10.1038/s41388-020-1356-7 (2020).
103 Gonzalez-Alonso, P. *et al.* The Hippo Pathway Transducers YAP1/TEAD Induce Acquired Resistance to Trastuzumab in HER2-Positive Breast Cancer. *Cancers (Basel)* **12**, doi:10.3390/cancers12051108 (2020).
104 You, B. *et al.* Inhibition of ERK1/2 down-regulates the Hippo/YAP signaling pathway in human NSCLC cells. *Oncotarget* **6**, 4357-4368, doi:10.18632/oncotarget.2974 (2015).
105 Dong, Q. *et al.* Rab11a promotes proliferation and invasion through regulation of YAP in non-small cell lung cancer. *Oncotarget* **8**, 27800-27811, doi:10.18632/oncotarget.15359 (2017).
106 Ghiso, E. *et al.* YAP-Dependent AXL Overexpression Mediates Resistance to EGFR Inhibitors in NSCLC. *Neoplasia* **19**, 1012-1021, doi:10.1016/j.neo.2017.10.003 (2017).
107 Salem, O. & Hansen, C. G. The Hippo Pathway in Prostate Cancer. *Cells* **8**, doi:10.3390/cells8040370 (2019).
108 Khandelwal, M. *et al.* RASSF1A-Hippo pathway link in patients with urothelial carcinoma of bladder: plausible therapeutic target. *Mol Cell Biochem* **464**, 51-63, doi:10.1007/s11010-019-03648-y (2020).
109 Jeong, W. *et al.* Activation of YAP1 is associated with poor prognosis and response to taxanes in ovarian cancer. *Anticancer Res* **34**, 811-817 (2014).
110 Xie, Y., Zhou, F. & Zhao, X. TNFAIP8 promotes cell growth by regulating the Hippo pathway in epithelial ovarian cancer. *Exp Ther Med* **16**, 4975-4982, doi:10.3892/etm.2018.6819 (2018).
111 Elbediwy, A. *et al.* Integrin signalling regulates YAP and TAZ to control skin homeostasis. *Development* **143**, 1674-1687, doi:10.1242/dev.133728 (2016).

112 Andl, T., Zhou, L., Yang, K., Kadekaro, A. L. & Zhang, Y. YAP and WWTR1: New targets for skin cancer treatment. *Cancer Lett* **396**, 30-41, doi:10.1016/j.canlet.2017.03.001 (2017).
113 Maugeri-Sacca, M. & De Maria, R. The Hippo pathway in normal development and cancer. *Pharmacol Ther* **186**, 60-72, doi:10.1016/j.pharmthera.2017.12.011 (2018).
114 Kovar, H., Bierbaumer, L. & Radic-Sarikas, B. The YAP/TAZ Pathway in Osteogenesis and Bone Sarcoma Pathogenesis. *Cells* **9**, doi:10.3390/cells9040972 (2020).
115 Ji, J. *et al.* Actin like-6A promotes glioma progression through stabilization of transcriptional regulators YAP/TAZ. *Cell Death Dis* **9**, 517, doi:10.1038/s41419-018-0548-3 (2018).
116 Ji, J. *et al.* PMEPA1 isoform a drives progression of glioblastoma by promoting protein degradation of the Hippo pathway kinase LATS1. *Oncogene* **39**, 1125-1139, doi:10.1038/s41388-019-1050-9 (2020).
117 Pan, D. The hippo signaling pathway in development and cancer. *Dev Cell* **19**, 491-505, doi:10.1016/j.devcel.2010.09.011 (2010).
118 Badouel, C. & McNeill, H. SnapShot: The hippo signaling pathway. *Cell* **145**, 484-484 e481, doi:10.1016/j.cell.2011.04.009 (2011).
119 Zheng, Y. & Pan, D. The Hippo Signaling Pathway in Development and Disease. *Dev Cell* **50**, 264-282, doi:10.1016/j.devcel.2019.06.003 (2019).
120 Zhang, Y., Zhang, H. & Zhao, B. Hippo Signaling in the Immune System. *Trends Biochem Sci* **43**, 77-80, doi:10.1016/j.tibs.2017.11.009 (2018).
121 Hong, L., Li, X., Zhou, D., Geng, J. & Chen, L. Role of Hippo signaling in regulating immunity. *Cell Mol Immunol* **15**, 1003-1009, doi:10.1038/s41423-018-0007-1 (2018).
122 Boro, M., Singh, V. & Balaji, K. N. Mycobacterium tuberculosis-triggered Hippo pathway orchestrates CXCL1/2 expression to modulate host immune responses. *Sci Rep* **6**, 37695, doi:10.1038/srep37695 (2016).
123 Zhang, Q. *et al.* Hippo signalling governs cytosolic nucleic acid sensing through YAP/TAZ-mediated TBK1 blockade. *Nat Cell Biol* **19**, 362-374, doi:10.1038/ncb3496 (2017).
124 Sunami, Y. *et al.* Canonical NF-kappaB signaling in hepatocytes acts as a tumor-suppressor in hepatitis B virus surface antigen-driven hepatocellular carcinoma by controlling the unfolded protein response. *Hepatology* **63**, 1592-1607, doi:10.1002/hep.28435 (2016).
125 Zhang, R. *et al.* Hepatic expression of oncogenes Bmi1 and Dkk1 is up-regulated in hepatitis B virus surface antigen-transgenic mice and can be induced by treatment with HBV particles or lipopolysaccharides in vitro. *Int J Cancer* **141**, 354-363, doi:10.1002/ijc.30742 (2017).
126 Tseng, T. C. *et al.* Serum hepatitis B surface antigen levels help predict disease progression in patients with low hepatitis B virus loads. *Hepatology* **57**, 441-450, doi:10.1002/hep.26041 (2013).

127 Kawanaka, M. *et al.* Quantitative Levels of Hepatitis B Virus DNA and Surface Antigen and the Risk of Hepatocellular Carcinoma in Patients with Hepatitis B Receiving Long-Term Nucleos(t)ide Analogue Therapy. *Liver Cancer* **3**, 41-52, doi:10.1159/000343857 (2014).
128 Brechot, C., Pourcel, C., Louise, A., Rain, B. & Tiollais, P. Presence of integrated hepatitis B virus DNA sequences in cellular DNA of human hepatocellular carcinoma. *Nature* **286**, 533-535, doi:10.1038/286533a0 (1980).
129 Shafritz, D. A., Shouval, D., Sherman, H. I., Hadziyannis, S. J. & Kew, M. C. Integration of hepatitis B virus DNA into the genome of liver cells in chronic liver disease and hepatocellular carcinoma. Studies in percutaneous liver biopsies and post-mortem tissue specimens. *N Engl J Med* **305**, 1067-1073, doi:10.1056/NEJM198110293051807 (1981).
130 Liu, S. *et al.* Associations between hepatitis B virus mutations and the risk of hepatocellular carcinoma: a meta-analysis. *J Natl Cancer Inst* **101**, 1066-1082, doi:10.1093/jnci/djp180 (2009).
131 Yotsuyanagi, H. *et al.* Precore and core promoter mutations, hepatitis B virus DNA levels and progressive liver injury in chronic hepatitis B. *J Hepatol* **37**, 355-363, doi:10.1016/s0168-8278(02)00180-0 (2002).
132 Westland, C. *et al.* Hepatitis B virus genotypes and virologic response in 694 patients in phase III studies of adefovir dipivoxil1. *Gastroenterology* **125**, 107-116, doi:10.1016/s0016-5085(03)00700-5 (2003).
133 Sumi, H. *et al.* Influence of hepatitis B virus genotypes on the progression of chronic type B liver disease. *Hepatology* **37**, 19-26, doi:10.1053/jhep.2003.50036 (2003).
134 Liu, J. *et al.* Spontaneous seroclearance of hepatitis B seromarkers and subsequent risk of hepatocellular carcinoma. *Gut* **63**, 1648-1657, doi:10.1136/gutjnl-2013-305785 (2014).
135 Marion, P. L., Salazar, F. H., Alexander, J. J. & Robinson, W. S. Polypeptides of hepatitis B virus surface antigen produced by a hepatoma cell line. *J Virol* **32**, 796-802 (1979).
136 Chisari, F. V. *et al.* Molecular pathogenesis of hepatocellular carcinoma in hepatitis B virus transgenic mice. *Cell* **59**, 1145-1156, doi:10.1016/0092-8674(89)90770-8 (1989).
137 Huang, S. N. & Chisari, F. V. Strong, sustained hepatocellular proliferation precedes hepatocarcinogenesis in hepatitis B surface antigen transgenic mice. *Hepatology* **21**, 620-626 (1995).
138 Ono, M. *et al.* Transactivation of transforming growth factor alpha gene by hepatitis B virus preS1. *Cancer Res* **58**, 1813-1816 (1998).
139 Andrisani, O. M. & Barnabas, S. The transcriptional function of the hepatitis B virus X protein and its role in hepatocarcinogenesis (Review). *Int J Oncol* **15**, 373-379, doi:10.3892/ijo.15.2.373 (1999).
140 Bouchard, M. J. & Schneider, R. J. The enigmatic X gene of hepatitis B virus. *J Virol* **78**, 12725-12734, doi:10.1128/JVI.78.23.12725-12734.2004 (2004).

141 Tang, H., Oishi, N., Kaneko, S. & Murakami, S. Molecular functions and biological roles of hepatitis B virus x protein. *Cancer Sci* **97**, 977-983, doi:10.1111/j.1349-7006.2006.00299.x (2006).
142 Wang, Y. *et al.* HBsAg and HBx knocked into the p21 locus causes hepatocellular carcinoma in mice. *Hepatology* **39**, 318-324, doi:10.1002/hep.20076 (2004).
143 Schluter, V., Meyer, M., Hofschneider, P. H., Koshy, R. & Caselmann, W. H. Integrated hepatitis B virus X and 3' truncated preS/S sequences derived from human hepatomas encode functionally active transactivators. *Oncogene* **9**, 3335-3344 (1994).
144 Luber, B. *et al.* Hepatoma-derived integrated HBV DNA causes multi-stage transformation in vitro. *Oncogene* **12**, 1597-1608 (1996).
145 Liu, H. *et al.* In vitro transfection of the hepatitis B virus PreS2 gene into the human hepatocarcinoma cell line HepG2 induces upregulation of human telomerase reverse transcriptase. *Biochem Biophys Res Commun* **355**, 379-384, doi:10.1016/j.bbrc.2007.01.160 (2007).
146 Hildt, E., Munz, B., Saher, G., Reifenberg, K. & Hofschneider, P. H. The PreS2 activator MHBs(t) of hepatitis B virus activates c-raf-1/Erk2 signaling in transgenic mice. *EMBO J* **21**, 525-535, doi:10.1093/emboj/21.4.525 (2002).
147 Tai, P. C., Suk, F. M., Gerlich, W. H., Neurath, A. R. & Shih, C. Hypermodification and immune escape of an internally deleted middle-envelope (M) protein of frequent and predominant hepatitis B virus variants. *Virology* **292**, 44-58, doi:10.1006/viro.2001.1239 (2002).
148 Kekule, A. S. *et al.* The preS2/S region of integrated hepatitis B virus DNA encodes a transcriptional transactivator. *Nature* **343**, 457-461, doi:10.1038/343457a0 (1990).
149 Pollicino, T., Cacciola, I., Saffioti, F. & Raimondo, G. Hepatitis B virus PreS/S gene variants: pathobiology and clinical implications. *J Hepatol* **61**, 408-417, doi:10.1016/j.jhep.2014.04.041 (2014).
150 Wang, H. C., Huang, W., Lai, M. D. & Su, I. J. Hepatitis B virus pre-S mutants, endoplasmic reticulum stress and hepatocarcinogenesis. *Cancer Sci* **97**, 683-688, doi:10.1111/j.1349-7006.2006.00235.x (2006).
151 Hong, L., Cai, Y., Jiang, M., Zhou, D. & Chen, L. The Hippo signaling pathway in liver regeneration and tumorigenesis. *Acta Biochim Biophys Sin (Shanghai)* **47**, 46-52, doi:10.1093/abbs/gmu106 (2015).
152 Patel, S. H., Camargo, F. D. & Yimlamai, D. Hippo Signaling in the Liver Regulates Organ Size, Cell Fate, and Carcinogenesis. *Gastroenterology* **152**, 533-545, doi:10.1053/j.gastro.2016.10.047 (2017).
153 Zhang, S. & Zhou, D. Role of the transcriptional coactivators YAP/TAZ in liver cancer. *Curr Opin Cell Biol* **61**, 64-71, doi:10.1016/j.ceb.2019.07.006 (2019).
154 Li, H. *et al.* Deregulation of Hippo kinase signalling in human hepatic malignancies. *Liver Int* **32**, 38-47, doi:10.1111/j.1478-3231.2011.02646.x (2012).

155 Tao, J. *et al.* Activation of beta-catenin and Yap1 in human hepatoblastoma and induction of hepatocarcinogenesis in mice. *Gastroenterology* **147**, 690-701, doi:10.1053/j.gastro.2014.05.004 (2014).
156 Zender, L. *et al.* Identification and validation of oncogenes in liver cancer using an integrative oncogenomic approach. *Cell* **125**, 1253-1267, doi:10.1016/j.cell.2006.05.030 (2006).
157 Perra, A. *et al.* YAP activation is an early event and a potential therapeutic target in liver cancer development. *J Hepatol* **61**, 1088-1096, doi:10.1016/j.jhep.2014.06.033 (2014).
158 Dong, J. *et al.* Elucidation of a universal size-control mechanism in Drosophila and mammals. *Cell* **130**, 1120-1133, doi:10.1016/j.cell.2007.07.019 (2007).
159 Lu, L. *et al.* Hippo signaling is a potent in vivo growth and tumor suppressor pathway in the mammalian liver. *Proc Natl Acad Sci U S A* **107**, 1437-1442, doi:10.1073/pnas.0911427107 (2010).
160 Lee, K. P. *et al.* The Hippo-Salvador pathway restrains hepatic oval cell proliferation, liver size, and liver tumorigenesis. *Proc Natl Acad Sci U S A* **107**, 8248-8253, doi:10.1073/pnas.0912203107 (2010).
161 Chen, Q. *et al.* Homeostatic control of Hippo signaling activity revealed by an endogenous activating mutation in YAP. *Genes Dev* **29**, 1285-1297, doi:10.1101/gad.264234.115 (2015).
162 Benhamouche, S. *et al.* Nf2/Merlin controls progenitor homeostasis and tumorigenesis in the liver. *Genes Dev* **24**, 1718-1730, doi:10.1101/gad.1938710 (2010).
163 Zhang, N. *et al.* The Merlin/NF2 tumor suppressor functions through the YAP oncoprotein to regulate tissue homeostasis in mammals. *Dev Cell* **19**, 27-38, doi:10.1016/j.devcel.2010.06.015 (2010).
164 Yimlamai, D. *et al.* Hippo pathway activity influences liver cell fate. *Cell* **157**, 1324-1338, doi:10.1016/j.cell.2014.03.060 (2014).
165 Song, H. *et al.* Hepatitis B Virus-Induced Imbalance of Inflammatory and Antiviral Signaling by Differential Phosphorylation of STAT1 in Human Monocytes. *J Immunol* **202**, 2266-2275, doi:10.4049/jimmunol.1800848 (2019).
166 Li, Y. *et al.* Epigenetic silencing of microRNA-193a contributes to leukemogenesis in t(8;21) acute myeloid leukemia by activating the PTEN/PI3K signal pathway. *Blood* **121**, 499-509, doi:10.1182/blood-2012-07-444729 (2013).
167 Chen, R., Liliental, J. E., Kowalski, P. E., Lu, Q. & Cohen, S. N. Regulation of transcription of hypoxia-inducible factor-1alpha (HIF-1alpha) by heat shock factors HSF2 and HSF4. *Oncogene* **30**, 2570-2580, doi:10.1038/onc.2010.623 (2011).
168 Liu, J. *et al.* Advanced Method for Isolation of Mouse Hepatocytes, Liver Sinusoidal Endothelial Cells, and Kupffer Cells. *Methods Mol Biol* **1540**, 249-258, doi:10.1007/978-1-4939-6700-1_21 (2017).

169 Werner, M. *et al.* All-In-One: Advanced preparation of Human Parenchymal and Non-Parenchymal Liver Cells. *PLoS One* **10**, e0138655, doi:10.1371/journal.pone.0138655 (2015).
170 Jiao, S. *et al.* A peptide mimicking VGLL4 function acts as a YAP antagonist therapy against gastric cancer. *Cancer Cell* **25**, 166-180, doi:10.1016/j.ccr.2014.01.010 (2014).
171 Zhou, W. *et al.* Predictive model for inflammation grades of chronic hepatitis B: Large-scale analysis of clinical parameters and gene expressions. *Liver Int* **37**, 1632-1641, doi:10.1111/liv.13427 (2017).
172 Liu, H. *et al.* Differentially Expressed Intrahepatic Genes Contribute to Control of Hepatitis B Virus Replication in the Inactive Carrier Phase. *J Infect Dis* **217**, 1044-1054, doi:10.1093/infdis/jix683 (2018).
173 Schwertheim, S. *et al.* Intranuclear inclusions in hepatocellular carcinoma contain autophagy-associated proteins and correlate with prolonged survival. *J Pathol Clin Res* **5**, 164-176, doi:10.1002/cjp2.129 (2019).
174 Cao, L. *et al.* BMI1 as a novel target for drug discovery in cancer. *J Cell Biochem* **112**, 2729-2741, doi:10.1002/jcb.23234 (2011).
175 Weiler, S. M. E. *et al.* Induction of Chromosome Instability by Activation of Yes-Associated Protein and Forkhead Box M1 in Liver Cancer. *Gastroenterology* **152**, 2037-2051 e2022, doi:10.1053/j.gastro.2017.02.018 (2017).
176 Mah, L. J., El-Osta, A. & Karagiannis, T. C. gammaH2AX: a sensitive molecular marker of DNA damage and repair. *Leukemia* **24**, 679-686, doi:10.1038/leu.2010.6 (2010).
177 Seley-Radtke, K. L. & Yates, M. K. The evolution of nucleoside analogue antivirals: A review for chemists and non-chemists. Part 1: Early structural modifications to the nucleoside scaffold. *Antiviral Res* **154**, 66-86, doi:10.1016/j.antiviral.2018.04.004 (2018).
178 Zoulim, F. & Durantel, D. Antiviral therapies and prospects for a cure of chronic hepatitis B. *Cold Spring Harb Perspect Med* **5**, doi:10.1101/cshperspect.a021501 (2015).
179 Ortega-Prieto, A. M. *et al.* 3D microfluidic liver cultures as a physiological preclinical tool for hepatitis B virus infection. *Nat Commun* **9**, 682, doi:10.1038/s41467-018-02969-8 (2018).
180 Zheng, Y. *et al.* Homeostatic Control of Hpo/MST Kinase Activity through Autophosphorylation-Dependent Recruitment of the STRIPAK PP2A Phosphatase Complex. *Cell Rep* **21**, 3612-3623, doi:10.1016/j.celrep.2017.11.076 (2017).
181 Wu, X. *et al.* Precision-cut human liver slice cultures as an immunological platform. *J Immunol Methods* **455**, 71-79, doi:10.1016/j.jim.2018.01.012 (2018).
182 Palma, E., Doornebal, E. J. & Chokshi, S. Precision-cut liver slices: a versatile tool to advance liver research. *Hepatol Int* **13**, 51-57, doi:10.1007/s12072-018-9913-7 (2019).

183 Paish, H. L. *et al.* A Bioreactor Technology for Modeling Fibrosis in Human and Rodent Precision-Cut Liver Slices. *Hepatology* **70**, 1377-1391, doi:10.1002/hep.30651 (2019).
184 Lopatin, U. Drugs in the Pipeline for HBV. *Clin Liver Dis* **23**, 535-555, doi:10.1016/j.cld.2019.04.006 (2019).
185 Antunovic, J., Lemieux, N. & Cromlish, J. A. The 17 kDa HBx protein encoded by hepatitis B virus interacts with the activation domains of Oct-1, and functions as a coactivator in the activation and repression of a human U6 promoter. *Cell Mol Biol Res* **39**, 463-482 (1993).
186 Kong, H. J. *et al.* Hepatitis B virus X protein regulates transactivation activity and protein stability of the cancer-amplified transcription coactivator ASC-2. *Hepatology* **38**, 1258-1266, doi:10.1053/jhep.2003.50451 (2003).
187 Niu, Y. *et al.* Hepatitis B virus X protein co-activates pregnane X receptor to induce the cytochrome P450 3A4 enzyme, a potential implication in hepatocarcinogenesis. *Dig Liver Dis* **45**, 1041-1048, doi:10.1016/j.dld.2013.06.004 (2013).
188 Niu, Y. *et al.* Farnesoid X receptor ablation sensitizes mice to hepatitis b virus X protein-induced hepatocarcinogenesis. *Hepatology* **65**, 893-906, doi:10.1002/hep.28924 (2017).
189 Caselmann, W. H. *et al.* A trans-activator function is generated by integration of hepatitis B virus preS/S sequences in human hepatocellular carcinoma DNA. *Proc Natl Acad Sci U S A* **87**, 2970-2974, doi:10.1073/pnas.87.8.2970 (1990).
190 Hildt, E., Saher, G., Bruss, V. & Hofschneider, P. H. The hepatitis B virus large surface protein (LHBs) is a transcriptional activator. *Virology* **225**, 235-239, doi:10.1006/viro.1996.0594 (1996).
191 Hildt, E. & Hofschneider, P. H. The PreS2 activators of the hepatitis B virus: activators of tumour promoter pathways. *Recent Results Cancer Res* **154**, 315-329, doi:10.1007/978-3-642-46870-4_23 (1998).
192 Chisari, F. V. *et al.* Structural and pathological effects of synthesis of hepatitis B virus large envelope polypeptide in transgenic mice. *Proc Natl Acad Sci U S A* **84**, 6909-6913, doi:10.1073/pnas.84.19.6909 (1987).
193 Meyer, M. *et al.* Hepatitis B virus transactivator MHBst: activation of NF-kappa B, selective inhibition by antioxidants and integral membrane localization. *EMBO J* **11**, 2991-3001 (1992).
194 Lauer, U., Weiss, L., Lipp, M., Hofschneider, P. H. & Kekule, A. S. The hepatitis B virus preS2/St transactivator utilizes AP-1 and other transcription factors for transactivation. *Hepatology* **19**, 23-31 (1994).
195 Chisari, F. V. Hepatitis B virus transgenic mice: insights into the virus and the disease. *Hepatology* **22**, 1316-1325, doi:10.1016/0270-9139(95)90645-2 (1995).
196 Rashid, H. O., Yadav, R. K., Kim, H. R. & Chae, H. J. ER stress: Autophagy induction, inhibition and selection. *Autophagy* **11**, 1956-1977, doi:10.1080/15548627.2015.1091141 (2015).

197 Wu, H. *et al.* Integration of Hippo signalling and the unfolded protein response to restrain liver overgrowth and tumorigenesis. *Nat Commun* **6**, 6239, doi:10.1038/ncomms7239 (2015).
198 Lu, P. D. *et al.* Cytoprotection by pre-emptive conditional phosphorylation of translation initiation factor 2. *EMBO J* **23**, 169-179, doi:10.1038/sj.emboj.7600030 (2004).
199 Chen, X. *et al.* XBP1 promotes triple-negative breast cancer by controlling the HIF1alpha pathway. *Nature* **508**, 103-107, doi:10.1038/nature13119 (2014).
200 Koumenis, C. ER stress, hypoxia tolerance and tumor progression. *Curr Mol Med* **6**, 55-69, doi:10.2174/156652406775574604 (2006).
201 Li, Z. *et al.* Structure of a Bmi-1-Ring1B polycomb group ubiquitin ligase complex. *J Biol Chem* **281**, 20643-20649, doi:10.1074/jbc.M602461200 (2006).
202 Ginjala, V. *et al.* BMI1 is recruited to DNA breaks and contributes to DNA damage-induced H2A ubiquitination and repair. *Mol Cell Biol* **31**, 1972-1982, doi:10.1128/MCB.00981-10 (2011).
203 Capparelli, C. *et al.* CDK inhibitors (p16/p19/p21) induce senescence and autophagy in cancer-associated fibroblasts, "fueling" tumor growth via paracrine interactions, without an increase in neo-angiogenesis. *Cell Cycle* **11**, 3599-3610, doi:10.4161/cc.21884 (2012).

8. Appendices

8.1 Publications

1. Xufeng Luo, Mengji Lu, A. Baba Hideo, Heiner Wedemeyer, Broering Ruth. *Toll-like receptor signalling induces the Hippo pathway activity, thereby counter-regulating innate immunity against Hepatitis B virus*. (submitted)
2. Xufeng Luo, Jun Wang, Xueshi Zhou, Ruth Broering, Lihua Huang. *Medications rather than Coronavirus affects liver function directly*. (submitted)
3. Broering, Ruth; Luo, Xufeng; Liu, Jia; Lu, Mengji. *Early innate responses to hepatitis B virus infection, an explanation for viral persistence?* Virologica Sinica. 2020 Jul 6. doi: 10.1007/s12250-020-00235-0. Online ahead of print.
4. Yange Wang, Xiaobin Fan, Nanhang Lei, Xing He, Xiaoxi Wang, Xufeng Luo, Dongmei Zhang and Weiqing Pan. *A MicroRNA Derived From Schistosoma japonicum Promotes Schistosomiasis Hepatic Fibrosis by Targeting Host Secreted Frizzled-Related Protein 1*. Front Cell Infect Microbiol. 2020 Mar 13;10:101. doi: 10.3389/fcimb.2020.00101.
5. X Luo, M Lu, HA Baba, G Gerken, H Wedemeyer, R Broering. *Hippo signalling counter regulates early innate immunity in hepatocytes exposed to Hepatitis B virus*. Z Gastroenterol 2020; 58(01): e59 (Conference abstract)
6. Zhang Z, Trippler M, Real CI, Werner M, Luo X, Schefczyk S, Kemper T, Anastasiou OE, Ladiges Y, Treckmann J, Paul A, Baba HA, Allweiss L, Dandri M, Gerken G, Wedemeyer H, Schlaak JF, Lu M, Broering R. *Hepatitis B virus particles activate toll-like receptor 2 signalling initial upon infection of primary human hepatocytes*. Hepatology. 2020 Jan 11. doi: 10.1002/hep.31112. Online ahead of print.
7. Luo X, Lu M, Baba HA, Gerken G, Wedemeyer H, Broering R. *Toll-like receptor signalling induces changes in the Hippo signalling pathway that counter regulates innate immune responses in hepatocytes.* Journal of Hepatology. 12 April 2019 (Conference abstract)

8. Luo X, Lu M, Baba HA, Gerken G, Wedemeyer H, Broering R. *The Hippo signalling is induced by Toll-like receptor 4 activation and regulatory balance innate immune responses in liver cells*. Z Gastroenterol 2019; 57(01): e83-e84. (Conference abstract)
9. Yonghui Li *, Li Gao *, Xufeng Luo *, Lili Wang, Xiaoning Gao, Wei Wang, Liping Dou, Jingxin Li, Chengwang Xu, Lixin Wang, Yang Yang, Clara Nervi, Clara D. Bloomfield, Guido Marcucci, and Li Yu. *Epigenetic Silencing of microRNA-193a Contributes to Leukemogenesis in t(8;21) Acute Myeloid Leukemia by Activating the PTEN/PI3K Signal Pathway*. Blood. 2013 Jan 17;121(3):499-509. doi: 10.1182/blood-2012-07-444729. (*Y.L., L.G., and X.L. contributed equally to this work)
10. Xufeng Luo *, Dongmei Zhang *, Jun Xie, Qin Su, Xing He, Ruipu Bai, Guangping Gao and Weiqing Pan. *MicroRNA-96 Promotes Schistosomiasis Hepatic Fibrosis in mice by suppressing Smad7*. Mol Ther Methods Clin Dev. 2018 Oct 10;11:73-82. doi: 10.1016/j.omtm.2018.10.002.
11. He X, Xie J, Zhang D, Su Q, Sai X, Bai R, Chen C, Luo X, Gao G, Pan W. *Recombinant Adeno-Associated Virus–Mediated Inhibition of MicroRNA-21 Protects Mice Against the Lethal Schistosome Infection by Repressing Both IL-13 and Transforming Growth Factor Beta 1 Pathways.* Hepatology. 2015 Jun;61(6):2008-2017. doi: 10.1002/hep.27671.
12. C Xu, H Fu, L Gao, L Wang, W Wang, J Li, Y Li, L Dou, X Gao, X Luo, Y Jing, C-S Chim, X Zheng and L Yu. *BCR-ABL/GATA1/miR-138 mini circuitry contributes to the leukemogenesis of chronic myeloid leukemia*. Oncogene. 2014 Jan 2;33(1):44-54. doi: 10.1038/onc.2012.557.
13. Li-Xin Wang, Zhen-Yang Mei, Ji-Hao Zhou, Yu-Shi Yao, Yong-Hui Li, Yi-Han Xu, Jing-Xin Li, Xiao-Ning Gao, Min-Hang Zhou, Meng-Meng Jiang, Li Gao, Yi Ding, Xue-Chun Lu, Jin-Long Shi, Xu-Feng Luo, Jia Wang, Li-Li Wang, Chunfeng Qu, Xue-Feng Bai, Li Yu. *Low Dose Decitabine Treatment Induces CD80 Expression in Cancer Cells and Stimulates Tumor Specific Cytotoxic T Lymphocyte*

Responses. PLoS One. 2013 May 9;8(5):e62924. doi: 10.1371/journal.pone.0062924.

14. Jihao Zhou, Yonghui Li, Yushi Yao, Lixin Wang, Li Gao, Xiaoning Gao, Xufeng Luo, Jingxin Li, Mengmeng Jiang, Minhang Zhou, Lili Wang, Li Yu. *The cancer-testis antigen NXF2 is activated by the hypomethylating agent decitabine in acute leukemia cells in vitro and in vivo*. Mol Med Rep. 2013 Nov;8(5):1549-55. doi: 10.3892/mmr.2013.1659.

8.2 Acknowledgement

Throughout the whole period of the doctoral study and the writing of this dissertation I have received a great deal of support and assistance.

First and foremost, I would like to thank my supervisor, Priv. Doz. Dr. rer. nat. Ruth Bröring, for giving me the opportunity and a lot of support to conduct the research in her group. Her expertise also gave me a lot of scientific support and inspiration to solve different problems during the experiments.

I would like to thank Prof. Guido Gerken and Prof. Heiner Wedemeyer for providing financial support and for providing lab space.

I would like to thank Prof. Mengji Lu for providing the lab space for BSL2 and scientific discussion of my project.

I am also grateful to Prof. Carsten Kirschning, who provided the knock-out mice that help me solving important questions within my experiments.

I give my great thanks to Mrs. Thekla Kemper and Mrs. Dorothe Möllmann for their excellent technical support and the Westdeutsche Biobank Essen for acquisition of liver samples.

I would also like to thank my colleagues from the lab of Gastroenterology and Hepatology, namely Matthias Hardtke-Wolenski, Martin Trippler, Laura Elisa Buitrago Molina, Stefan Schefczyk, Yaojie Liang, Julia Pietrek, Leonie Weber, Alexandra Frey, Natalie Vogel, Sabrina Rüschenbaum, Mona-May Langer, Stefanie Sichelschmidt, Adriana Schultz-Moreira, Tanvi Khera and Yanqin Du, who made the work in the lab more enjoyable and smoothly.

In addition, I would like to thank my family for their wise counsel and sympathetic ear. They are always there for me.

Finally, there are my friends, who were of great support in deliberating over our problems and findings, as well as providing happy distraction to rest my mind outside of my research.

8.3 Curriculum vitae

The curriculum vitae is not included in the online version for data protection reasons

8.4 Declarations required for the submission of the thesis

Declaration:

In accordance with § 6 (para. 2, clause g) of the Regulations Governing the Doctoral Proceedings of the Faculty of Biology for awarding the doctoral degree Dr. rer. nat., I hereby declare that I represent the field to which the topic "*Hepatitis B virus affects TLR2 signalling and Hippo pathway activity, thereby counter-regulates innate immunity and contributes to hepatocarcinogenesis"* is assigned in research and teaching and that I support the application of *Luo, Xufeng*.

Essen, date_____ _____

Priv. Doz. Dr. rer. nat. Ruth Bröring

Declaration:

In accordance with § 7 (para. 2, clause d and f) of the Regulations Governing the Doctoral Proceedings of the Faculty of Biology for awarding the doctoral degree Dr. rer. nat., I hereby declare that I have written the herewith submitted dissertation independently using only the materials listed, and have cited all sources taken over verbatim or in content as such.

Essen, date_____ _____

Xufeng Luo

Declaration:

In accordance with § 7 (para. 2, clause e and g) of the Regulations Governing the Doctoral Proceedings of the Faculty of Biology for awarding the doctoral degree Dr. rer. nat., I hereby declare that I have undertaken no previous attempts to attain a doctoral degree, that the current work has not been rejected by any other faculty, and that I am submitting the dissertation only in this procedure.

Essen, date_____ _____

Xufeng Luo